NORTHERN TERRITORY GEOLOGICAL SURVEY

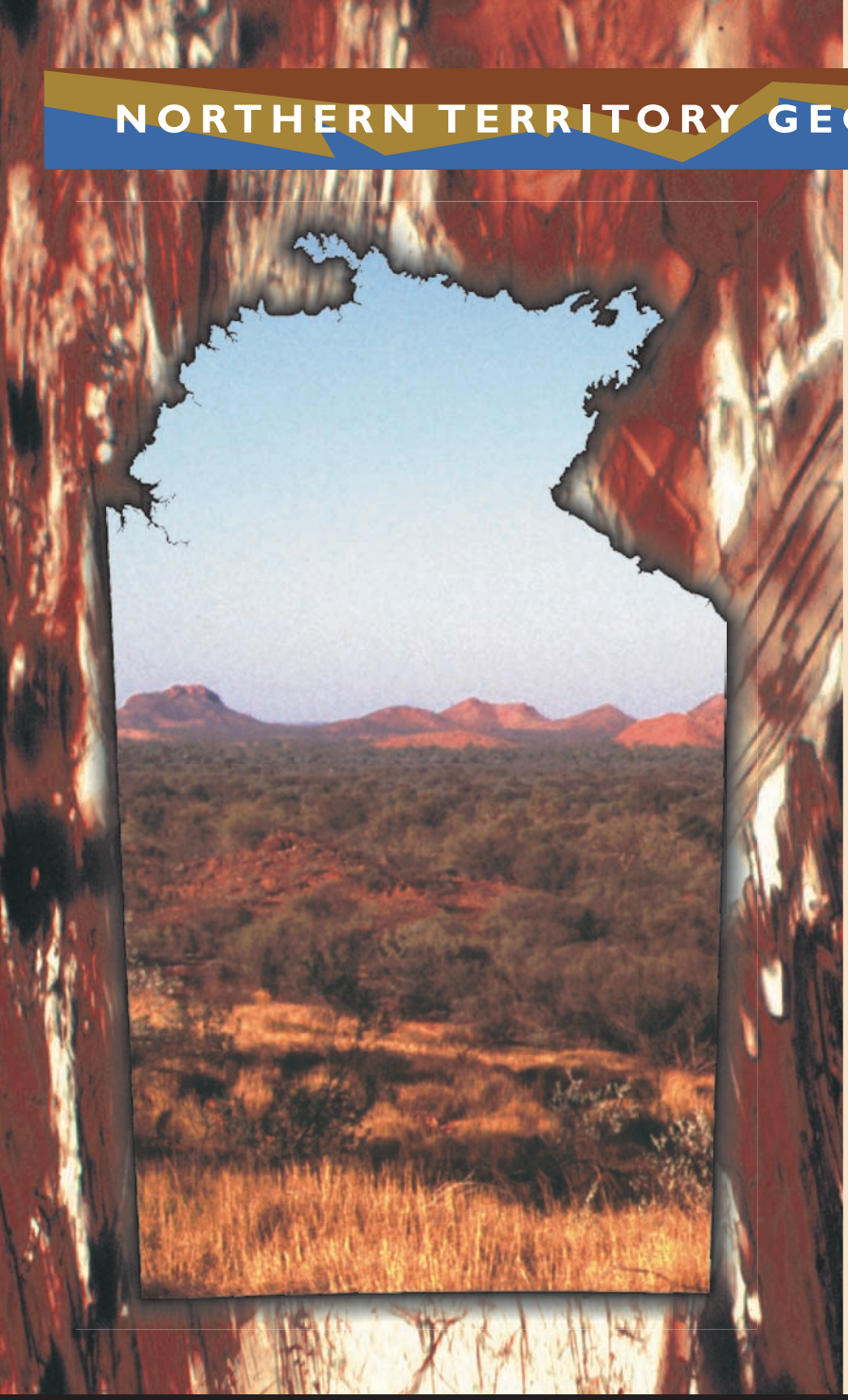

I. Scrimgeour
J. Raith

TECTONIC AND THERMAL EVENTS IN THE NORTHEASTERN ARUNTA PROVINCE

REPORT 12

DEPARTMENT OF MINES AND ENERGY

NORTHERN TERRITORY GEOLOGICAL SURVEY

TECTONIC AND THERMAL EVENTS IN THE NORTHEASTERN ARUNTA PROVINCE

Ian Scrimgeour
Johann Raith

Government Printer of the Northern Territory
Darwin, Australia 2001

REPORT 12

NORTHERN TERRITORY DEPARTMENT OF MINES AND ENERGY
MINISTER: Hon Daryl Manzie, MLA
SECRETARY: Peter Blake

NORTHERN TERRITORY GEOLOGICAL SURVEY
DIRECTOR: Dr R Dennis Gee

Scrimgeour I (Ian) and Raith J (Johann)*

Tectonic and thermal events in the northeastern Arunta Province

Darwin: Northern Territory Geological Survey, 2001.
(Report / Northern Territory Geological Survey ISSN 0814-7477; 12)
Bibliography
ISBN 0 7245 7031 4

BIBLIOGRAPHIC REFERENCE: Scrimgeour I and Raith J, 2001. Tectonic and thermal events in the northeastern Arunta Province. *Northern Territory Geological Survey, Report* 12.

KEYWORDS: Geology, Northern Territory, Arunta Province, tectonic events, thermal events, HUCKITTA, geochronology, metamorphism.

551.8099429

Northern Territory Geological Survey
GPO Box 2901
Darwin NT 0801
Web site: http://www.dme.nt.gov.au

* Dr. Johann Raith
Institute of Geosciences
University of Leoben
Peter-Tunner Strasse 5
A-8700 Leoben Austria
Email: raith@unileoben.ac.at

Printed and published for the Northern Territory Geological Survey
by the Government Printer of the Northern Territory

ABSTRACT

The northeastern Arunta Province in JINKA[1] and DNEIPER is comprised of three terranes with distinct protolith ages and tectonothermal histories, separated by major, broadly east trending Palaeozoic shear zones. North of the Delny Shear Zone (DSZ), metasediments of the Deep Bore and Cackleberry Metamorphics have a maximum depositional age of 1805 ± 7 Ma and were intruded by granite at 1780-1710 Ma. Granulite facies rocks of the Deep Bore Metamorphics underwent very low pressure partial melting at conditions of 2.8-4.0 kbar and 750-800°C during the Late Strangways Event at 1730 ± 7 Ma. The Cackleberry Metamorphics underwent low pressure, upper amphibolite facies metamorphism during the same event. Sapphirine-phlogopite schist within the Cackleberry Metamorphics is interpreted as a metamorphosed alteration zone, and represents an unusually low-T sapphirine occurrence. South of the DSZ is the Kanandra Granulite, comprising a sequence of pelite, psammite and mafic granulite with a maximum depositional age of about 1820 Ma. Granulite facies metamorphism at 5-7 kbar and 770-850°C is likely to have occurred at 1730 Ma, and was followed by near-isobaric cooling. The Late Strangways Event is the dominant Palaeoproterozoic event in the eastern Arunta Province, and is interpreted to have resulted in relatively limited crustal thickening, with a mantle-derived heat source, extensive melting of the deep crust and advection of heat by magma to the upper crust.

To the south of the Kanandra Granulite is a sequence of metasediments and mafic rocks of the Harts Range Group. Recent studies of the Harts Range Group suggest that it was deposited in a rift setting in the late Neoproterozoic or Cambrian, and underwent high-grade metamorphism (8-10 kbar, 800°C) in an extensional setting during the Ordovician (480-460 Ma). The northern margin of the Harts Range Group is defined by steeply south-dipping mylonites of the Entire Point Shear Zone (EPSZ) that juxtaposed Harts Range Group against Kanandra Granulite. Upper amphibolite facies reworking of the Kanandra Granulite by EPSZ mylonites occurred at 7 kbar and 700°C. Monazite within the EPSZ crystallised at 445 ± 5 Ma, coincident with the onset of compressional deformation elsewhere in the eastern Arunta Province. The northern Harts Range Group and Kanandra Granulite cooled through 550-500°C by 420-390 Ma.

Further reworking of the Kanandra Granulite occurred in steeply south-dipping, north-vergent mylonites of the 2-4 km wide Delny Shear Zone (DSZ) that decrease in grade from mid-amphibolite facies in the south to greenschist facies in the north. Exhumation related to movement on the DSZ juxtaposed Kanandra Granulite against Deep Bore and Cackleberry Metamorphics. The lowest grade mylonites in the DSZ were active at 365-360 Ma, and the terrane south of the DSZ cooled through 350-420°C by 350 Ma. Ductile deformation had largely ceased in the northeastern Arunta by the end of the Devonian, with no evidence for Carboniferous metamorphism and deformation that occurs elsewhere in the Arunta. The DSZ and EPSZ represent fundamental structures in the Arunta Province that accommodated large scale exhumation at the rear of a south-vergent orogenic wedge between the late Ordovician and the late Devonian.

[1] Names of 1:250 000 and 1:100 000 mapsheets in this report are shown in large and small capital letters respectively, eg HUCKITTA, JINKA.

CONTENTS

APPENDICES

FIGURES

TABLE

INTRODUCTION

The eastern Arunta Province of central Australia is a complex polymetamorphic terrane, with an evolution that extends from the Palaeoproterozoic to the Carboniferous. Until recently, the prevailing model for the evolution of the eastern Arunta Province was that all high-grade (upper amphibolite to granulite facies) metamorphism occurred during the Palaeoproterozoic, with subsequent exhumation of high-grade rocks occurring during the 400-300 Ma intraplate Alice Springs Orogeny, associated with mid-amphibolite to greenschist facies metamorphism (Collins and Shaw 1995).

Recent metamorphic and geochronological studies in the eastern Arunta Province (Mawby *et al* 1999, Hand *et al* 1999a, Buick *et al* in press) have led to a radical re-interpretation of the evolution of the region, with the recognition of a third, previously unrecognized high-grade intraplate event at about 480-460 Ma in the Harts Range region (Figure 1). This new event, termed the Larapinta Event by Hand *et al* (1999b) involved upper amphibolite to granulite facies metamorphism (8-12 kb, 800°C) of the Harts Range Group in an inferred extensional tectonic setting (Hand *et al* 1999a; Mawby *et al* 1999). Furthermore, recent detrital zircon work (Buick *et al* in press) suggests that deposition of the Harts Range Group occurred in the late Neoproterozoic to Cambrian, rather than the Palaeoproterozoic as previously believed. Juxtaposition of Ordovician granulite against the Palaeoproterozoic Strangways Metamorphic Complex to the south occurred along major shallowly dipping thrusts during the onset of compressional deformation at 450 Ma (Mawby *et al* 1999). However, the regional extent of Ordovician tectonism in the Arunta Province, and in particular the degree of reworking of Palaeoproterozoic crust during the Ordovician remains unclear.

The objective of this collaborative study is to examine the poorly understood northern margin of Palaeozoic high-grade metamorphism and deformation in the eastern Arunta Province. The area of study was the Huckitta Station region (Jinka and Dneiper, Figures 1, 2) where a 3-5 km wide zone of complexly reworked Proterozoic granulite separates Ordovician granulites of the Harts Range Group from a granite-dominated terrane that underlies unmetamorphosed Neoproterozoic sediments of the Georgina Basin. This zone of reworking represents the northern margin of the Palaeozoic metamorphic overprint in the eastern Arunta Province, and is of fundamental importance for understanding the tectonics of intraplate deformation in central Australia. This study characterises the nature, metamorphic grade and timing of the Palaeozoic shear zones throughout the region, and determines the timing and metamorphic grade of the Proterozoic high-grade thermal events. This was done in order to construct a revised geological

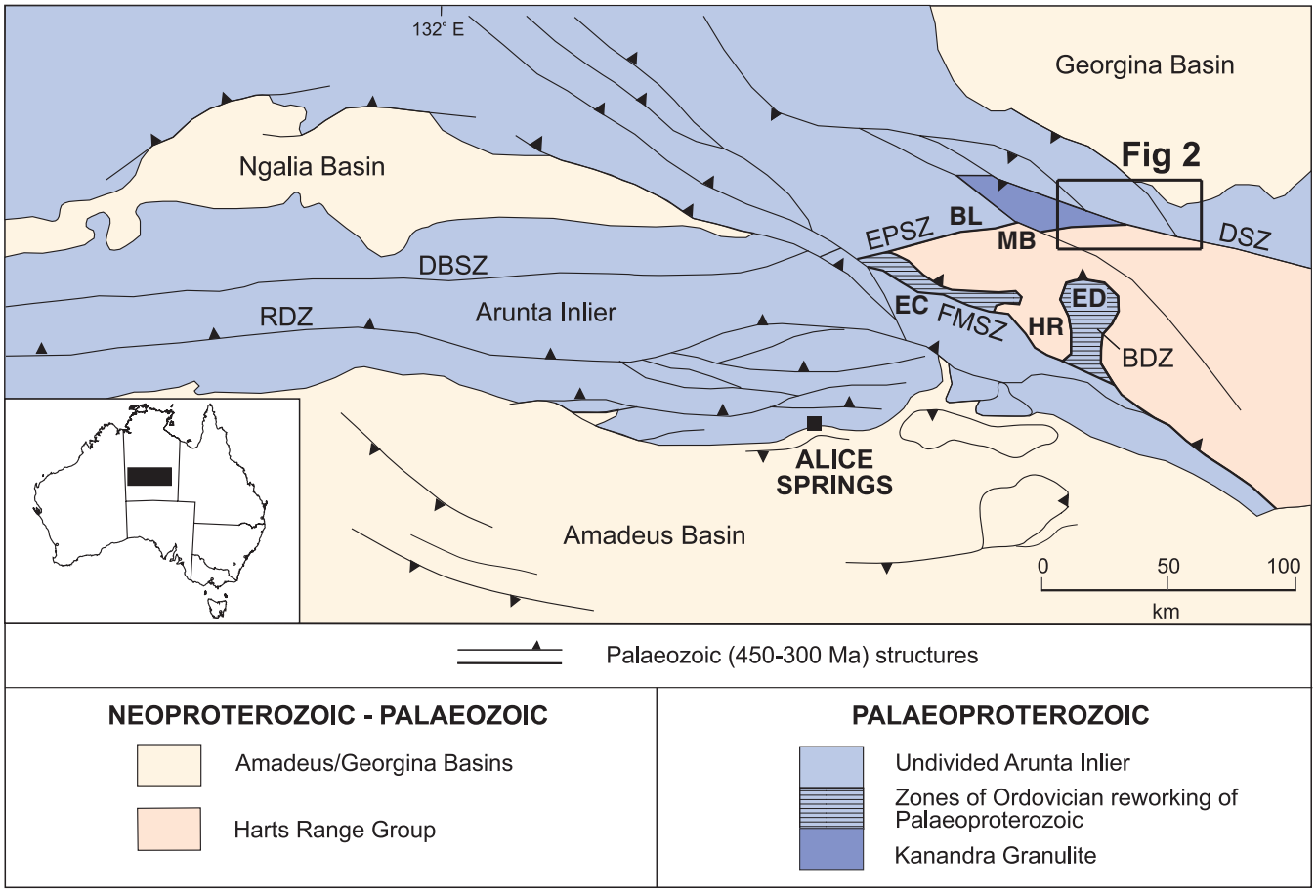

Figure 1 Map of part of the Arunta Province showing major Palaeozoic structures. Zones of documented Ordovician reworking of Proterozoic granulite are from Mawby *et al* (1999) and Hand *et al* (1999a, b). Abbreviations: HR – Harts Range; MB- Mallee Bore; EC – Edwards Creek; ED – Entia Dome; BL – Bleechmore Granulite; DBSZ – Desert Bore Shear Zone; RDZ – Redbank Deformed Zone; FMSZ – Florence-Muller Shear Zone; EPSZ – Entire Point Shear Zone; DSZ – Delny Shear Zone

framework for the Huckitta area and to gain a better understanding of Palaeozoic intraplate tectonics in the Arunta Province.

The map datum used in this study is GDA84, and the Australian Map Grid (AMG) zone is 53. A grid reference shown, for example, as NQ573905, is equivalent to AMG 557300E 7490500N, and can be found on the HUCKITTA 1:250 000 map (Freeman 1986) by referring to the letter codes for the 10 km square grid. All mineral abbreviations used are after Kretz (1983). Sample numbers have the prefix ISHU98, which has been abbreviated in the text to HU. A list of samples utilised in this study is given in Appendix 1. A complete set of representative samples has been retained in the NTGS Core Store, Alice Springs.

elements, separated by major west trending shear systems (Figure 2). The southernmost of these three elements comprises upper amphibolite to granulite facies metasediments belonging the Irindina Supracrustal Assemblage of the Harts Range Group (Shaw *et al* 1984). Dominant lithologies include migmatitic metapelite, metabasite, garnet-biotite gneiss and subordinate calc-silicate rock, marble and quartzite. The lithological associations and metamorphic grade are very similar to rocks of the Irindina Supracrustal Assemblage elsewhere in the eastern Arunta Province. Until recently, the Harts Range Group was believed to have been deposited and metamorphosed during the Palaeoproterozoic (Cooper *et al* 1988). However, it is now recognised that the Harts Range Group underwent peak metamorphism (>800°C, 8-12 kbar) during the Larapinta Event at 480-460 Ma (Mawby *et al* 1999, Hand *et al* 1999*a*,

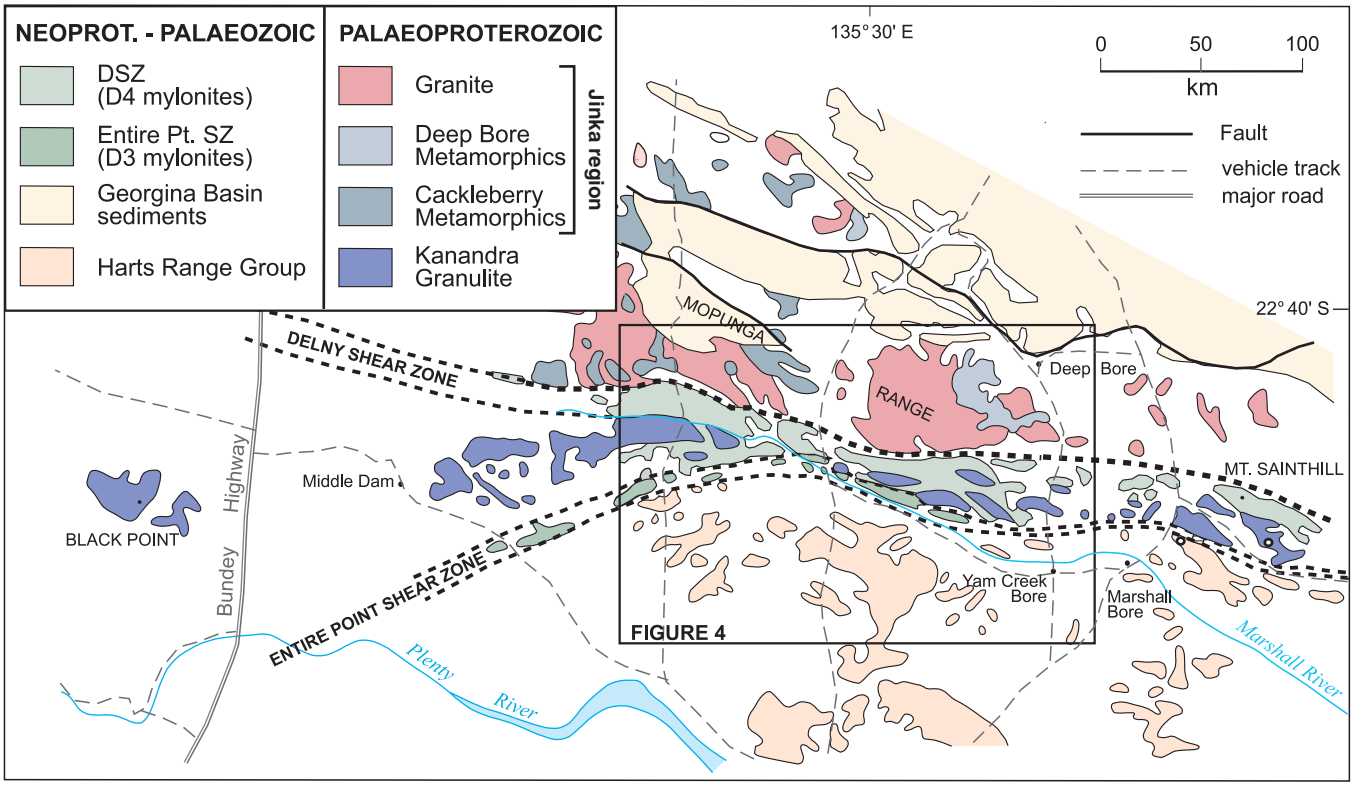

Figure 2 Regional geological map of the Huckitta region of the eastern Arunta Inlier, showing the two major shear zone systems (Entire Point Shear Zone and Delny Shear Zone). The location is given in Figure 1.

GEOLOGICAL SETTING AND PREVIOUS STUDIES

The Huckitta area is situated near the northern margin of the eastern Arunta Province, immediately south of the Neoproterozoic to Palaeozoic Georgina Basin (Figure 1). The Arunta Province has a complex stratigraphic, structural and metamorphic history extending from the Palaeoproterozoic to the Palaeozoic (Collins and Shaw 1995). This tectonic evolution can be broadly divided into a period of multiple high-grade events during the Palaeo- to Mesoproterozoic (1870-1560 Ma, Black and Shaw 1992; Collins and Shaw 1995; Vry *et al* 1996) and a period of intraplate tectonism during the Palaeozoic (500-300 Ma), which is largely concentrated in the southeastern Arunta Province (Dunlap and Teyssier 1995; Hand *et al* 1999*a*).

The Huckitta area can be divided into three main tectonic

Buick *et al* in press). The timing of deposition of the precursor sediments remains poorly constrained, but new detrital zircon data (Buick *et al* in press) suggests that deposition occurred in the late Neoproterozoic to Cambrian, in a probable rift setting. Ordovician high-grade metamorphism is interpreted to have occurred in an extensional environment, due to the apparent deepening of the overlying intracratonic seaway at the time (Mawby *et al* 1999, Hand *et al* 1999).

To the north of the Harts Range Group is the Kanandra Granulite, which belongs to the Palaeoproterozoic Strangways Metamorphic Complex (Shaw and Warren 1975). The Kanandra Granulite forms part of a 150-200 km long, west trending belt of intermittently outcropping pelitic and mafic granulites that includes the Bleechmore Granulite to the west (Figure 1; Shaw and Warren 1975). The Huckitta area occurs near the eastern end of this belt of granulite, where the Kanandra

Granulite is strongly reworked in amphibolite to greenschist facies mylonite zones. The Kanandra Granulite comprises felsic and mafic granulites with garnet-bearing pelitic and semi-pelitic migmatite and rare calc-silicate rock, intruded by deformed granite. Previous studies suggest that it has undergone medium-pressure granulite facies metamorphism (Warren *et al* 1987, Warren and Hensen 1989). The unit has yielded a Rb-Sr whole rock age of 1790 ± 35 Ma (Black *et al* 1983) that was interpreted to reflect the timing of granulite facies metamorphism.

The third major geological element in the Huckitta area, located to the north of the Kanandra Granulite, is informally termed the Jinka region. This comprises a narrow (5-25 km wide) belt of low-pressure amphibolite to granulite facies metasediments intruded by extensive pre-, syn- and post-tectonic granites. It extends from the Perenti Metamorphics (Freeman 1986) in the west to the Jervois Range (Freeman 1986, Cartwright *et al* 1997) in the east, a total distance of more than 100 km (Figure 2). Metasediments of the Deep Bore and Cackleberry Metamorphics occur in the Mopunga Range, in the central part of this terrane. The Jinka region escaped the significant Palaeozoic reworking and exhumation that affected the Kanandra Granulite, and is overlain by Neoproterozoic sediments that only underwent gentle folding at sub-greenschist facies conditions during the Palaeozoic.

The only previous detailed metamorphic studies in the Jinka region were in Jervois Range and Bonya Hills, 80 km east of Mopunga Range, where metamorphism of a sedimentary and volcanic sequence occurred at low-pressure amphibolite facies conditions (2-3 kbar, 520-600°C; Dobos 1978, Cartwright *et al* 1997). The timing of granite intrusion in the Jinka region has been constrained by SHRIMP U-Pb zircon studies (Zhao and Bennett 1995). Two foliated granites, the Jervois and Dneiper Granites, have emplacement ages of 1771 ± 6 Ma and 1771 ± 15 Ma, respectively, while the post-tectonic Mount Swan Granite has an age of 1713 ± 7 Ma. In the Jervois region, Cartwright *et al* (1997) obtained Pb-Pb and Sm-Nd ages of 1750 ± 19 and 1720 ± 20 Ma, respectively, for garnet interpreted to have grown during fluid flow that was associated with pegmatite intrusion soon after the metamorphic peak.

Two major shear zones separate the three tectonic elements in this region: the Entire Point Shear Zone, which separates the Harts Range Group from the Kanandra Granulite, and the Delny Shear Zone (DSZ), which separates the Kanandra Granulite from the Jinka region (Figure 2). The more simple term Delny Shear Zone is now used for the mylonite zone that was originally defined as the Delny-Mt Sainthill Shear Zone by Warren (1978). The Entire Point Shear Zone (EPSZ; formerly the Entire Point Fault; Shaw *et al* 1984, Collins and Teyssier 1989; Figures 1, 2), trends east-northeast, dips steeply south, and merges with the east-southeast striking Delny Shear Zone in the Huckitta area. The metamorphic grade of this zone is upper amphibolite facies (Shaw *et al* 1984, Kelsey 1998), and it has a largely strike-slip (sinistral) sense of movement (Collins and Teyssier 1989).

The Delny Shear Zone (Figures 1, 2), is a major east-southeast striking structure separating the Kanandra Granulite from the Jinka province and Georgina Basin. It is more than 150 km in length (Warren 1978), and is locally up to 3 km wide. A substantial gravity gradient is evident across the DSZ (Figure 3), implying that it is a major crustal feature. The DSZ comprises anastomosing, steeply south dipping, mid-amphibolite to greenschist facies mylonite zones (Shaw *et al* 1984). Warren (1978) considered the DSZ to be largely Proterozoic in age with a north-up sense of movement, but more recent studies (Collins and Teyssier 1989, Kelsey 1998) have concluded that significant movement on the DSZ was associated with the mid-Palaeozoic Alice Springs Orogeny, with south-up reverse movement. No chronological data exists for the Alice Springs Orogeny on HUCKITTA, but extensive Ar-Ar, K-Ar and Rb-Sr data from elsewhere in the Arunta Province suggest that it was a prolonged compressional event spanning the Devonian and Carboniferous (400-300 Ma; Dunlap and Teyssier 1995, Cartwright *et al* 1999).

LITHOLOGY, STRUCTURE AND METAMORPHISM

Kanandra Granulite

Field observations

In the Huckitta area (Figure 4), the Kanandra Granulite comprises pelitic granulite, mafic granulite, garnet-biotite migmatite, garnet leucogranite and biotite granite, with rare calc-silicates and small ultramafic bodies. Preserved granulite facies assemblages occur within large relics (0.01 to 1.5 km in width) between extensive anastomosing mylonites related to the DSZ and EPSZ. West of the Huckitta region, in the vicinity of Black Point (Figure 2), there are widespread but poorly exposed granulites that occur between the mylonites of the EPSZ to the south and the DSZ to the north.

The structural and metamorphic evolution of the Kanandra Granulite is represented by four phases on the basis of structural style, metamorphic grade and overprinting relationships ($D_{1\text{-}4}$ /$M_{1\text{-}4}$). However, each of these phases is more complex than a single fabric-forming event, particularly where the rocks are inferred to have undergone progressive mylonitic deformation. The distribution of lithologies and zones of reworking within the Kanandra Granulite are shown in Figure 4, along with stereonets summarizing the structural data relevant to the four events.

$D_{1\text{-}2}$ - granulite facies gneiss

Granulite facies gneiss comprising metasedimentary migmatite interlayered with mafic granulite have been intruded by garnet leucogranite, and post-D_1 biotite granite. The migmatitic gneiss can be subdivided into three groups:

(1) Relatively homogeneous garnet-biotite ± sillimanite migmatite (Figure 5) in which leucosomes contain coarse garnet. Sillimanite occurs locally but is typically restricted to biotite-rich selvages around leucosomes;

(2) Compositionally heterogeneous migmatite, dominated by garnet-sillimanite-biotite ± cordierite ± spinel metapelite with garnet-bearing leucosomes, psammitic layers and rare calc-silicate horizons; and

(3) A less common third lithology comprising biotite ± hornblende-bearing felsic migmatite that occurs at NQ551839. This lithology is likely to have had an igneous precursor.

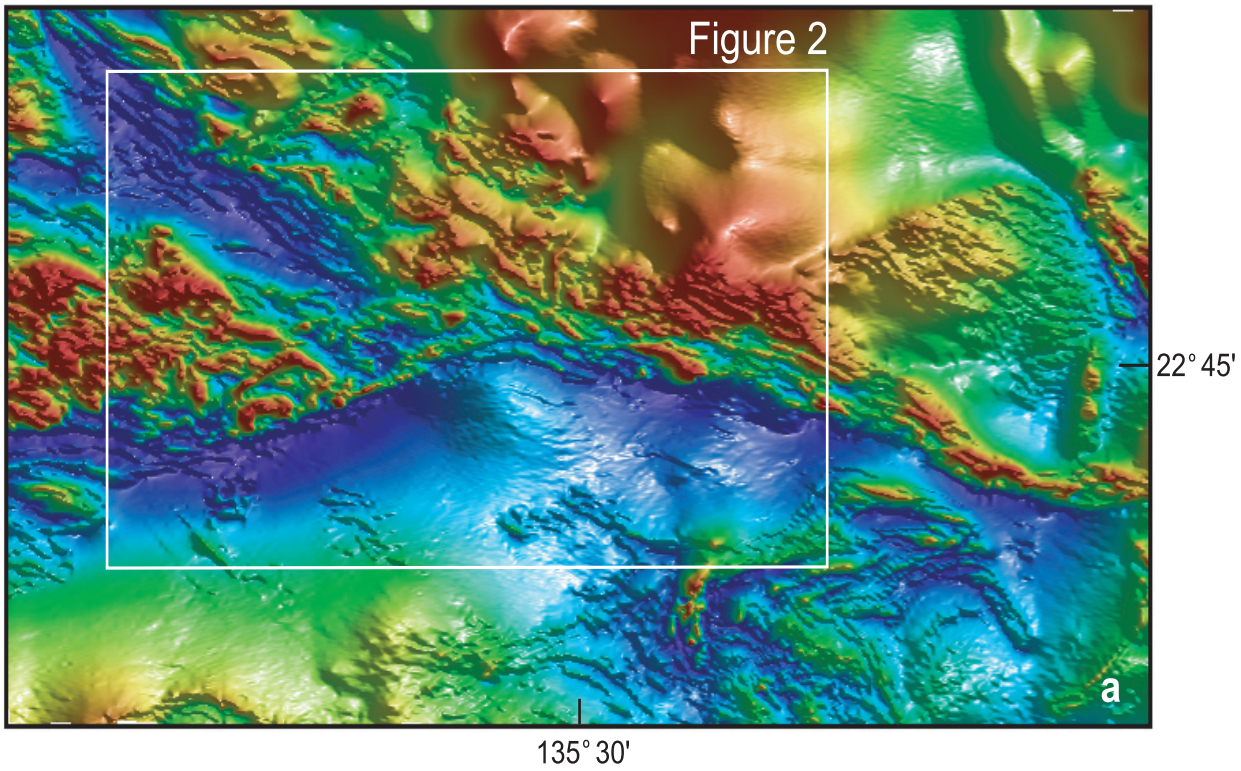

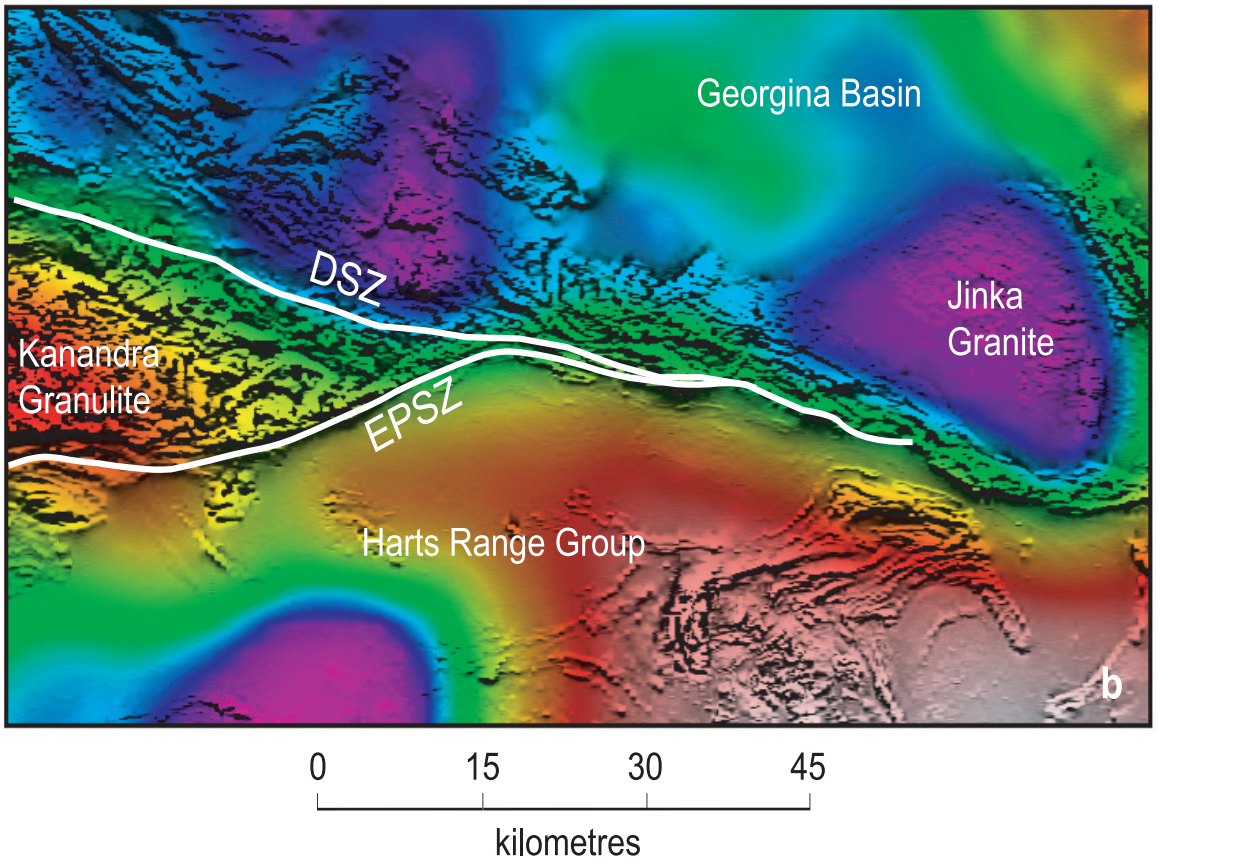

Figure 3 (a) Pseudocolour image of Bouguer gravity calculated using a density of 2.67 tm^{-3}, overlaid on greyscale first vertical derivative of total magnetic intensity. Gravity data acquired by AGSO. Location of area shown in Figure 2 is indicated; **(b)** Pseudocolour image of total magnetic intensity with synthetic sun illumination from the northeast

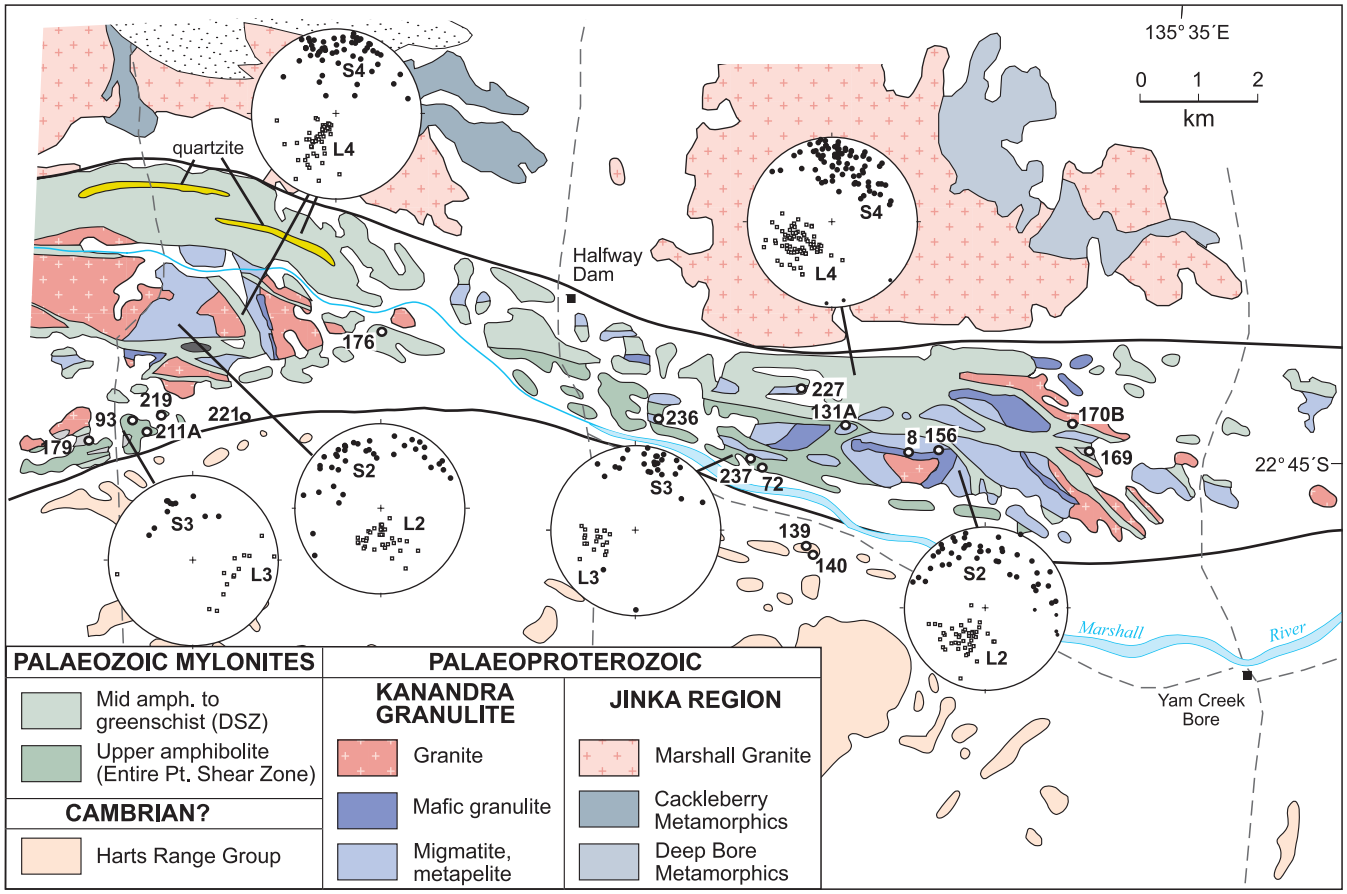

Figure 4 Map of the Kanandra Granulite in the Huckitta area, reworked by D_3 and D_4 shear zones. Bold lines represent the inferred margins of the Kanandra Granulite. Stereonets summarise the structural data for D_2-D_4 in the Kanandra Granulite, for structural domains to the east and west of Halfway Dam. Numbered localities refer to sample numbers referred to in the text and appendices (prefix ISHU98)

In addition to the migmatites two-pyroxene mafic granulite with orthopyroxene-bearing leucosomes occurs as layers and boudins up to 200 m wide within the migmatite. Rare, small ultramafic intrusions occur in the vicinity of NQ531843, and have largely recrystallised to tremolite and diopside.

Pelitic and semi-pelitic migmatites preserve an S_1 fabric, which is defined by parallel leucosomes and locally, by coarse oriented biotite and sillimanite or elongate aggregates of garnet, spinel and biotite. An early generation of leucosome is locally isoclinally folded and truncated by axial planar leucosomes. Leucosomes locally accumulate to form bodies of garnet leucogranite, up to tens of metres in width, which truncate S_1. The early surface S_0 is defined by psammitic layers within metapelite and is typically parallel to S_1. Granulite is intruded by extensive post-D_1, pre-D_2 biotite granite that locally contains garnet.

S_1 is overprinted by, and locally transposed into a planar high strain fabric of variable intensity (S_2; Figure 6), which is characterized by a well developed, south-plunging, quartz stretching lineation (L_2). In metapelite, this lineation is also defined by sillimanite, which forms part of a biotite-sillimanite fabric that envelops M_1 garnet. In zones of high D_2 strain, most leucosomes within metapelite are strongly deformed and transposed into S_2, although rare late melts are axial planar to F_2 folds, or truncate S_2 at low angles. Mafic granulites have recrystallised in S_2 to assemblages that contain two pyroxenes and hornblende. The S_2 fabric is folded openly along south plunging fold axes, and generally dips steeply southeast or southwest, with lineations plunging 170-220°. In some localities, S_2 is strongly mylonitic, but can generally be distinguished from subsequent mylonites by granulite facies assemblages in mafic rocks and localized occurrences of small leucosomes truncating the fabric in metapelite.

D_3 - upper amphibolite facies mylonites (Entire Point Shear Zone)

The Kanandra Granulite has been reworked within the EPSZ by mylonites (D_3) that formed at upper amphibolite facies conditions. These mylonites extend 2 km into the Kanandra Granulite, where they form an anastomosing network of shear zones 0.1-100 m in width. Pelite has recrystallised in D_3 mylonites to biotite-sillimanite-garnet assemblages and mafic lithologies have recrystallised to hornblende amphibolite that locally contain garnet. Sillimanite is fine grained and elongated in the lineation, whereas garnet forms larger porphyroclasts and less abundant, small subhedral grains. Calc-silicate layers within D_3 mylonites contain the assemblage diopside-quartz-calcite-scapolite-titanite ± anorthite.

West of Halfway Dam (Figure 4), the dominant mylonitic fabric (S_{3b}) trends in a west-southwesterly orientation. Mineral lineations (L_{3b}), defined by sillimanite in metapelite and quartz elongation in felsic rocks, range from near horizontal to moderately east or east-southeast plunging, on a plane which dips steeply towards 150-160°. Kinematic indicators consistently suggest a sinistral sense of strike-slip movement. East of Halfway Dam, the orientation of S_{3b} changes to become

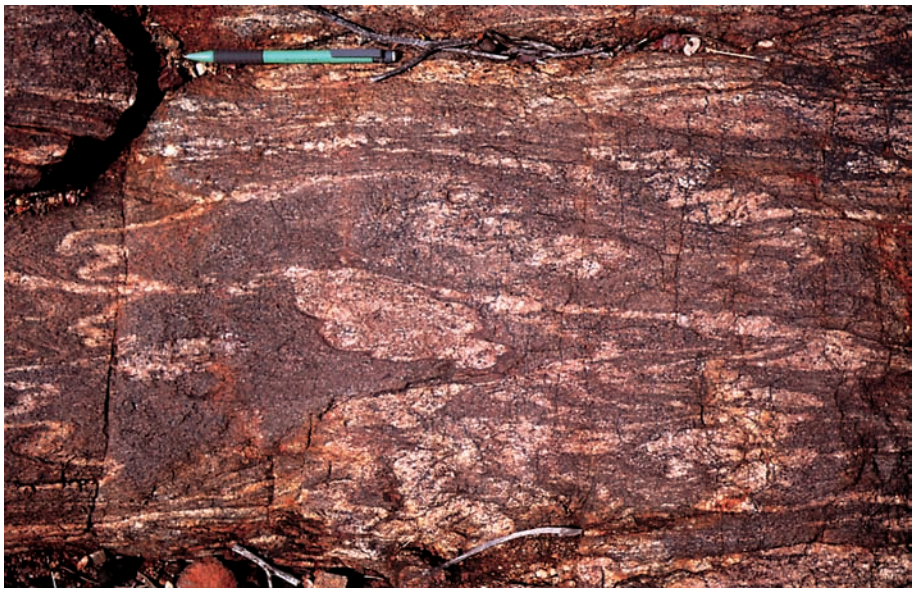

Figure 5 Typical migmatitic pelite in Kanandra Granulite with folded garnet-bearing leucosomes

Figure 6 Pelitic rock with S_2 fabric in Kanandra Granulite. This rock was sampled for shrimp U-Pb geochronology (HU195)

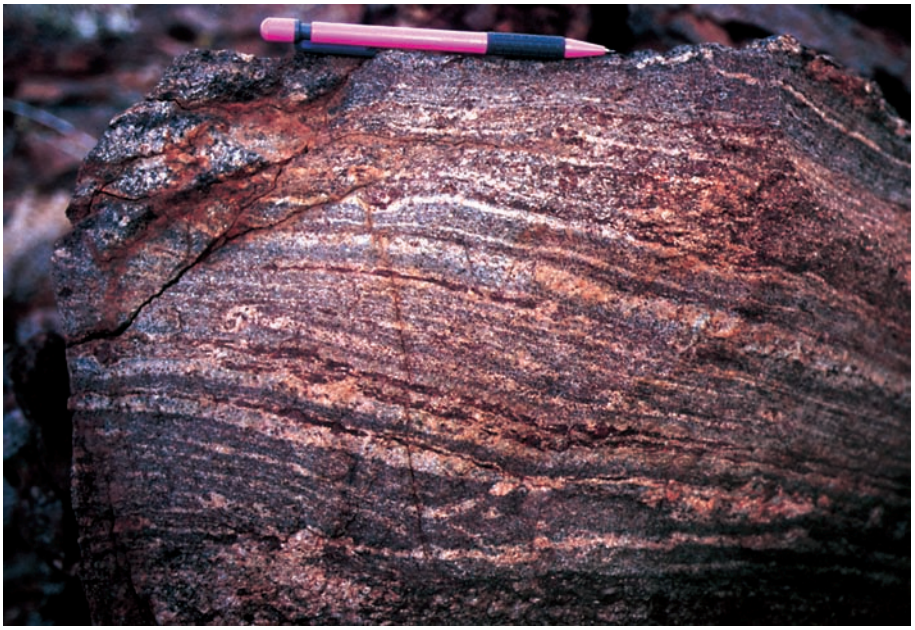

steeply south-southwest dipping, with a moderately west to west-southwest plunging lineation and kinematic indicators suggest sinistral-reverse oblique movement. In this region the northern margin of D_{3b} mylonitisation is unclear, as the D_{3b} mylonites are extensively reworked by subsequent, lower grade D_4 mylonites.

Less commonly, mafic rocks preserve a locally developed, steeply south dipping fabric with a south to southeast plunging mineral lineation, which contains garnet-hornblende-plagioclase-quartz assemblages. This fabric is best preserved within large boudins in the EPSZ, and is designated S_{3a}. It clearly postdates S_{1-2} granulite fabrics, but is strongly reworked by S_{3b} mylonites, which recrystallised the rock to finer grained garnet-hornblende assemblages. Geothermobarometry also suggests that S_{3a} and S_{3b} formed at different P-T conditions (see below).

D_4 - mid-amphibolite to greenschist facies mylonites (DSZ)

The Kanandra Granulite and D_3 high-grade mylonites have been substantially reworked in lower grade amphibolite to greenschist facies mylonite zones (D_4). The metamorphic grade in these mylonite zones decreases from mid amphibolite (biotite-muscovite ± sillimanite, staurolite or garnet in pelitic rocks) in the south to greenschist (chlorite-muscovite) in the north. These mylonites form the Delny Shear Zone (DSZ), and the intensity of D_4 deformation increases towards the north, where they form a zone of pervasive mylonitisation and retrogression approximately 1 000 m in width. In the northern parts of the DSZ, relict gneiss in low strain zones has undergone extensive hydrous retrogression to chlorite and muscovite. Mylonitic fabrics dip steeply south to southwest and mineral lineations plunge variably southwest. These mylonites have abundant kinematic indicators, particularly S-C fabrics, which show a consistent southwest over northeast (reverse) sense of movement. Zones of mylonitized quartzite of an uncertain origin are intercalated with strongly mylonitized and retrogressed granulite and granite within the northern DSZ to the west of Halfway Dam (Figure 4) and form quartz-muscovite schist and phyllite. The northern margin of the DSZ is defined by a 50 m wide zone of poor outcrop with abundant vein quartz and this is bounded to the north by granite of the Jinka region.

Petrology of pelites and mafic rocks

Cordierite-absent pelitic granulite

In most pelitic migmatite in the Kanandra Granulite, the peak metamorphic (M_1) assemblage comprises garnet, biotite, sillimanite, ilmenite, quartz, K-feldspar and plagioclase. M_1 garnet is typically elongated in S_1, and contains inclusions of biotite, sillimanite, quartz and ilmenite, with or without spinel. Within the matrix, S_1 is defined by the alignment of coarse sillimanite and biotite. Sillimanite locally contains inclusions of spinel. This fabric generally deflects around garnet, although sillimanite and biotite inclusion trails within garnet locally continue directly into the fabric in the matrix. Within leucosomes, M_1 garnet is typically equant and poikilitic, and has numerous quartz inclusions.

The M_1 assemblage has been overprinted by a biotite-sillimanite S_2 fabric of variable intensity. In rocks in which S_2 is weakly developed, fine-grained M_2 biotite and sillimanite occur along feldspar grain boundaries and also overgrow coarser M_1 sillimanite and biotite. M_1 sillimanite locally contains narrow fractures perpendicular to S_2, which are infilled with spinel-biotite-ilmenite ± corundum. These spinel-bearing intergrowths only occur in sillimanite-rich zones and are never in contact with quartz. Fractures in M_1 garnet contain M_2 biotite with minor sillimanite ± spinel. Where S_2 deformation is more intense, a biotite-sillimanite ± ilmenite fabric envelops and overgrows M_1 garnet, sillimanite and biotite, and M_1 garnet is significantly fractured and corroded and replaced by M_2 biotite ± sillimanite. Spinel is absent from more highly strained rocks. Within biotite-rich rocks, small subhedral garnet with fine-grained sillimanite inclusions occurs in the S_2 fabric and locally overgrows M_1 garnet.

Cordierite-bearing pelitic granulite

Peak (M_1) assemblages in cordierite-bearing rocks contain garnet porphyroblasts with inclusions of sillimanite, biotite, quartz, rutile and ilmenite, and coarse sillimanite, that variably defines the S_1 fabric and has inclusions of hercynitic spinel, ilmenite and rutile. In addition, the M_1 assemblage contains coarse granoblastic cordierite, quartz, K-feldspar and plagioclase. M_1 garnet, cordierite and sillimanite are overprinted by a fine grained M_2 biotite-sillimanite assemblage associated with the mylonitic S_2 fabric. M_1 garnet is locally fractured perpendicular to S_2, and these fractures are infilled by biotite. Cordierite, quartz and feldspar have recrystallised at grain boundaries associated with the growth of M_2 biotite and sillimanite. M_1 garnet and sillimanite are enveloped and corroded by fine grained intergrown biotite and M_2 sillimanite, with less abundant ilmenite and rutile. M_1 garnet locally has overgrowths of symplectitic garnet-quartz, whereas elsewhere it is overgrown by euhedral garnet with inclusions of fibrous sillimanite. This secondary garnet growth locally occurs at contacts between M_1 garnet and M_2 biotite-sillimanite. Small euhedral garnets with fine-grained sillimanite inclusions also occur in S_2.

D_3 pelitic mylonites

Within metapelites, the mineral assemblage associated with S_{3b} is garnet-biotite-sillimanite-K-feldspar-quartz-plagioclase-ilmenite ± muscovite. Fine grained biotite and sillimanite define the S_{3b} fabric and L_{3b} lineation. Porphyroclasts of M_1 garnet, sillimanite, quartz and feldspar are commonly present, and in general the porphyroclastic garnet is rounded (but not corroded), while M_1 sillimanite is partially corroded at contacts with biotite. In many D_{3b} mylonites, small euhedral garnet occurs in the S_{3b} biotite-sillimanite fabric (Figure 7). M_{3b} garnet contains rare inclusions of quartz, biotite and sillimanite. In less common bulk compositions, muscovite also occurs in S_{3b}, particularly in the vicinity of K-feldspar porphyroclasts.

D_4 pelitic mylonites

The mineral assemblage in most S_4 pelitic mylonites is dominated by biotite-muscovite-quartz-plagioclase-ilmenite, with or without sillimanite, garnet or staurolite. Less commonly, muscovite-absent garnet-biotite or sillimanite-biotite mylonites occur. Garnet and sillimanite are never stable together in S_4. Sillimanite-bearing mylonites typically contain coarse porphyroclastic sillimanite as well as finer grained sillimanite, which defines the S_4 fabric with biotite ± muscovite. Garnet-

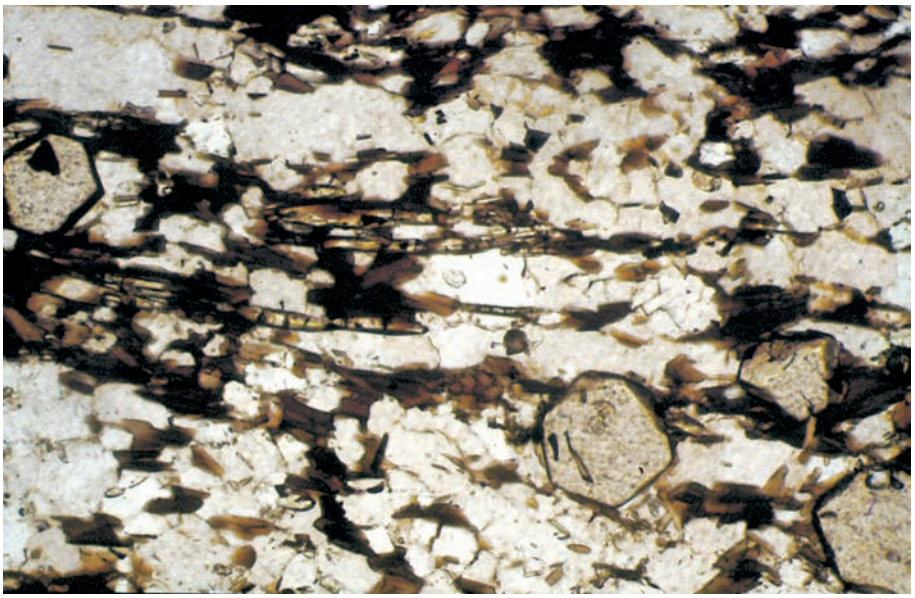

Figure 7 M_{3b} pelitic mylonite (ISHU98.227) showing euhedral garnet in the mylonitic fabric, which is defined by biotite and fine grained sillimanite. Colourless minerals are quartz, K-feldspar and plagioclase. Width of field of view is 2 mm. Plane-polarised light

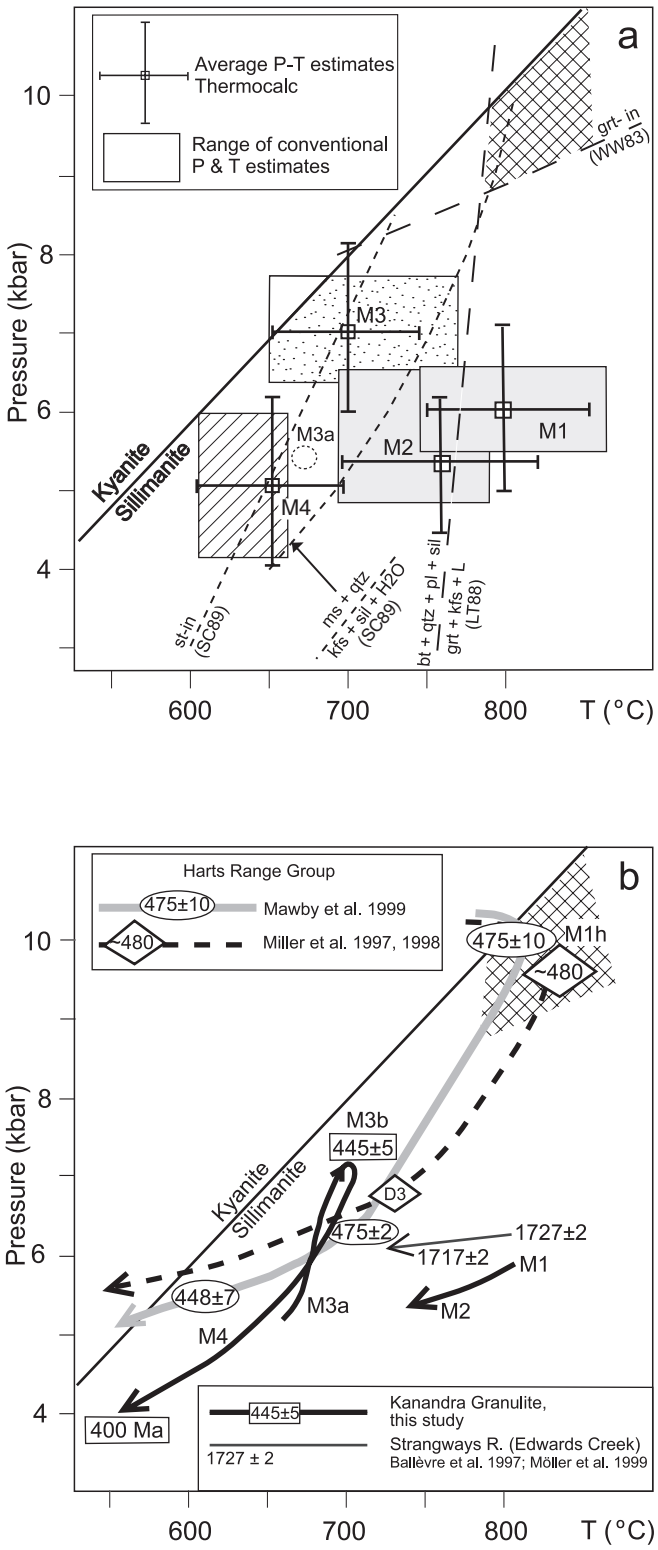

Figure 8 (**a**) Summary of P-T constraints for the Kanandra Granulite. Error bars represent 2σ uncertainties on combined average Thermocalc P-T estimates, except for M_4, which shows a 1σ uncertainty for a single estimate. Boxed fields represent estimates from conventional thermobarometry. The dashed circle represents the P-T estimate for M_{3a} (± ~100°C and 1.5-2 kbar). Short dashed lines represent the approximate upper stability limits of staurolite and muscovite in the KFMASH system (SC89 - Spear and Cheney 1989). Cross-hatched area represents the approximate P-T conditions of the Harts Range Group, based on experimentally determined melting reactions for appropriate compositions (Le Breton and Thompson 1988, Wyllie and Wolf 1993); **(b)** Proposed P-T paths for the two events in the Kanandra Granulite with age constraints, in comparison to P-T paths and age constraints for Strangways Complex granulites at Edwards Creek (Möller *et al* 1999), and the Harts Range Group at Mallee Bore (Miller *et al* 1997, 1998) and the Harts Range (Mawby *et al* 1999). 'D_3' on the Mallee Bore P-T path represents the P-T conditions of D_3 mylonitisation at Mallee Bore (Miller *et al* 1997). Discussion in text

bearing mylonites contain small euhedral garnet that occur in the fabric with biotite ± muscovite, and less abundant porphyroclastic garnet and locally preserved, corroded porphyroclastic sillimanite. Staurolite-bearing mylonites contain an assemblage of staurolite, muscovite, biotite, quartz, and ilmenite that define a strong mylonitic fabric with well developed S-C fabrics. Further north within the Delny Shear Zone, D_4 pelitic mylonites contain muscovite-biotite-chlorite-quartz assemblages and less deformed granulite relics have chlorite-muscovite pseudomorphs after garnet.

Mafic rocks

The peak (M_1) assemblage in mafic granulite comprises granoblastic orthopyroxene, clinopyroxene, hornblende and plagioclase, with minor ilmenite ± biotite ± quartz. Where mafic rocks have recrystallised in the S_2 fabric, the assemblage remains the same, but with a higher modal proportion of hornblende relative to pyroxene. In the S_{3a} fabric, mafic rocks have recrystallised to a garnet-hornblende-plagioclase-quartz-ilmenite ± rutile assemblage. In general the texture is granoblastic, although hornblende shows a variable degree of preferred orientation in the S_{3a} fabric. Garnet has abundant inclusions of hornblende, plagioclase, ilmenite and quartz. The coarse S_{3a} assemblage is partially recrystallised to a finer grained garnet-hornblende-plagioclase-ilmenite-quartz assemblage associated with mylonitic S_{3b} deformation. However, some S_{3b} mylonites contain garnet-absent hornblende amphibolite. S_4 mylonites contain equigranular hornblende-plagioclase-ilmenite ± quartz assemblages, grading into lower grade epidote-bearing assemblages in the northern DSZ.

P-T-t evolution of the Kanandra Granulite

M_1 event

A sample of cordierite metapelite (HU131A) and three samples of garnet-biotite-sillimanite pelites (HU57A, 168 and 236) were selected for thermobarometric calculations of M_1 in the Kanandra Granulite. The results are summarized in Figure 8 (a) and Appendix 3. Garnet-biotite thermometry on core analyses using the calibration of Hodges and Spear (1982) gives temperatures of 696-866°C with averaged temperature estimates for each sample ranging between 782 and 829°C. Pressure estimates using conventional barometers are typically between 5.2 and 6.6 kbar for a reference temperature of 800°C. Average P-T conditions using Thermocalc (Powell and Holland 1988, Holland and Powell 1998) yield relatively consistent results between samples which give a combined average P-T estimate of 793 ± 53°C and 5.9 ± 1.5 kbar (2σ error) for an aH_2O of 0.35. Due to the dependence of these estimates on biotite- and cordierite-bearing equilibria, the selected water activity has a significant influence on the results. For example, an aH_2O of 0.5 typically results in estimates approximately 50°C and 0.5 kbar higher, while an aH_2O of 0.1 results in unrealistic temperatures of <700°C.

Additional constraints on the peak M_1 conditions of the Kanandra Granulite are given by the presence of extensive garnet-bearing melts produced in metapelite during M_1. These are interpreted to have resulted from the biotite dehydration reaction:

biotite + quartz + plagioclase + sillimanite = garnet + K-feldspar + melt

Experimental studies by Le Breton and Thompson (1988) showed that this melting reaction is likely to commence at about 760-770°C for pressures of 6 kbar, thus giving a lower constraint on peak temperatures. The degree of melting and the formation of locally derived bodies of garnet leucogranite suggest that temperatures may have significantly exceeded this minimum value. In summary, the results of thermobarometry suggest that P-T conditions during M_1 in the Kanandra Granulite were 770-850°C and 5-7 kbar.

M_2 event

Thermobarometry relating to the development of the S_2 fabric in Kanandra Granulite was undertaken on two samples that contained the M_2 assemblage garnet-biotite-sillimanite-plagioclase-quartz-K-feldspar (HU131A, 179). Garnet-biotite thermometry using the Hodges and Spear (1982) calibration gives 692-792°C. The GASP barometer of Hodges and Crowley (1985) and Grt-Bt-Pl-Qtz barometer of Hoisch (1990) give 5.7-6.5 kbar for a reference temperature of 750°C for sample HU131A, and ~1 kbar lower for sample 179. Thermocalc estimates for aH_2O of 0.35 suggest P-T conditions of 753 ± 40°C and 5.4 ± 0.7 kbar for HU131A, and 760 ± 51°C and 4.9 ± 0.5 kbar for HU179 (1σ errors). In summary, M_2 temperatures are likely to have been about 50°C lower than M_1, at similar or slightly lower pressures.

P-T conditions and aH_2O of the Entire Point Shear Zone

Three metapelitic samples from the EPSZ yield consistent pressure-temperature estimates for the assemblage garnet-biotite-sillimanite-quartz-plagioclase-K-feldspar ± muscovite. The Hodges and Spear (1982) garnet-biotite thermometer gives 640-763°C for a pressure of 7 kbar, averaging between 680-700°C, whereas the garnet-phengite barometer of Green and Hellman (1982) gives temperatures ranging from 672-786°C. For temperatures of 700°C, the GASP barometer of Hodges and Crowley (1985) gives pressures between 6.4-7.6 kbar, and five other pelite barometers give results within the same range (Appendix 3). One muscovite-absent sample (HU93A) gives slightly lower temperatures of 619-725°C, and pressures of 6.1-6.6 kbar. A combination of average P-T estimates using Thermocalc for all four samples, plus one sample of a D_{3h} mylonite from the Harts Range Group (HU23) yields 692 ± 37°C and 6.8 ± 1.1 kbar (2σ errors) for water activity of 0.35 (see discussion below). Together, these data suggest that conditions during mylonitic deformation on the Entire Point Shear Zone were 670-720°C and 6.5-7.3 kbar. These pressures are 1-2 kbar higher than during granulite metamorphism.

Garnet-bearing recrystallised mafic rocks yield estimates that are less well constrained than those from the metapelite. However, the existence of two generations of garnet, hornblende, plagioclase and quartz in many mafic rocks provides constraints on the P-T trajectory during M_{3b}, as M_{3a} assemblages predate the mylonitic M_{3b} assemblage. For three samples containing the granoblastic M_{3a} assemblage, application of the garnet-hornblende thermometer of Graham and Powell (1982) gives estimates in the range 620-659°C, while the garnet-hornblende-plagioclase-quartz tschermakite barometer of Kohn and Spear (1990) gives 5.6-7.0 kbar for the Fe end-member, and 4.1-5.3 kbar for the Mg end-member. Application of these thermobarometers to samples containing the overprinting M_{3b} mylonitic garnet-hornblende-plagioclase assemblage (HU211A, 219) yields 580-701°C, and 6.1-8.6 kbar for the Fe end-member and 5.2-7.9 kbar for the Mg end-member. Although these estimates are relatively imprecise, they suggest that the mylonitic M_{3b} assemblage formed at higher pressures (and probably slightly higher temperatures) than the earlier, coarse grained M_{3a} assemblage. In particular, application of identical thermobarometers to the M_{3a} and M_{3b} assemblages within the one rock (211A) suggest a pressure increase of approximately 1-2 kbar from M_{3a} to M_{3b}. This inferred early up-pressure history leads to an unusual apparent P-T path for the Kanandra Granulite during the Ordovician, with an increase in pressure after the terrane was already at elevated temperatures (Figure 8b).

Numerous lines of evidence suggest that D_{3b} mylonitisation occurred at low aH_2O. Fluid independent barometers and thermometers consistently suggest conditions of 670-730°C and 6.4-7.6 kbar. Comparison of these estimates with averages for varying aH_2O using Thermocalc suggest aH_2O in the range 0.3-0.5 during D_3 mylonitisation. Higher water activities give temperatures of 750-850°C, which would preclude the stability of muscovite and thus appear unrealistic, while aH_2O of <0.3 results in estimates that are in the kyanite stability field. Additional evidence for aH_2O of <1.0 during D_3 is the abundance of calcite and scapolite, and absence of garnet or wollastonite in M_3 calc-silicate rocks at about 700°C, suggesting aCO_2 of > ~0.25 (Fitzsimons and Harley 1994). Furthermore, comparison with experimentally derived melting curves for granitic bulk compositions (Bohlen *et al* 1982) suggest that the lack of migmatisation of felsic lithologies subjected to 700°C during D_3 is consistent with aH_2O <0.5.

P-T conditions in the Delny Shear Zone

Due to a scarcity of garnet-bearing assemblages in M_4 mylonites, quantitative P-T estimates were only performed on one sample (HU170B), which contained garnet-biotite-muscovite-quartz-plagioclase, with rare ilmenite and K-feldspar. The garnet-biotite thermometer of Hodges and Spear (1982) and garnet-phengite thermometer of Green and Hellman (1982) both give temperatures between 607-660°C. Various pelite barometers of Hodges and Crowley (1985) and Hoisch (1990) give pressures between 3.3 and 6.0 kbar, but most typically between 4.0 and 5.5 kbar (Appendix 3). Average P-T estimates on this assemblage using Thermocalc are 653 ± 34°C and 5.1 ± 1.3 kbar for aH_2O of 1.0, and 631 ± 33°C and 4.9 ± 1.2 kbar for aH_2O of 0.8. Temperatures of 600-650°C at 5 kbar are consistent with the stability of the assemblages staurolite-muscovite-biotite-quartz (HU176) and sillimanite-biotite-muscovite-quartz (HU174) in differing bulk compositions in the KFMASH system (eg Xu *et al* 1994). These estimates reflect mid-amphibolite P-T conditions for the highest-grade mylonites in the DSZ, but chlorite- and epidote-bearing assemblages and quartz-chlorite-muscovite phyllites in the northern DSZ reflect a decrease in grade to lower

amphibolite and greenschist facies to the north. The hydrous nature of M_4 assemblages suggests that H_2O-rich fluid was present during metamorphism.

Deep Bore Metamorphics

Field observations

The Deep Bore Metamorphics (Shaw *et al* 1984) outcrop north of the DSZ (Figure 9), and comprise granulite facies metapelite with less abundant aluminous metapsammite, calc-silicate rock and mafic granulite. They outcrop poorly on rounded, spinifex covered hills and are generally deeply weathered. However, localised fresh outcrops of granulite are present (eg NQ573905).

The Deep Bore Metamorphics are intruded by the Marshall Granite, a weakly foliated to massive hornblende granite that was emplaced after granulite facies metamorphism. Creek outcrop at NQ569898 contains xenoliths of granulite within medium grained, undeformed Marshall Granite. A body of quartz norite, 250 m in diameter, also intrudes the Deep Bore Metamorphics, and contains metamorphic hornblende and epidote close to its margins with the Marshall Granite (Shaw *et al* 1984). The norite is interpreted to have intruded after granulite metamorphism but prior to intrusion of the Marshall Granite (Shaw *et al* 1984). Undeformed and unmetamorphosed dolerite dykes, including a west trending dyke at NQ557138 also intrude the granulite.

Paragneiss in the Deep Bore Metamorphics is typically cordierite-rich and forms rounded silicified outcrops. The most abundant lithologies are cordierite-biotite semi-pelitic gneiss, which locally contains sillimanite, orthopyroxene and/or spinel, and quartz-rich garnet-cordierite-biotite ± orthopyroxene metapsammite. The semi-pelitic gneiss is variably migmatitic and has cordierite porphyroblasts that occur within commonly discontinuous, leucocratic segregations (eg NQ565902, Figure 10). These porphyroblastic gneisses vary from being relatively undeformed to containing a gneissic layering, in which leucosome patches are strung out in the fabric with strongly elongated porphyroblasts.

Less abundant metapelitic migmatite also occurs in the Deep Bore Metamorphics, and is best exposed in southern outcrops at localities NQ586883 and NQ598880. It contains 30-60% K-feldspar rich leucosome, interlayered with a silica-undersaturated sillimanite-cordierite-spinel rich melanosome. These aluminous layers locally form schlieren migmatite (McLennan 1983), in which the melanosome forms discontinuous lenses and layers within the leucosome (Figure 11). The boundary between schlieren migmatite and adjacent quartz-rich, leucosome-poor semi-pelite and psammite is abrupt and reflects the preservation of S_0 compositional

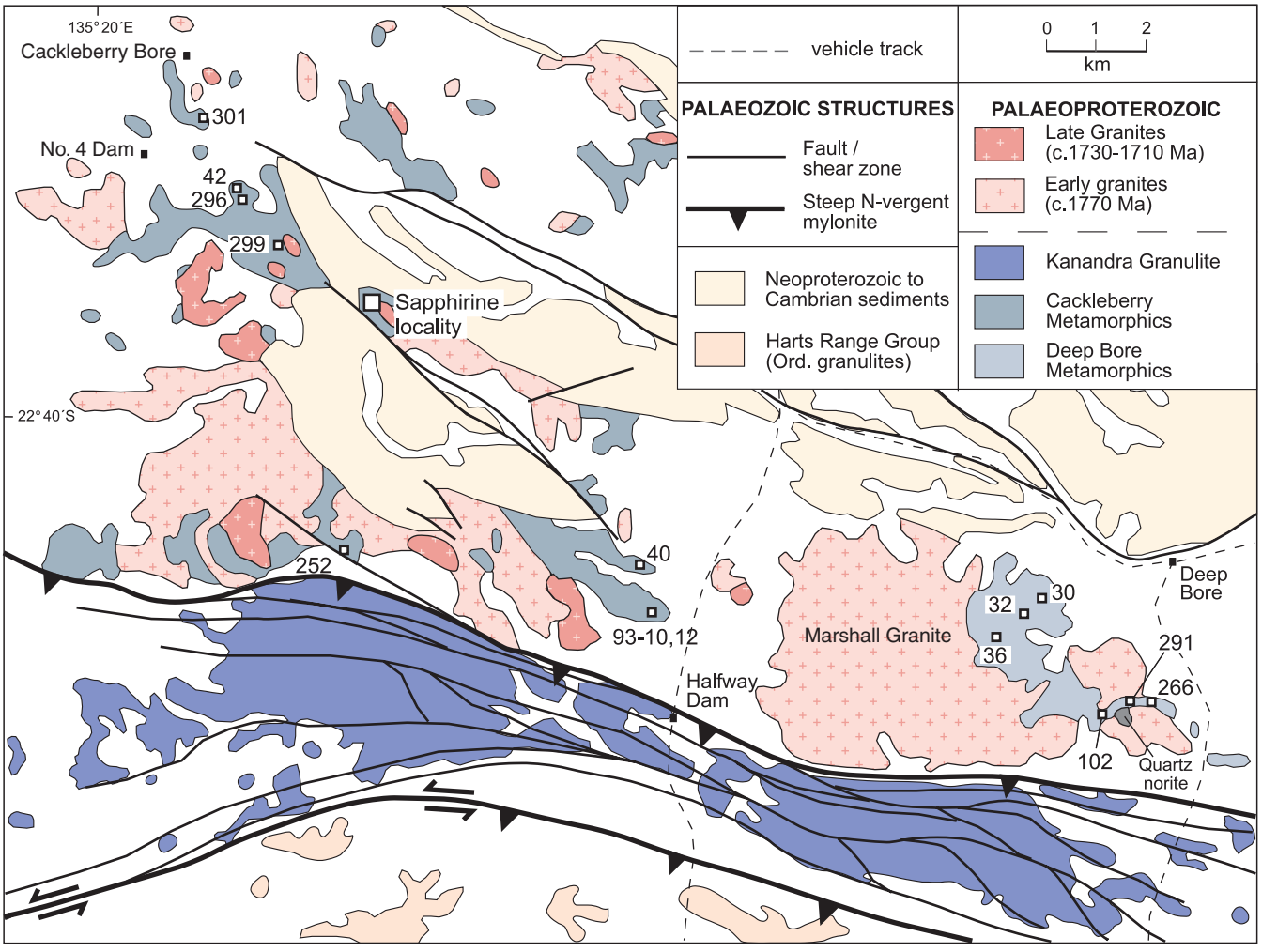

Figure 9 Map of the Mopunga Range region, adapted from Freeman (1986). Numbered localities indicate the location of samples referred to in the text and appendices

Figure 10 Cordierite-orthopyroxene migmatite from the Deep Bore Metamorphics. Leucosomes contain dark cordierite porphyroblasts, intergrown with spinel and sillimanite in the core. The outcrop shown was sampled for SHRIMP U-Pb geochronology (HU30)

layering. Parallel leucosomes and alignment of sillimanite define the regional fabric within aluminous migmatite. Detailed structural analysis of the Deep Bore Metamorphics is not possible due to poor outcrop, but measurements of the dominant fabric fall into two groups: steeply south dipping (50-85° towards 180-200°); and steeply northeast dipping (70-90° towards 040-060°). The fabric is generally weakly defined or absent in psammitic lithologies, and is more intense in more highly migmatised lithologies. No consistent lineations occur.

Calc-silicate layers are typically rich in diopside and quartz, although massive wollastonite rock locally occurs (eg NQ595880). The wollastonite zones are cut by late pegmatite and occur in regions with abundant epidote alteration, suggesting late hydrous alteration, which also led to chlorite-muscovite retrogression within pelite. Mafic units within the Deep Bore Metamorphics contain orthopyroxene, clinopyroxene, hornblende and plagioclase.

Much of the Deep Bore Metamorphics is deeply weathered, and is interpreted to have been retrogressed by fluid flow following granulite metamorphism. At NQ576884, randomly oriented quartz veins occur within gossanous outcrops in the metamorphics, immediately adjacent to the Marshall Granite. Abundant quartz veins and rocks that have undergone hydrous retrogression also occur at NQ579880.

Petrology

The pelitic to psammitic lithologies in the Deep Bore Metamorphics can be divided into four groups on the basis of bulk composition and mineralogy. These are designated assemblages I to IV, in order of increasing Al_2O_3 content. Assemblages I and II represent leucosome-free aluminous metapsammite, while assemblages III and IV represent semi pelitic to pelitic migmatites. In addition to these assemblages, granoblastic, cordierite-biotite-quartz-K-feldspar gneiss also

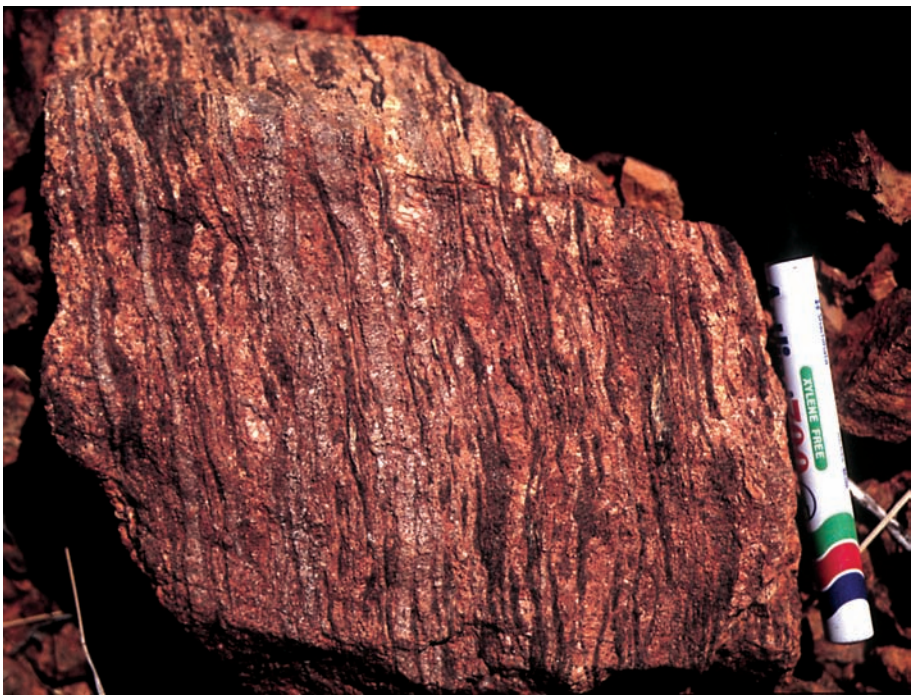

Figure 11 Typical 'schlieren migmatite' in the Deep Bore Metamorphics, with dark Crd-Spl-Mte-Sil melanosome and light coloured Qtz-Kfs leucosome

occurs. Late retrogression of cordierite, biotite and/or feldspar to muscovite and chlorite occurs in all lithologies, along with oxidation and hydration of hercynitic spinel to magnetite-diaspore intergrowths.

Assemblage I: Grt-Crd-Opx-Bt gneiss

Metapsammitic rocks of Assemblage I contain garnet, cordierite, orthopyroxene, biotite, quartz and minor magnetite. Feldspar is absent. Orthopyroxene forms large poikiloblasts containing biotite and quartz inclusions; biotite inclusions are aligned parallel to the dominant fabric. Garnet forms large porphyroblasts with rounded inclusions of quartz, and also occurs in a granoblastic fabric in contact with orthopyroxene, biotite, cordierite and quartz. Garnet porphyroblasts are commonly separated from quartz by secondary cordierite coronas that commonly contain vermicular quartz and biotite. Less commonly, orthopyroxene also occurs within cordierite coronas. A second generation of garnet overgrows primary garnet at contacts with cordierite coronas, and also forms coronas that enclose primary cordierite. Symplectites of biotite and quartz occur at embayed margins of orthopyroxene, and biotite also occurs along cordierite grain boundaries.

Assemblage II: Grt-Crd-Bt gneiss

Assemblage II contains garnet, cordierite, biotite, quartz and magnetite ± K-feldspar. Garnet is typically poikiloblastic and has large rounded inclusions of quartz, and less common inclusions of biotite and magnetite. Cordierite contains rounded quartz inclusions. Biotite occurs as large flakes that are randomly oriented or weakly aligned in a fabric. Quartz is typically coarse grained, and biotite (less commonly cordierite) is included within coarse quartz grains. Plagioclase is absent whereas K-feldspar is usually present. Garnet has coronas of secondary cordierite, and garnet, biotite and quartz are locally separated by cordierite that contains vermicular quartz ± K-feldspar, with minor secondary biotite and magnetite. Similar cordierite-bearing symplectites also separate magnetite and garnet.

Assemblage III: Crd-Bt-Spl ± Opx gneiss

In garnet-absent and cordierite-rich lithologies, typical assemblages contain cordierite, biotite, quartz and K-feldspar with or without spinel, orthopyroxene and sillimanite. Coarse cordierite porphyroblasts are enclosed within leucocratic K-feldspar-quartz ± biotite segregations that are interpreted to be crystallised melt. The cordierite porphyroblasts within the segregations contain inclusions of spinel, magnetite and less common sillimanite. Fibrous sillimanite also occurs at the embayed margins of some cordierite porphyroblasts. In HU30, orthopyroxene occurs with cordierite, biotite, quartz, K-feldspar and magnetite in the mesosome, and also occurs in leucosome that surrounds large cordierite porphyroblasts. Cordierite porphyroblasts contain spinel ± sillimanite inclusions, and are locally in contact with orthopyroxene in the enclosing leucosome. HU32C contains K-feldspar-quartz segregations that surround intergrowths of cordierite, spinel, magnetite and sillimanite. These minerals are overgrown and embayed by finer grained sillimanite and green biotite. The mesosome within these rocks consists of a granoblastic cordierite-biotite-K-feldspar-quartz-ilmenite assemblage, with or without orthopyroxene. Cordierite in the mesosome contains rounded inclusions of quartz. Fine grained retrograde symplectites of andalusite and quartz occur rarely along cordierite and K-feldspar grain boundaries.

Assemblage IV: Crd-Sil ± Spl migmatite

In strongly migmatitised pelite (schlieren migmatite), silica-undersaturated aluminous melanosome and quartz - K-feldspar leucosome are interlayered on a scale of 0.2-1.0 cm. The peak metamorphic assemblage in the melanosome is dominated by cordierite, with varying amounts of sillimanite, hercynitic spinel, magnetite, biotite and less common corundum and ilmenite. Cordierite contains inclusions of sillimanite, and minor biotite, which are oriented parallel to the migmatitic layering. K-feldspar is locally present in the melanosome, but quartz is typically absent, although it occurs in one spinel-absent sample as rounded inclusions within cordierite. Coarser grained sillimanite, forms discrete sillimanite-rich layers about 1 mm in width. Spinel and magnetite ± corundum occur as inclusions within cordierite and as larger aggregates which are generally elongated in the fabric. The leucosome consists of quartz, K-feldspar and minor biotite. Quartz in the leucosome is always separated from the cordierite-rich melanosome by a rim of K-feldspar.

Two types of retrograde assemblages can be distinguished. In the first, fine grained sillimanite ± biotite occurs along cordierite grain boundaries, and forms coronas around spinel. Late biotite also occurs as coronas around Fe-Ti oxides, and less commonly at the interface between leucosome and melanosome. The second retrograde assemblage comprises very fine grained andalusite-quartz symplectites that occur locally along cordierite grain boundaries.

P-T-t evolution of the Deep Bore Metamorphics

Assemblages I and II

Assemblage I (Grt-Crd-Opx-Bt-Qtz) is K-feldspar absent. This can be attributed to the influence of TiO_2 in stabilising biotite in preference to K-feldspar at granulite facies in metapsammites (Stevens *et al* 1997). Therefore, in considering reactions between phases in this rock, biotite as the only K-bearing phase is considered to be in excess. The absence of leucosome in the metapsammites also suggests that melt was not involved in the reactions. The existence of cordierite ± orthopyroxene coronas between garnet and quartz is attributed to the reaction:

$$\text{Grt} + \text{Qtz} (\pm \text{low-Fe Bt}) = \text{Crd} + \text{Opx} (\pm \text{high-Fe Bt}) \quad (1)$$

Similarly, in assemblage II, the existence of cordierite-K-feldspar-quartz ± ilmenite symplectites separating biotite, garnet and quartz reflects the reaction:

$$\text{Grt} + \text{Bt} + \text{Qtz} = \text{Crd} + \text{Ksp} (\pm \text{Ilm}) \quad (2)$$

These cordierite-producing reactions are traditionally regarded as being diagnostic of near-isothermal decompression (Harley 1989), but as they have a shallow positive slope in P-T space they also proceed with heating. Coronas of garnet surrounding cordierite, and less commonly orthopyroxene, reflect the reversal of reaction (1). This reversal suggests that the most likely interpretation of these textures is that they record near-isobaric heating and cooling.

Assemblage III

In assemblage III metapelite, the preservation of patches of leucosome centred on aggregates of aluminous minerals provides evidence for melting reactions associated with granulite metamorphism. Cordierite porphyroblasts, locally intergrown with spinel and magnetite (± sillimanite) and enclosed within patches of K-feldspar-rich leucosome are likely to have formed through the biotite fluid-absent melting reaction

$$Bt + Sil + Qtz = Crd + Spl + melt\ (Kfs\text{-}Qtz\text{-}H_2O) \quad (3)$$

The localised occurrence of fine-grained biotite and sillimanite consuming cordierite and spinel suggests a reversal of reaction (3) associated with crystallisation of the leucosome. In one sample, cordierite porphyroblasts contain spinel and ilmenite in their core, whereas orthopyroxene is present at the margins and in the adjacent melt segregation. This suggests, that reaction (3) was followed by the higher-T KFMASH divariant reaction

$$Bt + Qtz = Crd + Opx + melt\ (Kfs\text{-}Qtz\text{-}H_2O) \quad (4)$$

Biotite-quartz symplectites consuming orthopyroxene are consistent with the reversal of reaction (4) during cooling.

Assemblage IV

Assemblage IV pelitic migmatite, comprising a quartz-absent cordierite-sillimanite-spinel ± corundum melanosome and quartz-K-feldspar leucosome, is likely to have resulted from dehydration melting of biotite through reaction (3), resulting in the loss of all quartz to the melt, as well as the following quartz-absent reaction (Pattison and Tracy 1991, Whittington *et al* 1998):

$$Sil + Bt = Crd + Spl \pm Crn + Kfs + melt \quad (5)$$

This is supported by the existence of sillimanite, biotite and rare quartz inclusions within cordierite. The occurrence of late fine grained biotite and sillimanite along cordierite, K-feldspar and spinel grain boundaries with the quartz-absent melanosome reflects the reversal of reaction (5) with cooling.

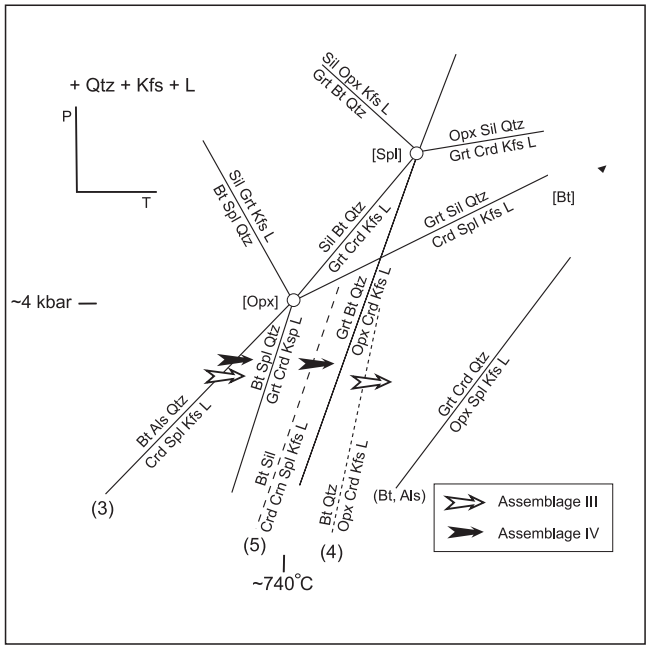

Constraints from petrogenetic grids and experimental studies

Figure 12 is a qualitative petrogenetic grid in the system K_2O-FeO-MgO-Al_2O_3-SiO_2-H_2O (KFMASH), adapted from Vernon *et al* (1990), Fitzsimons (1996), Greenfield *et al* (1998) and others, and projected from K-feldspar, quartz and melt. This grid does not include reaction (4), which is divariant in KFMASH, and reaction (5), which is quartz-absent. However, the relative locations of these reactions in P-T space are schematically represented in Figure 12, based on the inferred reaction sequence in well documented high-T, low-P terranes (Pattison and Tracy 1991) and on the grids of Grant and Frost (1990) and Pattison and Harte (1991). The location of the orthopyroxene-absent ([Opx]) invariant point is approximately 4 kbar and 740°C (Fitzsimons 1996). In rocks which undergo prograde heating at pressures below [Opx], the assemblage garnet + sillimanite is never stable, and dehydration melting of sillimanite-bearing assemblages is likely to be controlled by reaction (3). This is consistent with petrological observations from sillimanite bearing samples in the Deep Bore Metamorphics. The arrows indicate the reactions that are inferred to have occurred in Assemblages III and IV. The difference in the reaction sequence between Assemblages III and IV can be attributed to variable Al_2O_3 contents; in Assemblage III, sillimanite was exhausted by the progress of reaction (3), whereas in more aluminous assemblages, quartz was exhausted, allowing stabilisation of the assemblage sillimanite-spinel-cordierite. An upper temperature limit for metamorphism is provided by the lack of the stable assemblage spinel + orthopyroxene in all bulk compositions, suggesting that the (Bt, Als) reaction (Figure 12) was not crossed. The reaction sequence shown in Figure 12, at lower pressures than the [Opx] invariant point, has been recorded in metapelite from a number of well-documented, low-pressure contact aureoles, including Ballachulish, Scotland (Pattison 1989) and Laramie, Wyoming (Grant and Frost 1990). Both of these have well-constrained pressures of 3.0 ± 0.5 kbar at temperatures of up to 800°C. A similar reaction sequence has also been recorded from 'regional aureole' metamorphic rocks at Mt Stafford in the northern Arunta Province. These rocks underwent partial melting at pressures of 2.8-4.0 kbar and temperatures exceeding 800°C (Vernon *et al* 1990, Greenfield *et al* 1998).

Constraints on the P-T evolution of the Deep Bore Metamorphics can also be obtained from metapsammitic rocks that did not undergo migmatisation. Experimental studies on fluid-absent partial melting of various bulk compositions by Stevens *et al* (1997), established that at low pressures (4 kbar), metapsammitic rocks undergo fluid-absent partial melting at temperatures about 60°C higher than metapelite (Figure 13). The lower sodium content of the Deep Bore Metamorphics

Figure 12 Qualitative petrogenetic grid in the system KFMASH for fluid-absent metapelite (after Greenfield *et al* 1998). The relative position of the quartz-absent reaction (5) and the *divariant* reaction (4) in P-T space are from Grant and Frost (1990) and Pattison and Harte (1991). Arrows show the inferred reactions crossed by metapelites from Assemblages III and IV

compared to the plagioclase-bearing metapsammite of Stevens *et al* (1997) may result in an even higher solidus temperature for metapsammite than that predicted by experimental results, but nonetheless it is unlikely that peak metamorphic temperatures significantly exceeded 800°C.

P-T estimates

The results of thermobarometry on samples from the Deep Bore Metamorphics are summarised in Appendix 3 and Figure 13. Errors given below for conventional P-T estimates are single standard deviations of multiple (>4) estimates from different mineral pairs within a single sample. Various calibrations of garnet-biotite and garnet-orthopyroxene thermometers give temperatures between 670 ± 27° and 871 ± 20°C. The garnet-cordierite thermometer of Nichols *et al* (1992) gives temperatures between 708 ± 11° and 742 ± 38°C for three samples, whereas two samples give lower temperatures (500-600°C) that suggest re-equilibration. Due to the lack of plagioclase or sillimanite in garnet-bearing lithologies, the only applicable barometer was the garnet-orthopyroxene barometer (Harley and Green 1982). Application of this barometer to sixteen mineral pairs from three samples gives a pressure range of 2.1-3.7 kbar for an 800°C reference temperature. However, this barometer is highly temperature dependent, and reference temperatures of 750°C and 850°C resulted in pressures of 0.4-2.0 kbar and 3.8-5.4 kbar, respectively (Figure 7).

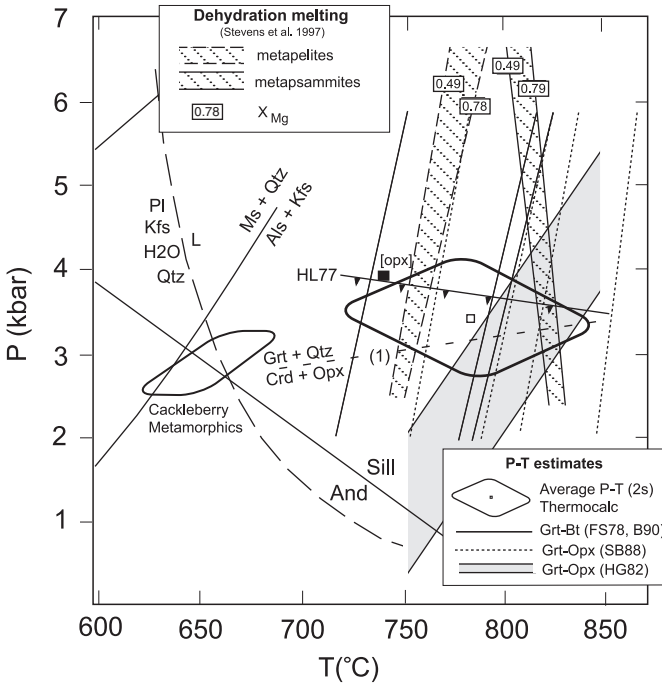

Figure 13 Constraints on P-T conditions of metamorphism in the Deep Bore Metamorphics. The position of the [Opx] invariant point is from Fitzsimons (1996). The line marked HL77 is the lower stability limit of the assemblage Grt + Sil in metapelites of intermediate bulk composition (Holdaway and Lee 1977), and the position of reaction (1) for intermediate bulk compositions is from Vielzeuf and Holloway (1988). Experimental constraints on the onset of partial melting in metapelites and metapsammites of differing bulk rock X_{Mg} are from Stevens *et al* (1997)

Average P-T estimates using Thermocalc (Powell and Holland 1988, Holland and Powell 1998) were calculated using garnet-bearing samples from the Deep Bore Metamorphics. Estimates on the assemblage Grt-Crd-Bt-Qtz ± Ksp were highly sensitive to aH_2O. However, an aH_2O of 0.3 resulted in P-T estimates in best agreement with conventional thermobarometry and experimental melting constraints. A combination of average P-T estimates for six samples of Deep Bore Metamorphics at an aH_2O of 0.3 gives 3.4 ± 0.8 kbar and 773 ± 59°C (2σ errors; Appendix 3).

Cackleberry Metamorphics

Field observations

The Cackleberry Metamorphics is a succession of metapelite and amphibolite with less abundant calc-silicate, quartzofeldspathic gneiss and cordierite-orthoamphibole rock (Shaw *et al* 1984). These rocks occur to the west of the Deep Bore Metamorphics and are unconformably overlain by unmetamorphosed Georgina Basin sediments (Figure 9).

Western end of the Mopunga Range

In outcrops at the western end of the Mopunga Range (NQ379988), the Cackleberry Metamorphics consists of pelitic gneiss containing biotite, cordierite and aluminosilicate (andalusite and/or sillimanite). The gneiss has a compositional layering reflecting S_0, and has garnet-bearing psammitic layers

Figure 14 Cordierite-bearing leucosome in metapelite from the Cackleberry Metamorphics, showing a biotite-aluminosilicate rich selvage, in which sillimanite is aligned in S_2 (parallel to pencil)

and more extensive coarser grained pelitic layers, which contain porphyroblasts of andalusite and cordierite. The dominant gneissic layering (S_1) is generally parallel to S_0, and contains leucocratic veins and segregations. Although the gneissic fabric is well developed, bedding is clearly preserved, and biotite is only weakly oriented in S_1.

F_2 folds that have a variable intensity and an associated biotite-sillimanite fabric fold the S_1 fabric. D_2 strain is strongly partitioned and has zones of high non-coaxial strain interlayered with low strain zones, at both thin-section and outcrop scale. The S_2 fabric most commonly strikes north, dips steeply and has a moderately south plunging stretching lineation. Cordierite-bearing melts occur in shear bands parallel to S_2 and more commonly as veins and large (>10 cm) melt patches, which are discordant to S_1 but weakly folded by F_2. Cordierite melts contain biotite-rich selvages in which sillimanite is aligned in S_2 (Figure 14). Cordierite-bearing leucosomes locally accumulate to form larger bodies with xenoliths of biotite-sillimanite country rock. In zones of low S_2-strain, cordierite porphyroblasts are pseudomorphed by sillimanite ± biotite.

Localised occurrences of biotite (± hornblende) granite and granodiorite, mapped by Shaw *et al* (1984) as Dneiper Granite, have a strong fabric and contain the L_2 lineation. Numerous granite bodies intrude the Cackleberry Metamorphics, as well as pegmatite and granite veins that truncate S_2 and are undeformed. These late granites are generally leucocratic, and locally contain euhedral K-feldspars. Rare, steeply dipping, anastomosing mylonite zones with biotite-muscovite assemblages truncate the gneiss. These mylonites also truncate the late granites.

Sapphirine locality

Silica-undersaturated, phlogopite-sapphirine bearing schist outcrops near the Huckitta-Dneiper boundary fence at NQ409966. The schist occurs in an area of predominantly granitic outcrop, on either side of a vehicle track, 50 m west of a gate in the boundary fence. The granite comprises gneissic Dneiper Granite and variably deformed leucocratic granite. Schist is intercalated with the deformed granite and includes a layer of phlogopite-rich schist that outcrops over 150 metres and is 1-2m wide. This layer is parallel to the regional S_2 fabric, which trends north and is nearly vertical with a lineation plunging 60° south. The phlogopite schist contains randomly oriented euhedral to subhedral pale blue sapphirine up to 1 cm in length and pale green porphyroblasts of pinitised cordierite. Other schist bands contain pale blue rounded corundum porphyroblasts. Retrogressed and weathered cordierite-orthoamphibole rock occurs in outcrops immediately adjacent to the phlogopite schist. Phlogopite is weakly aligned in S_2, and undeformed leucocratic veins truncate the schist bands.

North of Halfway Dam

North of Halfway Dam (NQ472910) the Cackleberry Metamorphics is poorly exposed, and largely comprises subcropping biotite schist, granite, vein quartz and cordierite-bearing felsic gneiss, with a steeply dipping fabric that strikes east-southeast. Rare pods and boudins of massive, fresh aluminous rock contain glassy purple-blue cordierite, biotite and randomly oriented fibrous sillimanite.

South of the Mopunga Range

Along the Dneiper-Huckitta fenceline south of Mopunga Range, the Cackleberry Metamorphics comprises poorly outcropping hornblende amphibolite lenses amongst strained granite. The amphibolite has a strong, near-vertical lineation, and locally contains phenocrysts of plagioclase. Shaw et al (1984) mapped this exposure as para-amphibolite. Fresh exposures occur where the fenceline track crosses a creek at NQ411903.

Petrology

Metapelite

Pelitic metamorphics at the western end of Mopunga Range contain a medium to fine grained assemblage of aluminosilicate, cordierite, biotite, quartz, K-feldspar and plagioclase, and locally have an S_2 sillimanite-biotite fabric. In domains of low D_2 strain, the pelite contains And-Crd-Bt-Ksp-Qtz-Plag. Andalusite contains inclusions of biotite and quartz, whereas cordierite contains inclusions of quartz, andalusite and biotite. Coarse symplectites of andalusite, biotite and quartz, with or without plagioclase and K-feldspar, locally

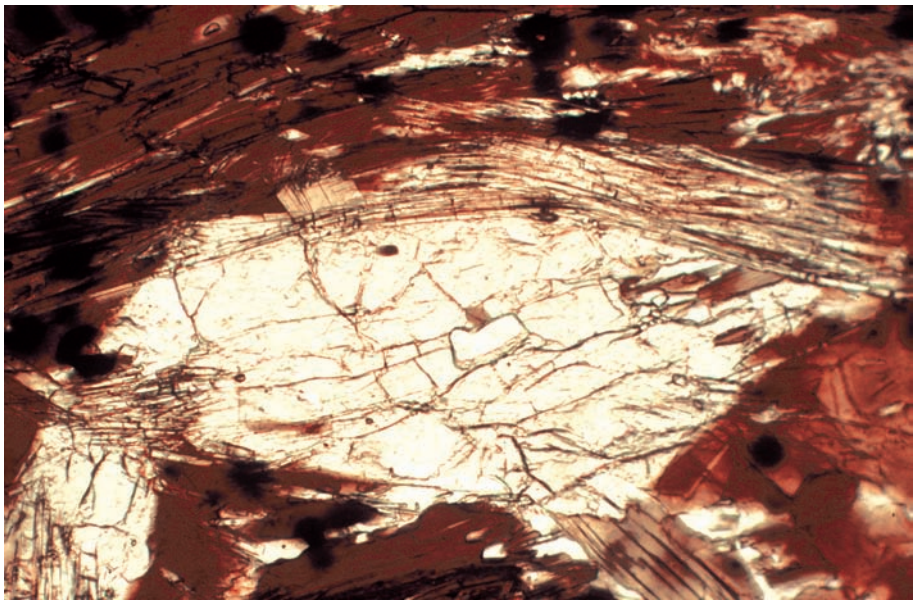

Figure 15 Andalusite and biotite within a selvage adjacent to cordierite-bearing leucosome, Cackleberry Metamorphics. Fibrous sillimanite intergrown with biotite defines S_2 and envelops andalusite. Width of field of view is 2 mm. Plane-polarised light

overgrow coarse biotite and andalusite at the expense of cordierite and K-feldspar. In places, random fibrous sillimanite occurs at cordierite, K-feldspar and plagioclase grain boundaries, where it is intergrown with biotite and not in contact with andalusite.

Cordierite-quartz-K-feldspar leucosomes occur within the pelites, and biotite and aluminosilicate selvages occur in the adjacent country rock. In rocks that lack an S_2 fabric, leucosomes have sharp edges and truncate the weak S_1 fabric. In selvages at the margins of leucosomes, cordierite is consumed by coarse andalusite-biotite-quartz symplectites. Elsewhere, selvages comprise coarse euhedral andalusite and randomly oriented biotite. The leucosomes contain quartz, feldspar, inclusion-free cordierite and rare biotite. Fine grained andalusite-quartz symplectites occur along cordierite grain boundaries, whereas in metapelite with an S_2 fabric, fine grained sillimanite and biotite locally occur in the leucosome, and are concentrated along cordierite and K-feldspar grain boundaries.

Rocks that contain an S_2 fabric display complex relationships between aluminosilicate polymorphs, and all contain co-existing andalusite and sillimanite. Most andalusite occurs in zones of low S_2 strain, both as porphyroblasts and within coarse symplectites consuming cordierite. Sillimanite (which most commonly has both fibrous and prismatic forms) occurs with biotite and quartz in narrow zones of high S_2 strain. Outside these zones, sillimanite occurs as randomly oriented fibres and prisms within cordierite and K-feldspar and along grain boundaries, and is generally not in contact with andalusite. Fibrolitisation of biotite also occurs locally. In cases where andalusite is in contact with sillimanite, folia of S_2 sillimanite and biotite envelop andalusite (Figure 15), and oriented fibres and prisms of sillimanite partially pseudomorph andalusite. Both sillimanite and andalusite are locally overgrown at contacts with cordierite by fine grained symplectites of andalusite and quartz, with or without biotite.

Metapsammite interlayered with the pelite contains fine to medium grained granoblastic garnet, biotite, quartz and plagioclase. K-feldspar was not identified in these rocks, but this is not conclusive, as much of the feldspar is highly sericitised.

Sapphirine-phlogopite schist

All samples of phlogopite-bearing schist from the sapphirine locality contain >50% coarse phlogopite aligned in a fabric of variable intensity, along with abundant apatite and rutile, accessory monazite and rare zircon. Quartz and feldspar are absent. The description below refers only to sapphirine-bearing schist, although sapphirine-absent phlogopite schist with coarse corundum and pinitised cordierite porphyroblasts also occurs.

Sapphirine, which is colourless in thin section, occurs as subhedral to euhedral prisms that contain inclusions of rutile, phlogopite and apatite. Less commonly, corundum and colourless spinel are also enclosed within sapphirine. Sapphirine is most commonly oriented parallel to the enclosing phlogopite fabric, and locally occurs as smaller prisms within the fabric. An amorphous, hydrous alteration product occurs as pseudomorphs after rounded porphyroblasts that contain inclusions of rutile, apatite and randomly oriented phlogopite. These alteration products are green in hand specimen and colourless in thin section. On the basis of the mineral composition of the alteration products they are interpreted to be pinitised cordierite.

The most common reaction textures in phlogopite-sapphirine schist are intergrowths of corundum, fine grained phlogopite and chlorite replacing sapphirine. This texture only occurs in open fractures crosscutting sapphirine, and at contacts between sapphirine and primary phlogopite. Less commonly, sapphirine is also consumed by fine grained reaction textures comprising spinel, chlorite and corundum. These spinel-bearing textures only occur within sapphirine grains adjacent to inclusions of corundum, in the absence of phlogopite. A relatively late generation of fractures within sapphirine is infilled by chlorite and diaspore. The remaining sapphirine is partly replaced by extremely fine grained hydrous alteration products.

Crd-Mus-Qtz assemblages

Pods of highly aluminous and magnesian rock north of Halfway Dam are massive and unfoliated, and contain an early cordierite-muscovite-quartz-ilmenite ± plagioclase assemblage. Cordierite contains inclusions of biotite, and muscovite has numerous inclusions of quartz. This cordierite-muscovite assemblage is overprinted and partly consumed by extensive swirling mats of fibrous sillimanite, which are intergrown with quartz and less abundant biotite and K-feldspar. Biotite is more abundant where sillimanite contacts muscovite and cordierite. The replacement of muscovite-cordierite-quartz by mats of fibrous sillimanite and biotite can be attributed to the reaction: Crd + Mus + Qtz = Bt + Ksp + Sil + H_2O. This reaction is not commonly included in pelitic P-T grids, as it is restricted to highly magnesian bulk compositions (Xu *et al* 1994). The reaction has a steep positive slope in P-T space (Xu *et al* 1994), and therefore proceeds with increase in temperature.

Origin of sapphirine-phlogopite schist

The phlogopite-sapphirine-cordierite schist in the Cackleberry Metamorphics represents an unusual paragenesis and there are few documented analogues worldwide. Whole rock geochemistry of sapphirine-phlogopite and corundum-phlogopite schists from the Cackleberry Metamorphics is given in Appendix 2. They are characterised by low SiO_2, FeO, K/Rb, V, Cu, Cr and Ni and high K_2O, Al_2O_3, Rb, Th and LREE. Low Cr and Ni contents preclude an ultramafic precursor, and the high Rb and lack of significant partial melting in surrounding rocks makes a restitic origin (eg Clifford *et al* 1975) unlikely. High-T metasomatism accompanying metamorphism (Vry and Cartwright 1994) is also considered unlikely, due to the similarity of prograde and retrograde assemblages. The schists occur adjacent to cordierite-orthoamphibole rocks, which have also been documented at a number of other localities throughout the Cackleberry Metamorphics (Shaw *et al* 1984). The presence of cordierite-orthoamphibole and sapphirine-bearing rocks is potentially important given the association between these lithologies and Cu-Pb-Zn mineralisation elsewhere in the eastern Arunta Province (Warren & Shaw 1985).

In a review of cordierite-orthoamphibole and sapphirine-bearing rocks in the Arunta Province, Warren (1979) proposed that most had a chlorite-rich precursor, as well as quartz and an aluminosilicate mineral such as illite or muscovite. Models for the formation of these rocks include hydrothermal alteration of volcanogenic rocks (Warren 1979), diagenetic alteration of sedimentary pelite in contact with hypersaline fluids (Warren and Hensen 1987) and metamorphism of evaporitic mudstones (Moine 1981). The bulk composition of sapphirine-phlogopite schist from the Cackleberry Metamorphics is broadly similar

to cordierite-orthoamphibole and sapphirine-bearing rocks from elsewhere in the Arunta Province, except that the sapphirine-phlogopite schist has significantly higher K_2O. The schist is similar to sapphirine-phlogopite schist occurring 5 km north of Aileron (NAPPERBY) that was interpreted by Warren and Hensen (1987) as having undergone potassium metasomatism. It also has chemical and mineralogical affinities with the phlogopite-rich outer zone of a sapphirine bearing xenolith at Mawson, Antarctica that was interpreted by Sheraton *et al* (1982) as having developed from metasomatism of a magnesian (chlorite-quartz) body during crystallisation of the enclosing granite. The high values for mobile elements such as Rb, Th and LREE in the sapphirine-phlogopite schist, with correspondingly low K/Rb, are consistent with metasomatic alteration (Warren and Hensen 1987).

In summary, a likely model for the origin of the sapphirine-phlogopite schist in the Cackleberry Metamorphics is via potassium metasomatism of a magnesian chlorite-rich precursor. This occurred prior to high-grade metamorphism and probably during intrusion of the adjacent Dneiper Granite at 1771 ± 15 Ma. The magnesian precursor is likely to have been either an evaporitic mudstone or, more probably, a volcanogenic pelite that was affected by early hydrothermal alteration.

P-T-t evolution of the Cackleberry Metamorphics

Interpretation of reaction textures

Complex textures in Cackleberry metapelite in the northwestern Mopunga Range can be summarised by the following reaction sequence:

1. Syn-S_1 - Crd-And-Bt-Kfs-Qtz-Pl assemblage;
2. Crystallisation of Crd-bearing melts, first generation of coarse-grained And-Bt-Qtz symplectites after Crd + Ksp;
3. Syn-S_2 - Sil-Bt-Qtz assemblage consuming Crd + Ksp;
4. Second generation of fine-grained And-Qtz ± Bt symplectites.

The critical reaction for interpreting this evolution is the biotite dehydration reaction:

$$Bt + Als + Qtz = Crd + Kfs + H_2O \quad (6)$$

This reaction has a shallow positive slope in P-T space (Grant 1985), and therefore progresses to the right with increasing temperature, or decreasing pressure, or a decrease in aH_2O. The existence of biotite, andalusite and quartz inclusions within cordierite suggests that reaction (6) contributed to the growth of cordierite in S_1. At temperatures above the haplogranite solidus (650-660°C at 3 kbar, Johannes and Holtz 1990), a similar reaction (Grant 1985, Spear *et al* 1999) produces cordierite-bearing melt:

$$Bt + Als + Qtz = Crd + L \pm Kfs \quad (7)$$

The slopes of reactions (6) and (7) and their position in P-T space for compositions of the Cackleberry Metamorphics have been calculated with Thermocalc (Powell and Holland 1988, Holland and Powell 1998) using analysed mineral compositions from sample HU42E (Figure 16). Reactions (6) and (7) are divariant (continuous) reactions in the KFMASH system, so are likely to proceed over a range of P-T conditions. The lack of significant congruent melting above the fluid-saturated haplogranite or pelite solidus implies that melting only occurred through dehydration reactions under H_2O-undersaturated conditions.

The breakdown of cordierite and K-feldspar to biotite, aluminosilicate and quartz is most commonly attributed to near-isobaric cooling (Clarke *et al* 1990), although it can also be attributed to the up-pressure and up-temperature portion of an anti-clockwise P-T path (Rubenach 1992). The inset in Figure 16 shows the apparent topology in P-T space of reactions (6) and (7), the muscovite-dehydration reaction, the haplogranite solidus and the sillimanite-andalusite equilibrium, as suggested by the reaction sequence in the Cackleberry Metamorphics. The existence of coarse andalusite-quartz-biotite symplectites in selvages around cordierite-bearing melts reflects back-reaction between country rock and crystallising melt and the reversal of reaction (7) within the andalusite field. According to petrographic relationships, this must have occurred prior to development of the sillimanite-bearing S_2

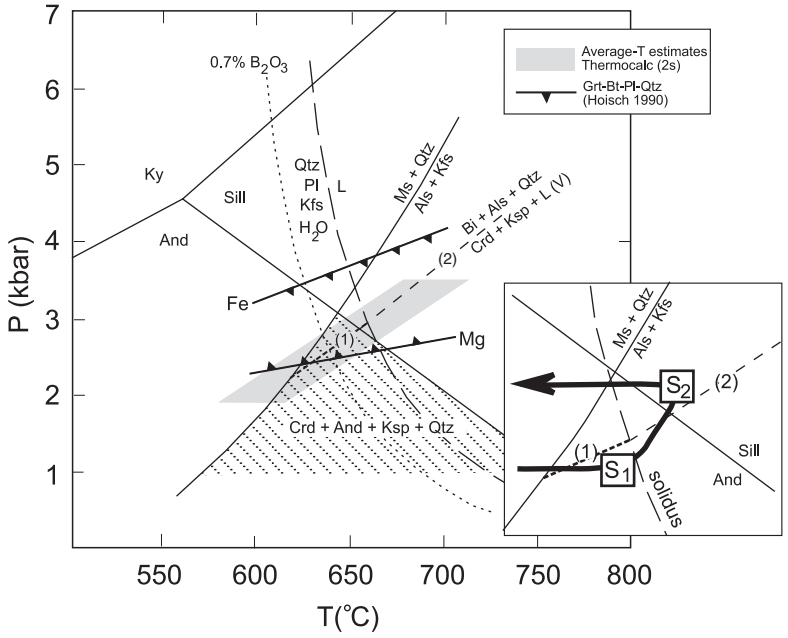

Figure 16 Constraints on the P-T conditions of metamorphism in the Cackleberry Metamorphics. The location of cordierite-producing reactions for an X_{Mg} (Crd) of 0.55 are from Pattison (1989). The haplogranite solidus is from Johannes and Holz (1990) and the solidus with the addition of 0.7% B_2O_3 is from Manning and Pichavant (1983). Discussion in text

fabric. This would allow two possibilities for the P-T evolution of the Cackleberry Metamorphics:

1. Bt-And-Qtz symplectites represent cooling from the thermal peak, and the S_2 fabric represents a second independent thermal event at a higher pressures; or

2. The sillimanite fabric represents an increase in pressure following melt crystallisation but prior to significant cooling, as part of an anti-clockwise P-T path.

Although either scenario is possible given the lack of age constraints on S_1 and S_2, it is proposed that the entire high-grade evolution of the Cackleberry Metamorphics occurred during a single event with an anti-clockwise P-T-t evolution, as shown in the inset on Figure 16. Late, very fine-grained andalusite-bearing symplectites overgrowing sillimanite at contacts with cordierite and K-feldspar reflect cooling into the andalusite field.

Stability of co-existing andalusite and sillimanite

The Cackleberry Metamorphics in northwestern Mopunga Range represent a region where andalusite and sillimanite coexist over an area of 3 x 2 km. Although there are some clear timing relationships between andalusite and sillimanite growth (Figure 15), there are many examples of andalusite and sillimanite in contact, but with no evidence of reaction. Locally, sillimanite nucleates on, but does not replace andalusite. Replacement of sillimanite by andalusite only occurs in zones of high S_2 strain, primarily by growth of oriented fibres and prisms within andalusite. More commonly, sillimanite grows at the expense of K-feldspar and cordierite via reaction (6).

Similar inertness of andalusite in the presence of later sillimanite has been recorded from a number of low pressure terranes (Vernon 1987, Kerrick and Woodsworth 1989) and has been variously attributed to:

1. Minor-element partitioning resulting in the equilibrium co-existence of the polymorphs (Kerrick and Speer 1988); or

2. The sluggish kinetics of the polymorphic inversion resulting in the metastable persistence of andalusite into the sillimanite stability field (Pattison 1992).

Electron microprobe analysis of co-existing aluminosilicates from three samples (HU42E, 42F and 301A) enable the determination of the equilibrium constant (K_{eq}) between co-existing sillimanite and andalusite, ie

$$K_{eq} = K_D = X_{Al2SiO5}^{Sill}/X_{Al2SiO5}^{And}, \text{ where } X_{Al2SiO5} = 1 - X_{MAlSiO5}$$

(M = minor elements; Kerrick and Speer 1988). This value is close to unity (0.995-1.001) for the Cackleberry Metamorphics and there is no evidence of systematic partitioning of minor elements between andalusite and sillimanite. Therefore, the co-existence of the two aluminosilicates is more likely to be due to kinematic overstepping, which suggests that peak temperatures in the sillimanite field were within ~40°C of the andalusite-sillimanite equilibrium (Walther and Wood 1984, Kerrick and Woodsworth 1989).

P-T constraints from petrogenetic grids

An important consideration when assessing the P-T conditions of metamorphism in the Cackleberry Metamorphics is the location of the andalusite-sillimanite equilibrium in P-T space. This has been the source of considerable uncertainty (eg Kerrick 1990). The aluminosilicate triple point of Pattison (1992), which is based on the P-T conditions of the andalusite-sillimanite equilibrium in the Ballachulish aureole of Scotland (645 ± 20°C, 3.0 ± 0.4 kbar), is used in this study as it is in better agreement with thermobarometric constraints on naturally occurring assemblages than experimental data of Richardson *et al* (1969) and Holdaway (1971).

The stability field of the S_1 muscovite-absent assemblage And-Ksp-Crd-Bt-Qtz is up-temperature of the muscovite-quartz breakdown reaction, and is within the andalusite stability field. This restricts the stability of this assemblage to <3 kbar at 600-700°C (Figure 16), although this constraint varies depending on choice of aluminosilicate phase diagram. The presence of andalusite in selvages around cordierite-bearing melts suggests that temperatures accompanying crystallisation of the melt were below or close to the andalusite-sillimanite transition, which is likely to be in the range 625-665°C at 3 kbar, or 680-720°C at 2 kbar, (Pattison 1992). As reaction (7) is only likely to produce melt at temperatures above the haplogranite solidus (Grant 1985), this constrains temperatures to >660°C, implying that the pressure must have been 3 kbar or less during melting (Figure 16). Although these constraints point to a limited area in P-T space in which melting can occur in the andalusite stability field (Figure 16), significant uncertainties remain. These include the exact location of the andalusite-sillimanite equilibrium, which may in reality occur at higher temperatures (Richardson *et al* 1969), and the possible role of fluorine or boron (indicated by the presence of minor tourmaline and rare topaz in the Cackleberry Metamorphics) in stabilising melt to lower temperatures (Manning and Pichavant 1983; Figure 16).

The assemblages observed in the Cackleberry Metamorphics are comparable with those of other terranes where P-T conditions of 3 kbar and 650-680°C have been estimated (Ballachulish, Scotland, Pattison 1992; Zone 2b-c, Mt Stafford, Arunta Province, Greenfield *et al* 1998).

P-T estimates

Temperature estimates for the S_1 phase of Cackleberry metamorphism were made on domains with no S_2 sillimanite fabric, and are summarised in Appendix 3. Thermocalc estimates (Powell and Holland 1988, Holland and Powell 1998) for the assemblage And-Bt-Crd-Ksp-Qtz give consistent temperatures for five samples, with combined averages of 620 ± 17°C at a pressure of 2 kbar, 671 ± 17°C at 3 kbar, and 718 ± 19°C at 4 kbar, assuming an aH_2O of 1.0 (2σ errors). Varying aH_2O has little effect. Pressure estimates were made using the assemblage Grt-Bt-Pl-Qtz from garnet-bearing metapsammite from the western Mopunga Range (HU42C). Application of the barometer of Hoisch (1990) to this assemblage gave pressures between 2.3-3.1 kbar for the Mg end-member and 3.5-3.9 kbar for the Fe end-member, at 650°C. Grt-Bt thermometry on this sample yielded unrealistically low temperatures (500-600°C) and this was possibly due to retrograde Fe-Mg exchange. Precise P-T estimates were not possible on the S_2 biotite-sillimanite-quartz fabric, although the presence of sillimanite and absence of melt suggest that S_2 formed at higher pressures than S_1.

Sapphirine-phlogopite schist

The mineral and whole rock compositions in the sapphirine-phlogopite schist can be represented graphically by projecting

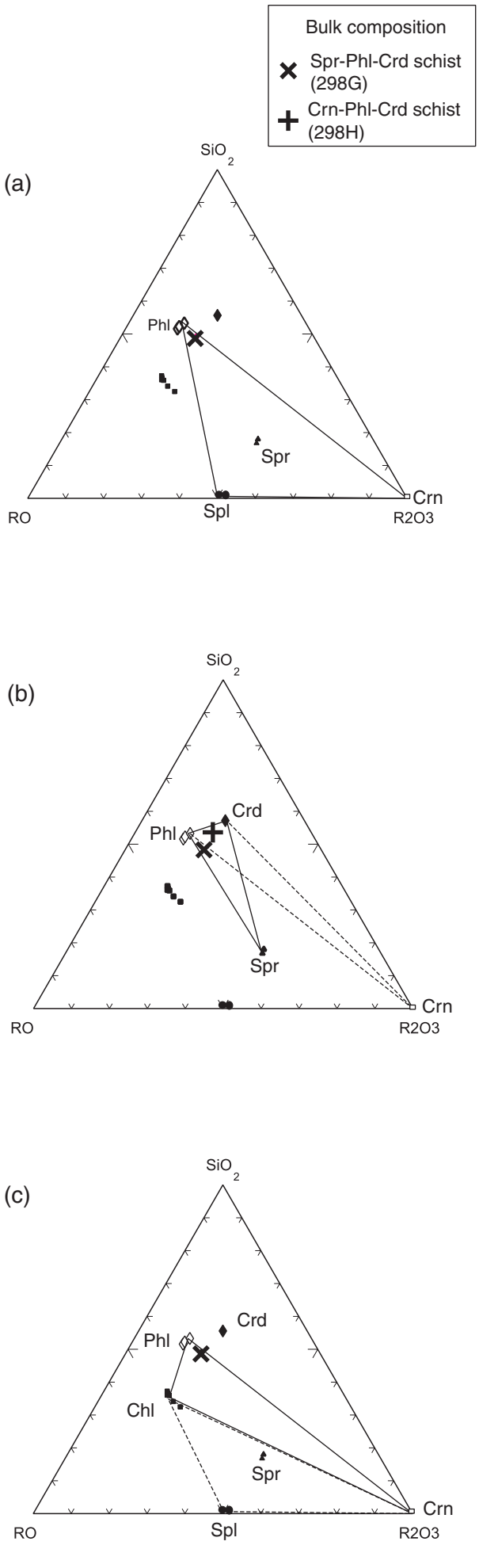

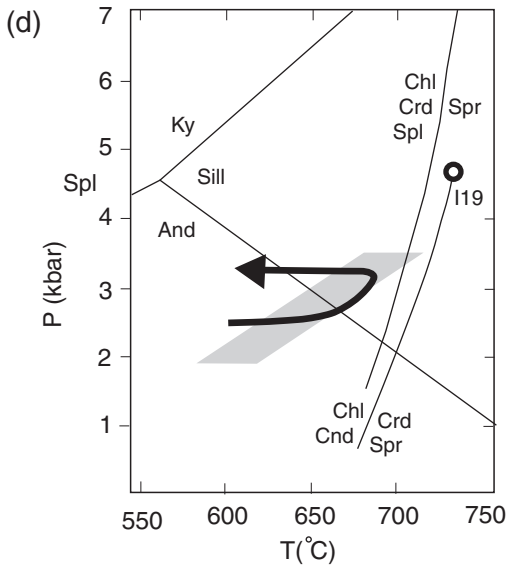

Figure 17 SiO_2-RO (MgO+FeO) - R_2O_3 (Al_2O_3+Fe_2O_3) diagrams, projected from K_2O, for phlogopite schists from the Cackleberry Metamorphics, showing mineral paragenesis during **(a)** prograde **(b)** peak and **(c)** retrograde evolution. The whole rock geochemistry of representative Crn-Phl-Crd and Spr-Phl-Crd schists are shown, on either side of the Phl-Crn tie line. The dashed line in (b) represents peak paragenesis for Crn-Phl-Crd schist and the dashed line in (c) represents spinel-bearing retrograde paragenesis within sapphirine; **(d)** P-T diagram showing the positions of reactions pertinent to the evolution of sapphirine-phlogopite schists (after Ackermand *et al* 1975) and the approximate P-T conditions of pelites in the Cackleberry Metamorphics (this study)

from K_2O into the triangle SiO_2-RO-R_2O_3, where R = (Mg + Fe) and R_2 = (Al_2 + Fe_2) [Figure 17 (a-c)]. Phlogopite is the only K-bearing mineral (with the exception of late, low-grade alteration products), and is interpreted to have been present at all stages of the high-grade evolution. Therefore, most reactions in these highly magnesian rocks can be interpreted in terms of the MASH (MgO-Al_2O_3-SiO_2-H_2O) system. An insight into the prograde evolution is given by spinel and corundum inclusions within sapphirine. These are likely to reflect the prograde growth of sapphirine through the reactions: Spl + Cnd + Chl = Spr + H_2O and Cnd + Chl = Crd + Spr, with phlogopite as an excess phase. At low pressures, these reactions occur at 700-710°C in the MASH system [Figure 17 (d); Ackermand *et al* 1975]. The difference in peak mineral assemblages between Spr-Phl-Crd and Cnd-Phl-Crd schists can be understood in terms of their differing bulk compositions, which lie on either side of the Cnd-Phl tie line on the SiO_2-RO-R_2O_3 diagram [Figure 17 (b)].

The crossing of the reaction Crd + Spr = Cnd + Chl on the retrograde P-T path resulted in stabilisation of the assemblage Phl-Chl-Crn at the expense of Phl-Crd-Spr [Figure 17 (c)], as seen in sapphirine breakdown reaction textures in cordierite-bearing samples. The subsequent breakdown of sapphirine to diaspore and chlorite in narrow fractures also represents the progress of this reaction but at temperatures below the corundum-diaspore equilibrium (400-450°C at low P; Haas 1972). Therefore, the second phase of sapphirine breakdown represents retrogression at greenschist facies. Reaction textures

are consistent with low pressure, as reaction (7) terminates at invariant point I19 of Seifert (1974) at 4.8 kbar and 735°C. In summary, the mineral assemblages and reaction textures are consistent with the sapphirine-bearing assemblages forming at similar P-T conditions to nearby metapelites (3 kbar, 680°C), with a simple heating-cooling path.

Summary of P-T evolution of the Mopunga Range region

The P-T constraints outlined above and summarised in Appendix 3 suggest that granulite facies metamorphism in the Deep Bore Metamorphics reached 2.6-4.0 kbar and 750-800°C, while peak conditions in Cackleberry Metamorphics were 2.5-3.0 kbar and 650-680°C. The observation that inferred retrograde reactions represent reversals of the prograde heating reactions suggests that the terrane underwent a near-isobaric heating-cooling path. However, the existence of a sillimanite fabric *postdating* melt crystallisation in Cackleberry Metamorphics is not consistent with a simple isobaric heating-cooling path and suggests either an increase in pressure at or soon after the thermal peak, or a second independent higher pressure event. In summary, the metamorphics of the Mopunga Range region are interpreted to have undergone a near-isobaric, possibly anti-clockwise P-T evolution at pressures of 2.5-4.0 kbar.

Harts Range Group

Field observations

Scattered outcrops of metasediments that occur south of the Entire Point Shear Zone (EPSZ) were mapped as the Irindina Supracrustal Assemblage of the Harts Range Group by Shaw *et al* (1984). The following description refers only to rocks of the Harts Range Group that occur within 5 km of the Kanandra Granulite in the Huckitta area. This region lies along strike from the Harts Range Group in the Mallee Bore region, where Miller *et al* (1997) documented metamorphism of 8-12 kbar and >800°C, which has been dated at 480-460 Ma (Mawby *et al* 1999, Buick *et al* in press). As part of this study, outcrops were sampled south of the Marshall River between Yam Creek Bore and Halfway Dam, and in the vicinity of the Dneiper-Huckitta boundary fence. A small number of outcrops were also visited between the Marshall River and Mt Sainthill. For the purpose of this description, fabrics in the Harts Range Group have been designated $S_{1h\text{-}3h}$, to distinguish them from $S_{1\text{-}3}$ in the Kanandra Granulite.

The Harts Range Group in the Huckitta area consists mostly of migmatitic, dominantly metasedimentary gneiss. Rock types include abundant biotite ± garnet bearing felsic and semi-pelitic gneiss, subordinate metabasite, garnet-hornblende-biotite gneiss, metapelite and calc-silicate rock, and rare quartzite and marble. The mineral assemblage in pelitic migmatite comprises garnet, biotite, sillimanite, quartz, K-feldspar and plagioclase. The peak mineral assemblage in metabasite comprises garnet-hornblende-plagioclase ± clinopyroxene ± quartz with garnet-bearing leucosomes (Figure 18; NQ542810), although more commonly metabasite is recrystallised to hornblende-plagioclase amphibolite. Calc-silicates typically contain scapolite, diopside, quartz, calcite, anorthite and titanite (eg NQ403816). Grossular garnet locally occurs in calc-silicates with scapolite, quartz, plagioclase and hornblende. Coarsely crystalline quartzite occurs at NQ581812 and 657812. Metamorphic grade in the Harts Range Group is transitional granulite facies, with widespread retrogression to upper amphibolite facies. Metapelite locally shows retrogression to greenschist facies muscovite and chlorite bearing assemblages. This retrogression is spatially related to late pegmatite intrusion and accompanying fluid flow (eg NQ523773).

The sequence is dominated by a planar fabric (S_{2h}), which has transposed an earlier migmatitic layering (S_{1h}). Boudins of metabasite within the fabric contain garnet and clinopyroxene leucosomes that pre-date S_{2h}. Garnet-bearing leucosomes also occur within metapelites, although these are typically transposed into S_{2h}. The S_{2h} fabric dips moderately to the northwest and has shallow southwest plunging, mineral elongation lineations (L_{2h}). The foliation S_{2h} is locally folded by moderately to shallowly west-plunging, tight folds that are inclined to the north and also fold L_{2h}. Mafic lithologies have recrystallised in S_{2h} to hornblende amphibolite with rare garnet, whereas pelite has recrystallised to biotite-sillimanite-garnet assemblages.

A steep south-dipping mylonitic fabric (S_{3h}) is strongly developed in the Harts Range Group within 1 km of its contact

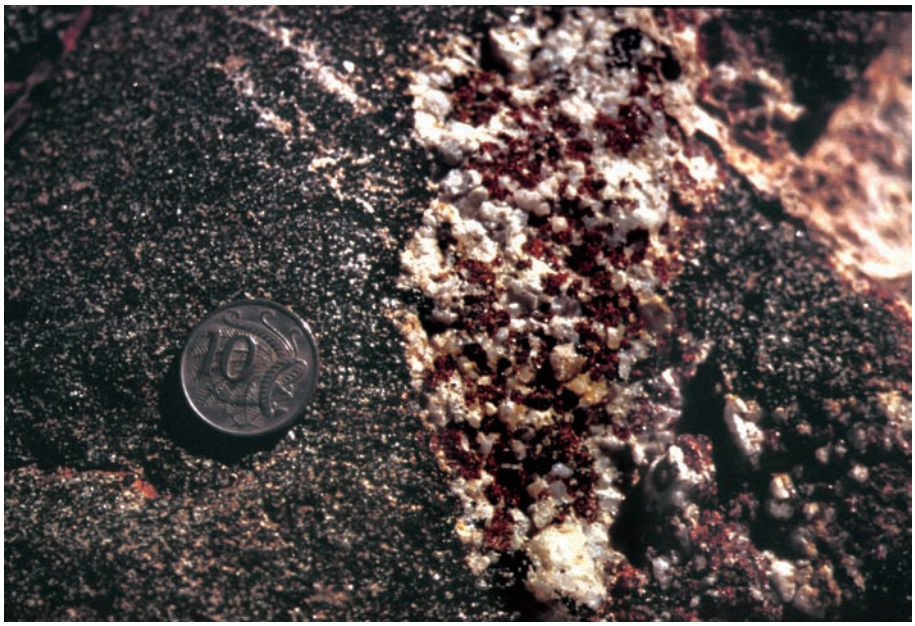

Figure 18 Metabasite in Harts Range Group containing garnet-bearing leucosome (NQ541810)

with the Kanandra Granulite. Metapelite has a biotite-sillimanite ± garnet fabric that envelops porphyroclastic garnet, quartz and feldspar, and has a shallow west plunging sillimanite lineation. A good section from the Harts Range Group into the Kanandra Granulite is exposed 2-3 km south of Mt Sainthill. In this region the S_{3h} fabric intensifies to the north into a 250 m wide mylonite zone comprising the EPSZ, that separates Harts Range Group from Kanandra Granulite. This fabric continues to the north, where it becomes S_{3b} in Kanandra Granulite.

P-T estimates

Pressure-temperature estimates of peak metamorphism in the Harts Range Group were obtained from two samples, a metapelite (HU140) containing garnet ($Alm_{67}Py_{19}Grs_{9}Sps_{6}$), biotite ($X_{Fe}$=0.50), sillimanite, plagioclase (An_{46}), quartz and K-feldspar; and a metabasite (HU139) containing garnet ($Alm_{53}Py_{10}Grs_{32}Sps_{5}$), hornblende ($X_{Fe}$=0.52), clinopyroxene ($X_{Fe}$=0.46), plagioclase ($An_{40}$) and quartz. Temperature estimates for sample 140 are 798-832°C at 9 kbar using the garnet-biotite thermometer of Hodges and Spear (1982). The GASP barometer of Hodges and Crowley (1985) gives 9.2-9.5 kbar (at 800°C). The Grt-Bt-Pl-Qtz barometer of Hoisch (1990) gives 9.4 kbar and 9.3 kbar for the Mg and Fe end-members, respectively. For sample 139, the Grt-Cpx-Pl-Qtz barometer of Newton and Perkins (1982) gives 9.0 kbar, while the Grt-Hbl-Pl-Qtz barometer of Kohn and Spear (1990) gives 9.0 and 11.2 kbar for the Fe and Mg end-members respectively. Average P-T estimates using Thermocalc give 772 ± 85°C and 8.4 ± 1.4 kbar for sample HU139, and 793 ± 57 and 8.5 ± 1.4 kbar for sample HU140 (1σ, aH_2O=0.8). These estimates are consistent with experimental studies on garnet-producing melting reactions for pelitic and mafic compositions similar to those of the Harts Range Group (Le Breton and Thompson 1982, Wyllie and Wolf 1993, Wolf and Wyllie 1994). They are also consistent with P-T estimates of peak metamorphism in the Harts Range Group in the Harts Range, 60-120 km to the southwest of the Huckitta area (800°C, 10.5 kbar; Mawby *et al* 1999) and Mallee Bore region, 80 km to the west (800-875°C, 8-12 kbar; Miller *et al* 1997; Figure 1).

GEOCHRONOLOGY

A combination of geochronological techniques has been used to place age constraints on the metamorphic and structural evolution of the Huckitta region. The location of samples is shown in Figure 23, and a complete list of all geochronological data from HUCKITTA is given in Table 1.

SHRIMP U-Pb geochronology

Three samples from HUCKITTA were selected for SHRIMP U-Pb dating as part of this study. Zircon dating in the Deep Bore Metamorphics and Kanandra Granulite was undertaken by Julie Smith (AGSO) as part of the NTGS-AGSO geochronology project (Smith 2000a), while monazite dating of the Entire Point Shear Zone was performed by Richard Armstrong (PRISE, Australian National University).

Unit	Sample	Easting	Northing	Method	Age (Ma)	Interpretation	Source*
Delny SZ	HU255m	53 541 512	7 488 350	Ar-Ar muscovite	349 ± 2	cooling through about 350°C	1
Harts Range Group	HU279m	53 552 300	7 477 280	Ar-Ar muscovite	349 ± 2	cooling through about 350°C	1
Delny SZ	HU241	53 555 841	7 485 486	Ar-Ar muscovite	350 ± 3	cooling through about 350°C	1
Delny SZ	HU250	53 540 724	7 486 616	Ar-Ar muscovite	356 ± 2	cooling through about 350°C	1
Delny SZ	HU251	53 541 088	7 489 774	Ar-Ar muscovite	362 ± 3	deformation	1
Harts Range Group	-	53 547 480	7 470 600	K-Ar biotite	363 ± 4	cooling through about 350°C	4
Delny SZ	HU253	53 541 083	7 490 275	Ar-Ar muscovite	364 ± 3	deformation	1
Delny SZ	HU243m	53 555 260	7 484 611	Ar-Ar muscovite	366 ± 2	cooling through about 350°C	1
Harts Range Group	HU263	53 553 070	7 482 740	Ar-Ar hornblende	390 ± 5	deformation/cooling	1
Entire Point SZ	HU156	53 555 640	7 484 400	Ar-Ar hornblende	403 ± 10	cooling through about 500°C	1
Harts Range Group	HU279h	53 552 300	7 477 280	Ar-Ar hornblende	417 ± 10	cooling through about 500°C	1
Entire Point SZ	HU156	53 555 640	7 484 400	Sm-Nd mineral isochron	434 ± 6	cooling through about 650°C	1
Entire Point SZ	HU237	53 552 475	7 484 190	SHRIMP U-Pb monazite	445 ± 5	deformation	1
Cackleberry Mets	93-10	53 548 900	7 490 000	K-Ar biotite	1550 ± 18	cooling through about 350°C	4
Kanandra Granulite	HU284	53 557 130	7 486 080	Ar-Ar hornblende	1552 ± 14	cooling through about 500°C	1
Cackleberry Mets	93-12	53 548 900	7 490 000	K-Ar hornblende	1595 ± 18	cooling through about 500°C	4
Cackleberry Mets	HU252	53 541 421	7 490 490	Ar-Ar hornblende	1601 ± 10	cooling through about 500°C	1
Kanandra Granulite	HU283	53 555 305	7 483 840	Ar-Ar hornblende	1620 ± 12	cooling / excess Ar	1
Mt. Swan Granite	89-551	53 495 373	7 505 731	SHRIMP U-Pb zircon	1713 ± 7	granite intrusion	2
Bonya Schist	93JV79	53 610 500	7 485 000	Sm-Nd garnet	1720 ± 20	garnet growth during high-T fluid flow	3
Deep Bore Mets	HU30	53 557 342	7 490 500	SHRIMP U-Pb zircon	1730 ± 7	metamorphism	3
Bonya Schist	93JV79	53 610 500	7 485 000	Pb-Pb garnet	1750 ± 19	garnet growth during high-T fluid flow	1
Dneiper Granite	89-554	53 504 799	7 509 420	SHRIMP U-Pb zircon	1771 ± 15	granite intrusion	2
Jervois Granite	89-567	53 625 280	7 485 660	SHRIMP U-Pb zircon	1771 ± 6	granite intrusion	2
Deep Bore Mets	HU30	53 557 342	7 490 500	SHRIMP U-Pb zircon	1805 ± 7	maximum protolith age	1

*Source: 1 – this study; 2 – Zhao & Bennett 1995; 3 - Cartwright et al 1997; 4 - J. Mawby, unpublished data. Location data for Cartwright et al (1997) and Mawby (unpublished data) are approximate. Data from this study is accurate to within 100 m. Mets – Metamorphics; SZ – Shear Zone.

TABLE 1. Summary of all geochronological data from HUCKITTA.

Zircon, Deep Bore Metamorphics

The sample selected for SHRIMP dating from the Deep Bore Metamorphics is a Crd-Bt-Opx-Ksp-Qtz gneiss (sample HU30, NQ573905). It contains coarse cordierite porphyroblasts with spinel, magnetite and sillimanite inclusions, within discrete segregations of K-feldspar-quartz leucosome that are weakly aligned in the regional fabric (Figure 10). The mesosome of the rock comprises quartz, cordierite, biotite, K-feldspar, magnetite and orthopyroxene. The sample was selected to help constrain the history of the protolith and metamorphism in the region. The analytical methods are outlined in Scrimgeour *et al* (in press). The majority of the zircons in this sample are subhedral, with a length to width ratio of 2:1, and a mean length of 150 µm. Less commonly, zircons are euhedral, approximately 200 µm long with a length to width ratio of 3:1. Cathodoluminescence imaging shows that most of the grains have unzoned weakly luminescent rims. The cores have oscillatory or irregular zones and are locally embayed. Zircon rims have low Th/U (0.006-0.031) in comparison with cores (0.323-0.614).

Thirty-eight analyses were made on thirty-one grains. The analytical data are summarised in Appendix 4 and are plotted on a concordia diagram in Figure 19. Three analyses were discarded from the pooled ages because of discordance. Two analyses (408.1 and 425.1) obviously contain inheritance and another analysis (401.1) also contains a component of inheritance as interpreted from the cathodoluminescence image. Two distinct populations have been identified in the Deep Bore zircons based on imagery, chemistry and age (Figure 19). The core age population and rim age population both have chi-square values that indicate single populations (1.59 and 0.86 respectively). The core population has a weighted mean $^{207}Pb/^{206}Pb$ age of 1805 ± 7 Ma (tσ) based on twenty concordant analyses. Analyses of the rim population gives a weighted mean $^{207}Pb/^{206}Pb$ age of 1730 ± 7 Ma (tσ) based on twelve concordant analyses.

The aluminous and heterogeneous nature of the Deep Bore Metamorphics indicates a sedimentary precursor, and therefore the detrital zircon cores with an age of 1805 ± 7 Ma provide a maximum age of deposition. The homogeneous nature of the detrital zircon population suggests a volcaniclastic origin, in which case the 1805 Ma age would represent the time of deposition. This is within error of the age of volcaniclastic sedimentation of the Patmungala Beds in the northern Arunta Province on MOUNT DOREEN at 1799 ± 7 Ma (Young *et al* 1995). It also provides further evidence for a major 1805 Ma magmatic event throughout the northern Arunta Province and Tanami Region. In the northern Arunta Province, the Barrow Creek Granite Suite has been dated at 1803 ± 6 and 1809 ± 5 Ma (Hussey *et al* 1999), while the Yaningidjara Orthogneiss in the Reynolds Range intruded at 1806 ± 6 Ma (Vry *et al* 1996). Similarly in the Tanami Region, recent SHRIMP U-Pb dating (Smith 2000b) indicates widespread granite intrusion at 1805 Ma.

The rim population is interpreted to represent a metamorphic age based on the lack of zoning, very low Th/U ratios, and the single age population (Rubatto *et al* 1999, Rubatto and Gebauer 2000). The 1730 ± 7 Ma age provides further evidence for high grade Palaeoproterozoic metamorphism in the eastern Arunta Province at this time. It is within error of Pb-Pb and Sm-Nd ages of 1720 ± 20 and 1750 ± 19 Ma, respectively, for garnets in skarn that were interpreted by Cartwright *et al* (1997) to have grown during cooling after peak metamorphic conditions in the Jervois region on HUCKITTA. This age is also in agreement with SHRIMP U-Pb zircon ages of 1727 ± 2 Ma for a concordant leucosome in granulite at Edwards Creek (Möller *et al* 1999), and 1728 ± 3 Ma for the syn-tectonic Wuluma Granite (Lafrance *et al* 1995), both of which are in the Strangways Range. It is also in accord with a conventional U-Pb age of 1730 ± 1 Ma for U-rich zircons within an amphibolite from the Entia Gneiss Complex in the Harts Range (Cooper *et al* 1998), and is within error of a possible metamorphic age of 1715 ± 19 Ma for the Atneequa Granitic Complex south of the Harts Range (Zhao and Bennett 1995). In general, the geochronological data suggests that high grade metamorphism in the Deep Bore Metamorphics forms part of the regionally extensive Late Strangways Event (Black and Shaw 1992, Collins and Shaw 1995).

Zircon, Kanandra Granulite

Zircon from a semipelitic migmatite in the Kanandra Granulite (sample HU195, NQ426863) was dated in order to characterise the detrital population and define the timing of metamorphism. The dated rock contained quartz, K-feldspar, plagioclase, biotite, garnet, ilmenite and rare sillimanite-bearing layers. Leucosomes defined a fabric that was transposed into a granulite facies, high strain S_2 fabric.

A total of 52 detrital zircon cores were analysed, with most analyses giving ^{207}Pb-^{206}Pb ages of 1820-2000 Ma (Figure 20). Two grains give Archaean ages (2500 Ma). The most abundant zircon population has Pb-Pb ages of 1850-1880 Ma, while the youngest analysed zircon has a Pb-Pb age of 1817 ± 15 Ma. This is interpreted to be the maximum age of deposition for the sedimentary protolith of the Kanandra Granulite. The detrital zircon population may have undergone partial resetting of the U-Pb system at 1820 Ma (Smith 2000a). Metamorphic rims were too narrow for an age to be calculated, but the three youngest analyses are interpreted as reflecting metamorphic

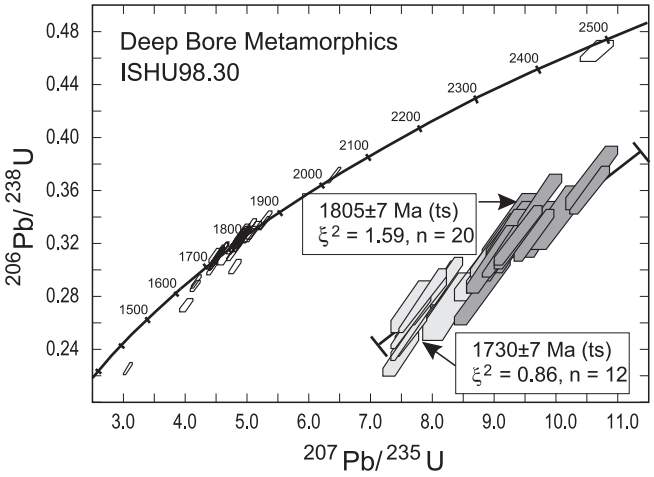

Figure 19 U-Pb concordia plot of SHRIMP data for the Deep Bore Metamorphics. Dark shaded and light shaded analyses were used in the calculation of the $^{207}Pb/^{206}Pb$ age of the cores (1805 ± 7 Ma) and rims (1730 ± 7 Ma) respectively. Error ellipses are 1σ for each analysis. Concordia curve is labelled in Ma

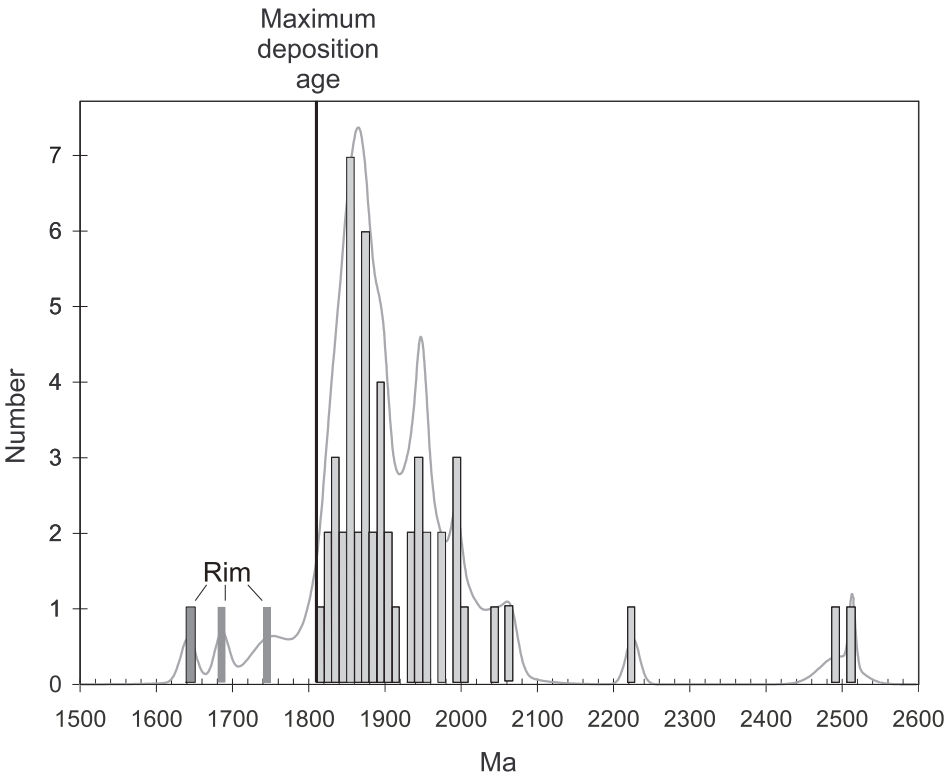

Figure 20 Cumulative probability histogram of zircons analysed from Kanandra Granulite (sample HU195), showing a maximum depositional age of about 1817 Ma

growth between 1642 and 1747 Ma. As the Late Strangways Event is the only known metamorphic event within this time interval in the eastern Arunta Province, it is interpreted that metamorphism of the Kanandra Granulite occurred at 1730-1720 Ma.

Monazite, D_3 mylonite, Kanandra Granulite

An S_{3b} mylonite reworking the Kanandra Granulite (sample HU237, NQ525842) was selected to date upper amphibolite facies mylonitic deformation in the Entire Point Shear Zone. Fine-grained biotite, sillimanite, quartz, K-feldspar, plagioclase, and minor ilmenite and muscovite define the mylonitic fabric. Most garnet is porphyroclastic, but smaller subhedral garnet occurs in the fabric. In thin section, monazite occurs as small rounded grains that are 5-100 µm in diameter and aligned in the fabric. The lineation on the mylonitic fabric plunges moderately towards 265°. Thermobarometry on the mylonitic assemblage yielded 700°C and 7 kbar. The analytical methods used are outlined in Scrimgeour and Raith (in press).

The sample yielded clear, light yellow monazite of good quality. The separated monazite grains were of variable size and form, but were generally quite rounded, and BSE imaging showed some zonation. Sixteen analyses on eleven different monazites (Appendix 4) are plotted on a conventional Wetherill U-Pb concordia diagram (Figure 21) and within the measured uncertainties, all analyses conform to a single concordant age population. Pb-Pb, Th-Pb and U-Pb ages can be calculated for this dataset and all show that the monazite grains are 445 Ma old and that there are no older (inherited) grains or parts of grains. The calculated ages are listed in Appendix 4. Although there is some variation in the three ages calculated, they do agree within the 95% confidence limits cited. Taking all data points into account, the 'Concordia Age' for these monazites as calculated using Isoplot/Ex (Ludwig 1998, 1999) is 445 ± 5 Ma (2σ error, including decay constant error; MSWD calculated for concordance and equivalence = 0.57, probability = 0.97). This age is interpreted to represent the timing of crystallisation of monazite at upper amphibolite conditions within the EPSZ.

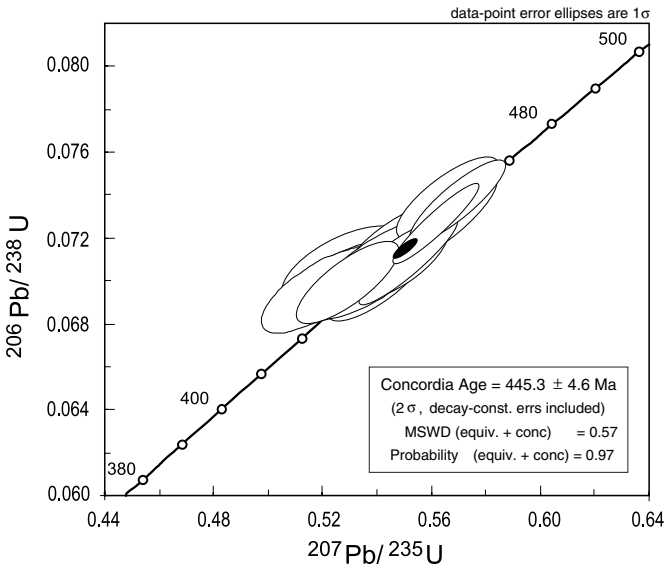

Figure 21 U-Pb concordia plot of SHRIMP monazite data for sample HU237 from the Entire Point Shear Zone. The black ellipse shows the calculated Concordia Age. Concordia curve is labelled in Ma

Sm-Nd geochronology

Garnet amphibolite (D_3), Kanandra Granulite

Sample HU156 is a mafic rock from the Kanandra Granulite (NQ556844), which contains the M_{3a} assemblage of garnet-hornblende-plagioclase-quartz with less abundant ilmenite and apatite. It occurs within a large region of Kanandra Granulite that escaped intense S_{3b} mylonitisation (Figure 23) and contains a weakly defined S_{3a} fabric with a south-southeast plunging

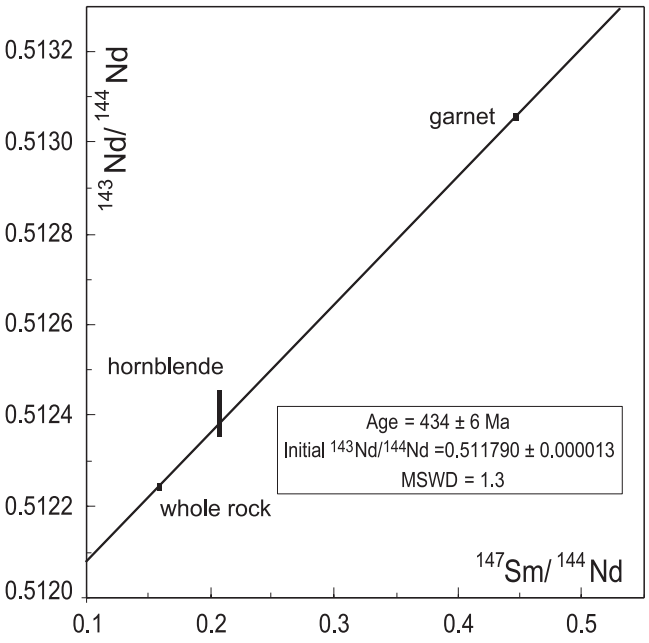

Figure 22 Sm-Nd garnet-hornblende-whole rock isochron for sample ISHU98.156, Kanandra Granulite

mineral lineation. Although the S_{3a} fabric is locally overprinted by subsequent S_{3b} mylonites, the sample selected for dating has no overprinting fabric. The texture is granoblastic with a grainsize typically between 0.3-1.5 mm. Garnet contains numerous inclusions of hornblende, quartz and plagioclase, while hornblende locally has inclusions of quartz. Sm-Nd analysis was performed on Finnigan MAT 261 and 262 mass spectrometers at the University of Adelaide. Sample preparation and analytical techniques follow those of Mawby *et al* (1999). Typical internal precision on the La Jolla Nd-standard during the course of the study was 0.511835 ± 20 (2σ). The Sm and Nd blanks contribution was 0.3 ng. Isochron calculations follow Ludwig (1999). The results of Sm-Nd isotopic analysis of sample HU156 are presented in Figure 22 and Appendix 4, and give an 3-point garnet-hornblende-WR mineral isochron age of 434 ± 6 Ma.

Given the SHRIMP U-Pb age of 445 ± 5 Ma for monazite growth during M_{3b}, the Sm-Nd age of 434 ± 6 Ma for the M_{3a} assemblage appears to be inconsistent with field and petrological evidence suggesting that M_{3a} predates M_{3b}. There are at least two explanations for this inconsistency. A problem in the interpretation of Sm-Nd mineral isochrons is uncertainty relating to the closure temperature of the Sm-Nd in garnet, which may be as low as 600-650°C (Burton *et al* 1995) or as high as 750-800°C, depending on factors such as grain size and cooling rate (Becker 1997). An additional source of uncertainty in comparing U-Pb monazite and Sm-Nd garnet ages in upper amphibolite facies rocks is the relative timing of monazite growth, which is controlled by monazite-producing mineral reactions that do not necessarily coincide with the peak of metamorphism (Lanzarotti and Hanson 1996). In spite of these uncertainties, we propose that the most likely interpretation of the geochronological data is that the monazite age reflects the timing of D_{3b} mylonitisation, and the Sm-Nd age reflects cooling through the closure temperature following peak conditions at 445 Ma. This interpretation is supported by the slow rate of cooling following M_{3b} (see discussion below), and the relatively fine grain size of garnet in sample HU156 (0.5-1 mm), both of which lead to a lowering in the closure temperature of Nd in garnet (Becker 1997).

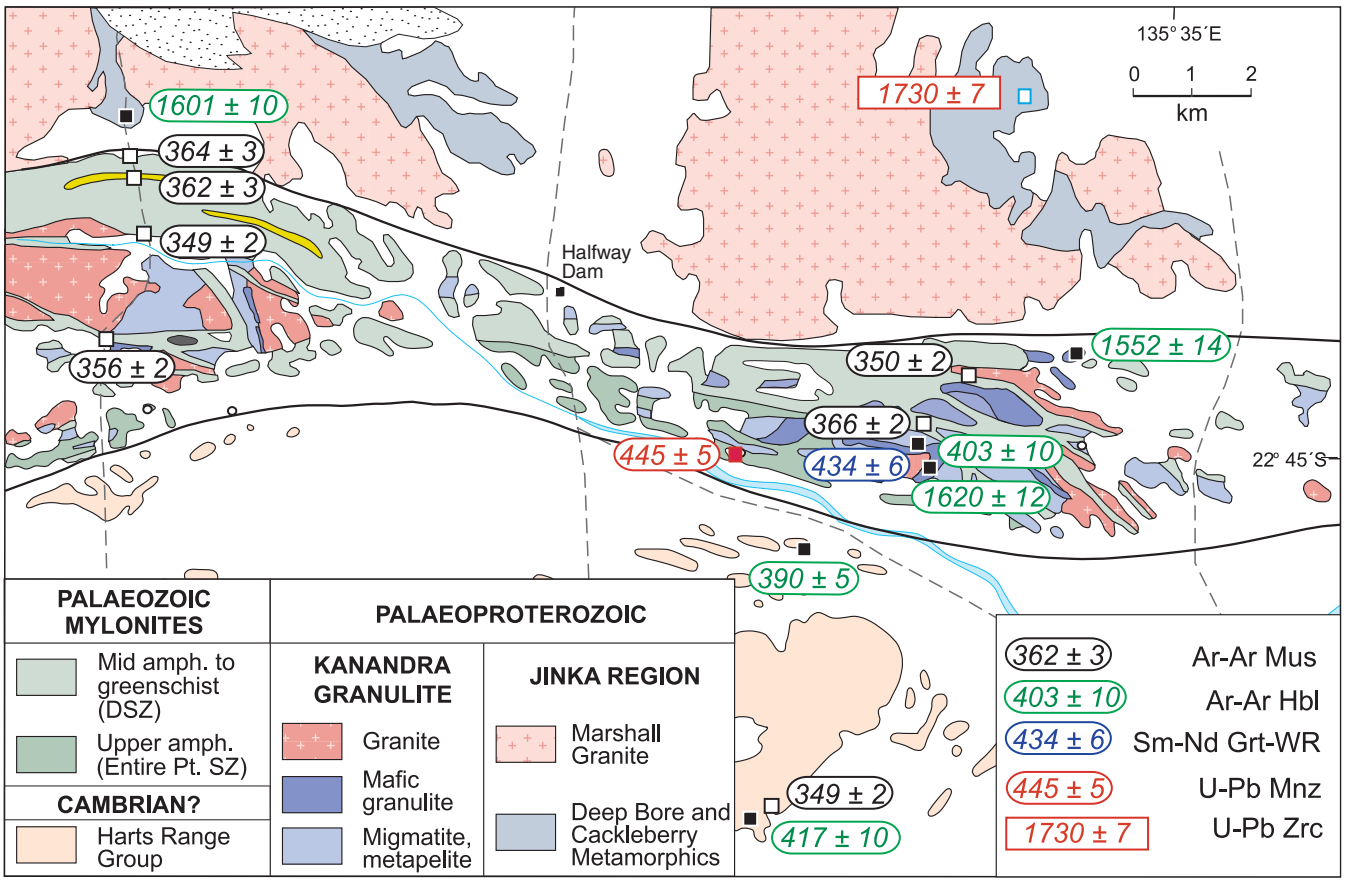

Figure 23 Map of Huckitta Station region showing locations of samples for U-Pb, Sm-Nd and Ar-Ar geochronology

^{40}Ar-^{39}Ar geochronology

^{40}Ar-^{39}Ar step heating analysis of hornblende and muscovite was undertaken to date low grade deformation in the Delny Shear Zone, as well as the timing of cooling through 500-550°C and 350-420°C across the terrane. ^{40}Ar-^{39}Ar spectra of all analysed samples are given in Figures 24 and 25.

Timing of deformation – DSZ

Samples of chlorite-muscovite-quartz phyllite were collected from along the Dneiper-Huckitta fenceline track near the northern margin of the DSZ. These schists represent the lowest grade mylonites in the DSZ and are interpreted to have crystallised under greenschist facies conditions. ^{40}Ar-^{39}Ar analyses of muscovite separated from these two samples (HU251 and 253) provide well defined plateau ages of 362 ± 3 Ma and 364 ± 3 Ma. These ages probably give the timing of muscovite crystallisation, and therefore also of deformation, and reflect the final stage of ductile movement on the DSZ.

Timing of cooling and exhumation

Kanandra Granulite and EPSZ

Two sampling traverses were made across the Kanandra Granulite, where it is variably reworked by the EPSZ and DSZ, to assess the timing and rate of Palaeozoic cooling. Five

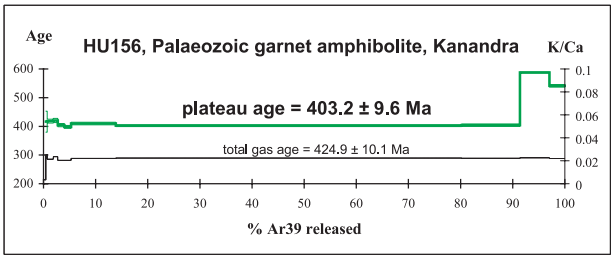

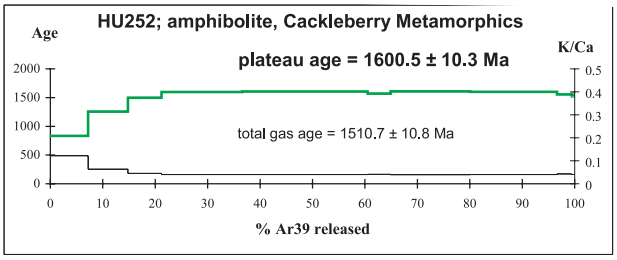

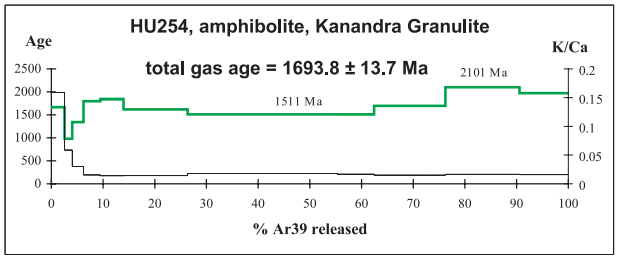

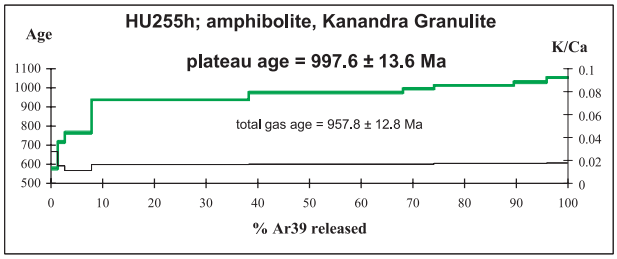

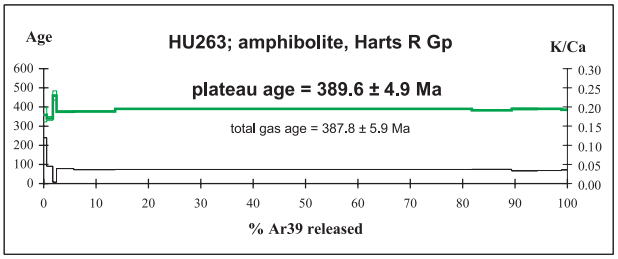

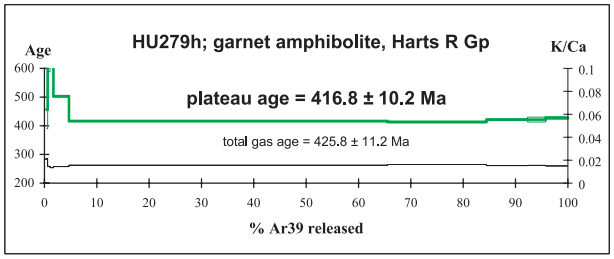

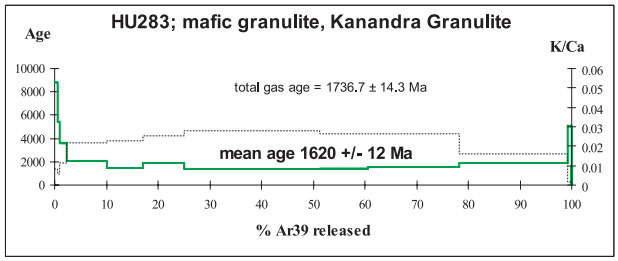

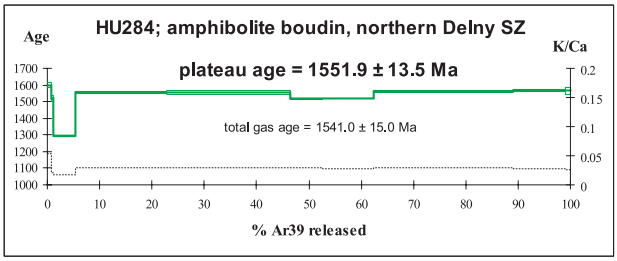

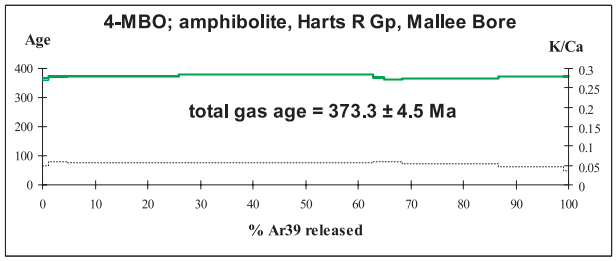

Figure 24 ^{40}Ar-^{39}Ar spectra from hornblende, HUCKITTA

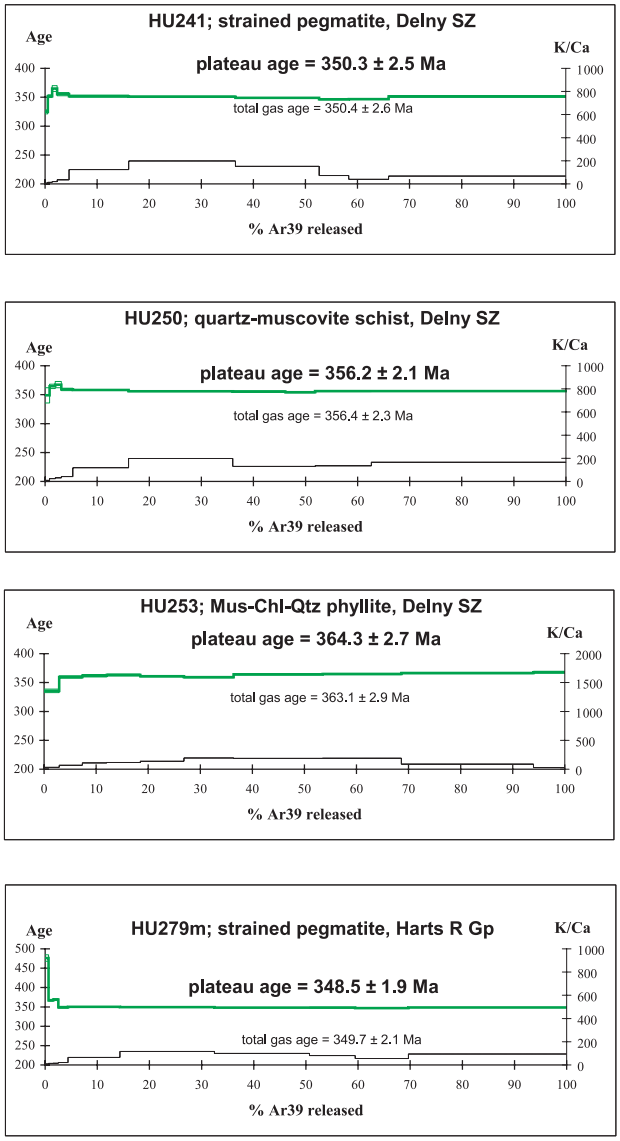

Figure 25 ^{40}Ar-^{39}Ar spectra from muscovite, HUCKITTA

hornblende samples were analysed, including a sample from the same garnet-hornblende amphibolite in the EPSZ that yielded a Sm-Nd isochron of 434 ± 9 Ma (HU156). The Ar-Ar age of hornblende from HU156 of 403 ± 10 Ma is interpreted to reflect cooling through 500-550ºC following Ordovician metamorphism. In contrast, hornblende separated from a nearby mafic granulite (HU283) has an Ar-Ar age of 1620 ± 12 Ma, and reflects Proterozoic cooling, although it should be noted that this result is possibly modified by a Palaeozoic input of radiogenic Ar. Hornblende from a boudin of granulite from the northern DSZ (HU284) gives an Ar-Ar plateau age of 1552 ± 14 Ma, interpreted to reflect cooling through 500-550ºC. Two samples of amphibolite from boudins within the DSZ show partial resetting and have erratic spectra with geologically meaningless ages of 1693 ± 14 and 998 ± 14 Ma.

Four muscovite separates from within the DSZ and EPSZ show much more consistent plateau ages that cluster from 349 ± 2 Ma to 366 ± 4 Ma. These give the probable timing of cooling through 350-420°C and are interpreted as reflecting exhumation due to late Devonian deformation on the DSZ.

Harts Range Group – Mallee Bore

Hornblende from garnet-hornblende metabasite (MBO-4) from the Harts Range Group at Mallee Bore in ALCOOTA gives a well defined ^{40}Ar-^{39}Ar plateau age of 373 ± 5 Ma. Previous SHRIMP U-Pb zircon and monazite geochronology at Mallee Bore, has shown that high grade metamorphism occurred at 480-460 Ma (Miller *et al* 1998, Buick *et al* in press). Buick *et al* also identified two generations of titanite at Mallee Bore. An early generation of titanite gave a SHRIMP U-Pb age of 420-410 Ma, interpreted to reflect cooling following Ordovician metamorphism, whereas titanite in a late, relatively low-T shear zone gave a U-Pb age of 390-380 Ma. This younger titanite age was interpreted as reflecting the timing of shearing during the Alice Springs Orogeny. The 373 Ma hornblende age from this study therefore is interpreted to reflect cooling following deformation at 390-380 Ma.

Harts Range Group – Huckitta

Hornblende from a highly strained amphibolite of the Harts Range Group immediately south of the EPSZ (HU263), has yielded a plateau age of 390 ± 5 Ma. Further south, a hornblende ± garnet amphibolite (HU279h) has given an older plateau age of 417 ± 10 Ma. Immediately adjacent to the sample site of HU279h, a metapelite next to strained pegmatites has undergone retrogression to muscovite and chlorite assemblages. Muscovite related to this retrogression has provided an Ar-Ar plateau age of 349 ± 2 Ma. This age may relate directly to the age of pegmatite intrusion, or it may reflect subsequent cooling.

Two interpretations for the differing hornblende ^{40}Ar-^{39}Ar ages of 417 ± 10 and 390 ± 5 Ma from the Huckitta region are possible. There may be a difference in the timing of cooling through 500-550°C following Ordovician metamorphism. Alternatively, it is possible that the 417 Ma age reflects cooling following Ordovician metamorphism, whereas the 390 Ma age reflects a subsequent recrystallisation event early in the Alice Springs Orogeny, similar to the interpretation of the two generations of titanite at Mallee Bore. The latter scenario appears to be more likely, given that the 390 Ma age is derived from a recrystallised high strain zone, and that deformation of this age has been recorded throughout the eastern Arunta Province (381 ± 7 Ma, Strangways Range, Ballèvre *et al* 2000; 380-390 Ma, Mallee Bore, Buick *et al* in press).

Cackleberry Metamorphics

A hornblende-plagioclase amphibolite with a steeply east plunging mineral lineation was sampled within the Cackleberry Metamorphics about 100 m north of the northern margin of the DSZ. The amphibolite has a granoblastic texture in thin section, with partial alteration of plagioclase to sericite that may reflect proximity to the DSZ. Hornblende separated from this rock gives an ^{40}Ar-^{39}Ar age of 1601 ± 10 Ma, which is similar to a hornblende K-Ar age of 1595 ± 18 Ma obtained from amphibolite (sample 93-10) north of Halfway Dam by J Mawby (unpublished data). These dates strongly suggest that the Cackleberry Metamorphics cooled through 500-550°C at 1600 Ma. This is coincident with high grade metamorphism in the Reynolds Range region (Buick *et al* 1998) and the Chewings Orogeny in the southern Arunta Province (Collins and Shaw 1995), and suggests that the Mopunga Range underwent a thermal or exhumation event at this time. A K-Ar biotite age of 1550 ± 18 Ma from a foliated monomineralic rock (sample 93-12, Mawby, unpublished data) suggests relatively slow cooling following the 1600 Ma event.

DISCUSSION

The Late Strangways Event in the northeastern Arunta Province

Given the newly recognised regional extent of the Late Strangways Event and the current exposure of different crustal levels across the eastern Arunta Province, new insights can be gained into the thermal and tectonic evolution of the region. The 1730 ± 7 Ma age for peak metamorphism in Mopunga Range provides evidence that the Late Strangways Event was the dominant Palaeoproterozoic high-grade event throughout the eastern Arunta Province. While there are no precise constraints on the timing of high-grade metamorphism in the Kanandra Granulite, the existence of poorly defined metamorphic rims that grew between 1745-1642 Ma supports the notion that granulite facies metamorphism was synchronous with that in the Strangways Metamorphic Complex and the Deep Bore Metamorphics. Furthermore, the evolution of the Kanandra Granulite is very similar to that in the Edwards Creek region of the Strangways Range, where a peak M_1 assemblage (800°C, 6-8 kbar) is overprinted by a planar S_2 fabric with associated cooling textures (Warren 1983, Ballèvre *et al* 1997). SHRIMP U-Pb dating of zircons in leucosomes related to these two events by Möller *et al* (1999), derived ages of 1727 ± 2 Ma for M_1, and 1717 ± 2 Ma for M_2.

Regional extent of high-T, low-P metamorphism in the Jinka region

Figure 26 is an interpreted solid geology map of the northern margin of the eastern Arunta Province, showing the inferred extent of low pressure, metamorphosed supracrustal rocks and granites within the Jinka region (adapted from Shaw and Warren 1975, Freeman 1986). In the east, the Bonya Hills and Jervois Range were metamorphosed to lower and middle amphibolite facies at 2-3 kbar, although rare sillimanite occurrences and migmatite suggest localised increases in metamorphic grade (Shaw *et al* 1984). To the west of Mopunga Range, cordierite-orthopyroxene and cordierite-sillimanite granulites of the Perenti Metamorphics were estimated by Warren and Hensen (1989) to have been metamorphosed at 4 kbar, which is likely to be a maximum estimate given the lack of garnet within pelitic lithologies. Metamorphic grade decreases to the west-northwest and is upper greenschist to lower amphibolite facies in the Delmore Metamorphics (Shaw *et al* 1975; Figure 26). Therefore, the east-west extent of high-T, low-P metamorphism in the Jinka province is likely to be about 150 km. Across this terrane, metamorphic temperatures vary from 500°C to 800°C at pressures of 2-4 kbar (Dobos 1978, this study). Although the resolution of existing barometric data does not allow clear temperature-depth relationships to be established, it is likely that the documented variations in temperature partly reflect lateral changes in metamorphic grade, as is typical of most high-T, low-P terranes (Collins and Vernon 1991). However, in regions with more extensive outcrop such as the Bonya Hills and Cackleberry Metamorphics, there are no detectable changes in grade over distances of 5 km and this suggests that lateral temperature gradients during metamorphism were relatively low.

Tectonic implications, and possible heat sources for metamorphism

Temperatures of 750-800°C at 3 kbar for the Deep Bore Metamorphics imply remarkably high thermal gradients of 65-75°Ckm^{-1} in the upper crust. Many low pressure granulite-amphibolite terranes, particularly at pressures below 4 kbar, are spatially related to large igneous intrusions, most commonly as well defined contact aureoles (Pattison and Tracy 1991). However, the heat source for high-T, low-P metamorphism in the Mopunga Range region is less well defined, due the relatively sparse outcrop, poor field relationships and abundant intrusions of varying ages.

In the Strangways Range, the Late Strangways Event involved compressional deformation that occurred in either an intraplate (Goscombe 1992) or plate margin setting (Zhao and McCulloch 1995). The upright fabrics throughout the Jinka region are also consistent with upper crustal compression similar to most other Australian Proterozoic high-T, low-P terranes (Loosveld and Etheridge 1990, Collins *et al* 1991). Therefore, it is unlikely that metamorphism occurred during lithospheric extension as proposed for a number of very low-P granulite terranes (eg Dempster *et al* 1991). In the Mopunga Range, significant strain only occurred during or immediately after peak metamorphic temperatures were attained; deformation and maximum P-T conditions were essentially coeval. This suggests that metamorphism is unlikely to have occurred as a conductive response to deformation and crustal thickening, in which case metamorphism would have most

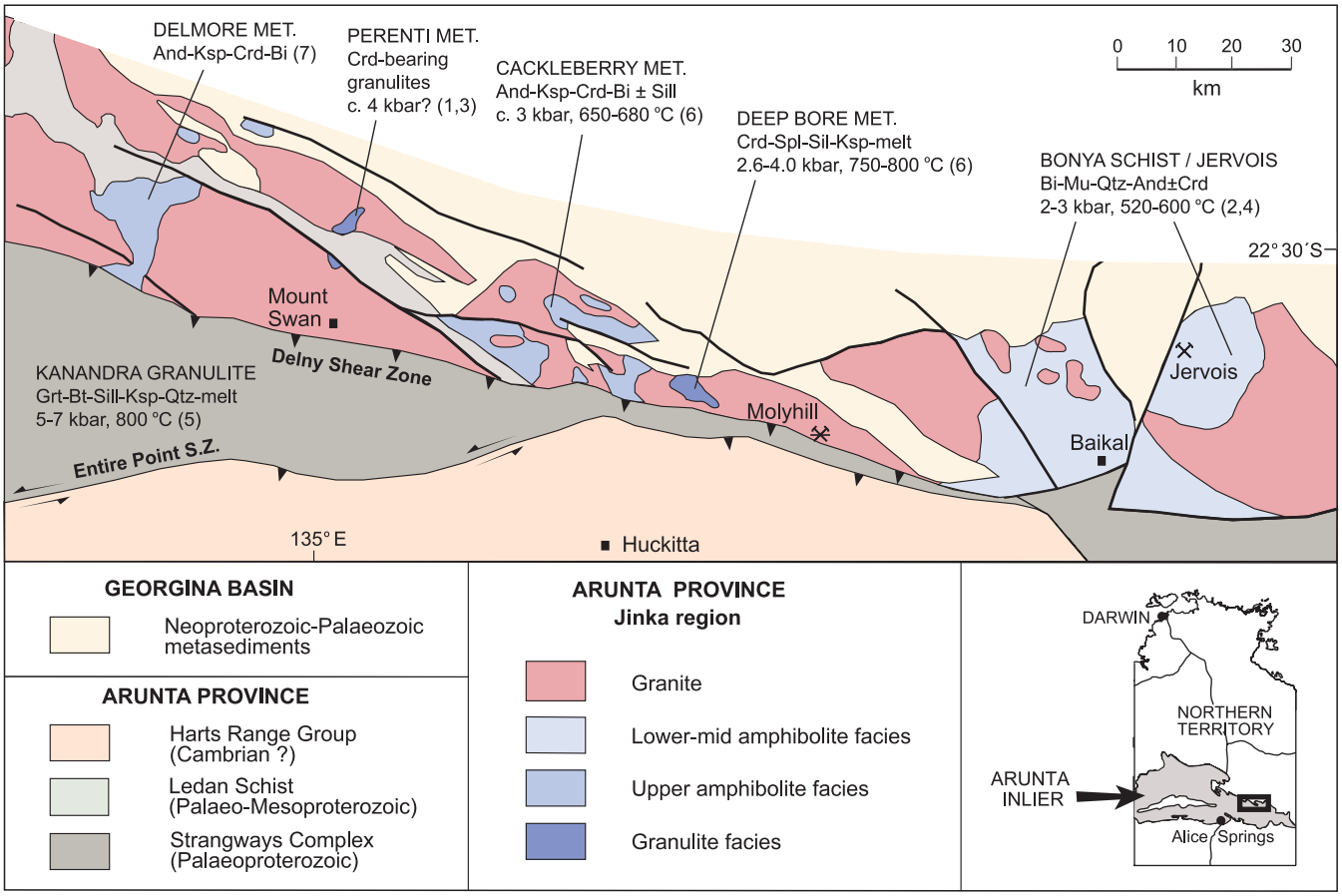

Figure 26 Solid geology map of the Jinka province, adapted from Shaw and Warren (1975) and Freeman (1986), showing diagnostic mineral assemblages in metapelites and P-T estimates (where available) for metamorphic units in the Jinka terrain. References: 1- Shaw *et al* (1984); 2 - Dobos (1978); 3 - Warren and Hensen (1979); 4 - Cartwright *et al* (1997); 5, 6 - this study; 7 - Shaw *et al* (1975)

likely outlasted deformation (De Yoreo *et al* 1991). The existence of high-T, low-P metamorphism during the Late Strangways Event suggests that crustal thickening must have been relatively limited (less than about 45 km), as denudation would otherwise have occurred below the levels currently exposed (Sandiford and Powell 1991). Such an interpretation is also consistent with isobaric cooling paths in Palaeoproterozoic granulites from all exposed crustal levels in the eastern Arunta Province. These imply a lack of significant vertical movement within the crust following peak metamorphism (for example Strangways Range, Ballèvre *et al* 1997; Kanandra Granulite, this study). Most exhumation of currently exposed middle to lower crust from the Late Strangways Event is interpreted to have occurred during later events, most notably during the Palaeozoic (Collins and Teyssier 1989).

The Jinka region is dominated by granite, which comprises more than half of the exposures (Figure 26). It includes voluminous granites belonging to the 1730-1710 Ma suite of Zhao and McCulloch (1995). Recent work by Sandiford and Hand (1998) has suggested that in many Australian Proterozoic high-T, low-P terranes, burial of high-heat producing granites beneath a sedimentary cover may have significantly contributed to the thermal perturbation. This ambient process may apply in regions such as the southeastern Reynolds Range (Figure 1), where high-T, low-P metamorphism was long-lived, had a clockwise P-T path (Buick *et al* 1998) and was spatially related to voluminous granite intrusions with high radiogenic heat production that intruded more than 100 Ma prior to metamorphism (Hand *et al* 1995). However, in the Mopunga Range and Kanandra Granulite, reaction textures suggest a cooling-dominated history following peak metamorphism, consistent with a relatively short-lived thermal event. Furthermore, high-T, low-P metamorphism was broadly synchronous with the intrusion of a regional, high radiogenic, heat-producing granite suite at 1730-1710 Ma (Zhao and McCulloch 1995), suggesting that long-lived radiogenic heating cannot be invoked as a heat source in the Mopunga Range. Therefore, magmatic advection of heat by the voluminous granites that dominate the Jinka province is considered a more likely heat source for high-T, low-P metamorphism. Intrusion of mafic bodies, such as the quartz norite in the vicinity of the Deep Bore Metamorphics (Shaw *et al* 1984), must also be invoked to account for the high temperatures associated with granulite facies metamorphism in the upper crust. This advective input of heat was superimposed on a regionally elevated geotherm, as shown by coeval granulite conditions that prevailed in the lower to middle crust in the Strangways Range, (Möller *et al* 1999).

The existence of elevated temperatures in the middle to lower crust, along with geochemical evidence for extensive partial melting of the lower crust (Zhao and McCulloch 1995) implies the existence of a mantle-derived thermal perturbation during the Late Strangways Event. A consequence of extensive lower crustal melting is the advection of magmas to the upper crust and this resulted in high-T, low-P "regional aureole" metamorphism and associated melt-enhanced deformation in the Mopunga Range. This is similar to models for high-T, low-

P metamorphism in the Anmatjira Range region of the northern Arunta as proposed by Collins and Vernon (1991) and Collins *et al* (1991). However, an important aspect of the high-T, low-P metamorphism in the Mopunga Range is that it is inferred to have been regionally extensive, and to have occurred synchronously with deeper crustal metamorphism and compressional deformation.

Palaeozoic tectonics in northeastern Arunta Province

450-440 Ma event in eastern Arunta Province

SHRIMP U-Pb dating of monazite from the Entire Point Shear Zone suggests that juxtaposition of the Harts Range Group and Kanandra Granulite occurred at 445 ± 5 Ma. This postdates peak metamorphism in the Harts Range Group, which has been dated at 480-460 Ma (Mawby *et al* 1999, Buick *et al* in press). There is no evidence for high-T deformation in the Kanandra Granulite during peak metamorphism of the Harts Range Group. Instead, evidence from this study shows that prograde heating and burial of Kanandra Granulite occurred at 450-440 Ma, following or during retrograde decompression of the Harts Range Group to 6-7 kbar (Figure 8 (b), Mawby *et al* 1999, Hand *et al* 1999*a*).

Transpressional deformation on the EPSZ at 445 ± 5 Ma forms part of a more widespread, newly recognized 450-440 Ma event in the eastern Arunta Province. In the Harts Range, metasediments of the Harts Range Group are separated from Palaeoproterozoic granulites of the Entia Gneiss Complex and Strangways Metamorphic Complex by shallowly dipping south-vergent detachments (the Bruna Detachment Zone and Florence-Muller Shear Zone; Ding and James 1985, Collins and Teyssier 1989, Hand *et al* 1999b). These south-directed thrusts (D_3 of Mawby *et al* 1999) formed at upper amphibolite facies and have Sm-Nd isochron ages of 448 ± 7 Ma and 445 ± 51 Ma. This postdates peak metamorphism of the Harts Range Group (Mawby *et al* 1999). Mawby *et al* interpreted D_3 in the Harts Range as reflecting a change from extensional to compressional deformation in the eastern Arunta Province. This is due to apparently south-directed reverse kinematics in D_3 shear zones (James *et al* 1989) as well as a change in the distribution of sedimentation in the surrounding basins at 450 Ma (Shaw *et al* 1991). P-T conditions during D_3 in the Harts Range were 600-650°C and 5-6 kbar (Mawby *et al* 1999) and this suggests that the EPSZ mylonites now exposed in the Huckitta area formed at deeper crustal levels than D_3 mylonites in the Harts Range.

Further evidence for an event at 450-440 Ma was provided by Möller *et al* (1999) who derived an age of 443 ± 6 Ma from zircon overgrowths in a staurolite-bearing shear zone in the Edwards Creek region in the Strangways Complex. Although no 450-440 Ma ages have yet emerged from the Mallee Bore area, Miller *et al* (1997) documented localised mylonitisation at 680-730°C and 5.8-7.7 kbar that overprints the peak metamorphic assemblage in the Harts Range Group (480-460 Ma, Miller *et al* 1998). These mylonites are tentatively correlated with other 450-440 Ma mylonites in the eastern Arunta Province, as they occur within 10-15 km of the inferred western continuation of the EPSZ. The apparently widespread distribution of mylonites of this age in the eastern Arunta Province indicates that the event that formed them was of regional significance. It led to the structural juxtaposition of the Harts Range Group and Entia Gneiss Complex against Proterozoic granulites that had experienced no previous high-grade Palaeozoic deformation. The evidence of new zircon growth in the Strangways Range at 445 Ma (Möller *et al* 1999) suggests that reworking of the Strangways Metamorphic Complex occurred at the same time (450-440 Ma) both north and south of Harts Range. The timing of the apparent onset of intraplate compressional deformation in the Arunta Province at 450-440 Ma is 40-50 Ma earlier than the traditionally accepted date of the onset of the Alice Springs Orogeny (400 Ma; Dunlap and Teyssier 1995).

Regional extent of Entire Point Shear Zone

On the basis of combined geological and geophysical evidence, the EPSZ is inferred to extend west into ALCOOTA, where it does not outcrop but is interpreted to pass immediately north of the Mallee Bore region and south of the Bleechmore Granulite. This inferred extension of the EPSZ is dextrally offset by the Woolanga Lineament and is reworked in the Wallaby Knob Schist. However, it can be traced on magnetic images as an east-west trending structure that truncates Proterozoic rocks and extends across the Arunta Province to the south of the Ngalia Basin (Figure 27). In the southwestern Arunta Province, this structure is known as the Desert Bore Shear Zone and it extends to the Western Australian border on northern MOUNT RENNIE. The correlation of the Desert Bore Shear Zone with the EPSZ remains tentative, but the linear nature of the former suggests that it is also a steeply dipping strike-slip structure.

Silurian-Devonian deformation, exhumation and cooling

The Alice Springs Orogeny is a long-lived intraplate event, with deformation occurring over a period of 100-150 Ma (Dunlap and Teyssier 1995, Hand *et al* 1999a). There is uncertainty as to whether deformation, metamorphism and exhumation were slow and continuous or episodic in nature. A complex episodic evolution has been postulated on evidence from surrounding sedimentary basins (Shaw *et al* 1991) and on the basis on differing ages for metamorphism in different regions (eg 343 ± 8 Ma for the Entia Dome, Hand *et al* 1999a; 381 ± 7 Ma for the Strangways Range, Ballèvre *et al* 2000). In addition, there are extreme variations in Palaeozoic cooling ages across the eastern Arunta. Data suggests that some regions (the southern Harts Range) had cooled through 500°C by 400 Ma while others (the Entia Dome) cooled through 500°C at 330 Ma (Dunlap and Teyssier 1995, Hand *et al* 1999a). Mawby *et al* (1998) suggested that the apparent northward younging of cooling ages might be attributable to exhumation on the DSZ relatively late in the Alice Springs Orogeny. However, Ar-Ar data presented in this study shows that the Huckitta region south of the DSZ cooled through 500°C at 420-400 Ma, at a similar time to the southwestern Harts Range. This indicates that the model of northward younging cooling ages towards the DSZ is not valid and that younger cooling ages in the Entia Dome are probably a localised effect.

Ar-Ar and Sm-Nd cooling ages for the Kanandra Granulite and northern Harts Range Group suggest a slow continuous cooling history extending from the late Ordovician to the late Devonian. In particular, a combination of U-Pb monazite, Sm-Nd garnet, Ar-Ar hornblende and Ar-Ar muscovite ages from the same area (the vicinity of HU156, NQ556844) suggests a

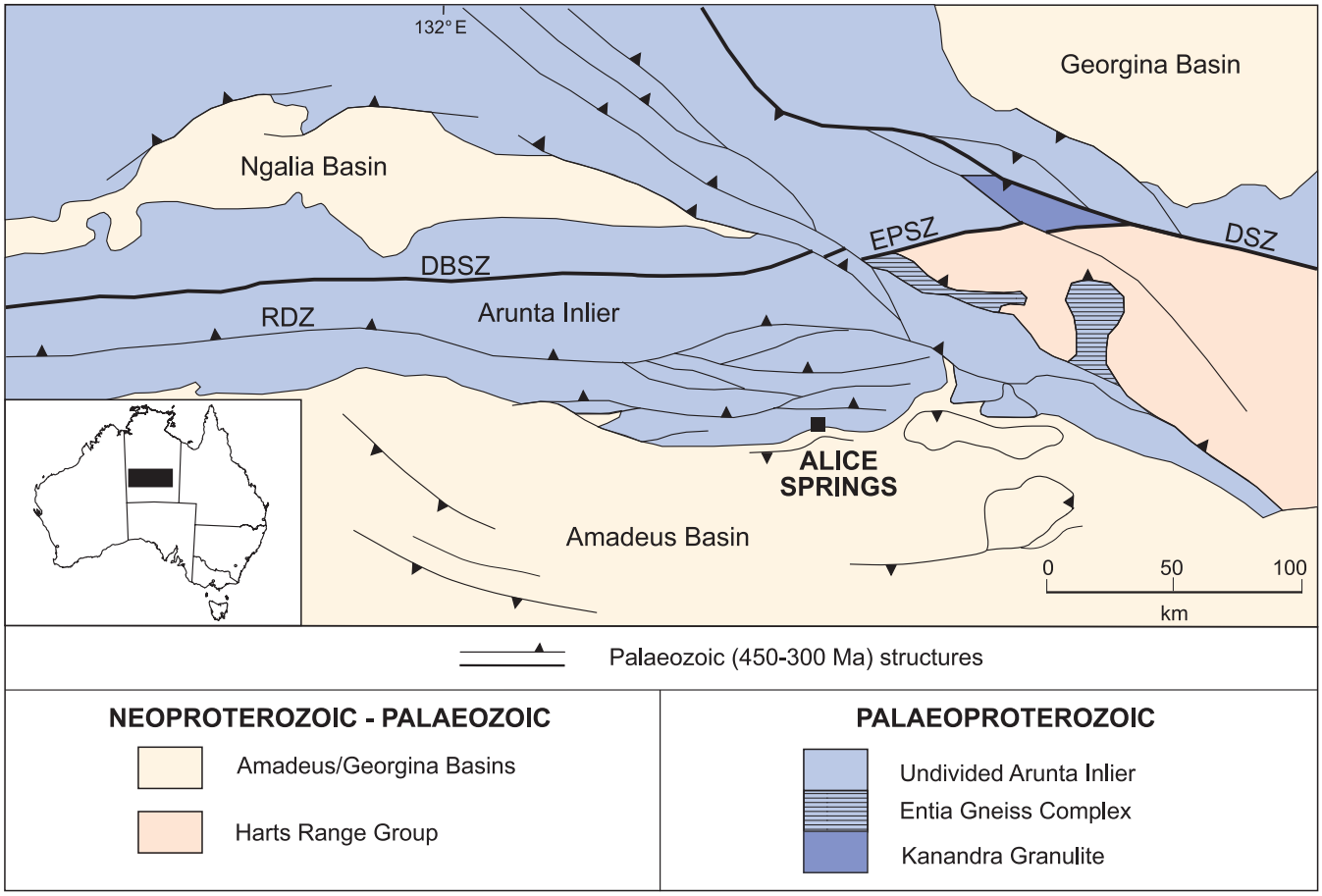

Figure 27 Map of the Arunta Province, showing the inferred extension of the Entire Point Shear Zone (EPSZ) to the west to form the Desert Bore Shear Zone (DBSZ). RDZ – Redbank Deformed Zone; DSZ – Delny Shear Zone

steady cooling rate of 4°CMa^{-1} over an 80 Ma period from 445 Ma (Figure 28). The presence of sillimanite, and P-T estimates of 600-650°C and 5 kbar for some D_4 (DSZ) mylonites in the Kanandra Granulite implies that at least some of the deformation on the DSZ occurred prior to cooling through 500°C at 403 ± 10 Ma. The 400 Ma cooling age also implies that either temperatures remained elevated for at least 40 Ma after upper amphibolite metamorphism at 445 Ma, or there was a later thermal pulse at 400 Ma associated with the Alice Springs Orogeny. Zonation characteristics in porphyroclastic garnet from the EPSZ suggest that temperatures were elevated above 600°C for more than 20 Ma during Palaeozoic metamorphism (Kelsey 1998), and this implies that the Kanandra Granulite may have experienced a prolonged high-T history. Therefore, it is likely that the mid-amphibolite DSZ mylonites reflect renewed deformation between 445 Ma and 400 Ma following slow cooling as a consequence of exhumation of the Kanandra Granulite, rather than a second thermal event. Thermal modeling by Kelsey (1998) suggested that the Kanandra Granulite had an elevated ambient thermal regime immediately prior to Palaeozoic deformation and that this was due to high heat-producing granite in the basement covered by insulating sedimentary cover. This ambient thermal perturbation may also have localised strain in an intraplate settting in this region (Sandiford and Hand 1998).

Given the evidence for a long-lived Palaeozoic thermal event in the eastern Arunta, it is likely that the Kanandra Granulite and northern Harts Range Group continuously cooled from the Late Ordovician, rather than being subjected to episodic thermal events at progressively lower temperatures. This progressive cooling was related to exhumation of the metamorphic terrane, which may have occurred in a series of deformation events, at 450-440 Ma, 390-380 Ma and 365-360 Ma.

Comparison with sedimentary record in Georgina and Amadeus Basins

Any analysis of Palaeozoic structural and chronological data in the Arunta Province must take into account the sedimentary record in the surrounding intracratonic basins. The relationship between deformation and sedimentation during the Ordovician

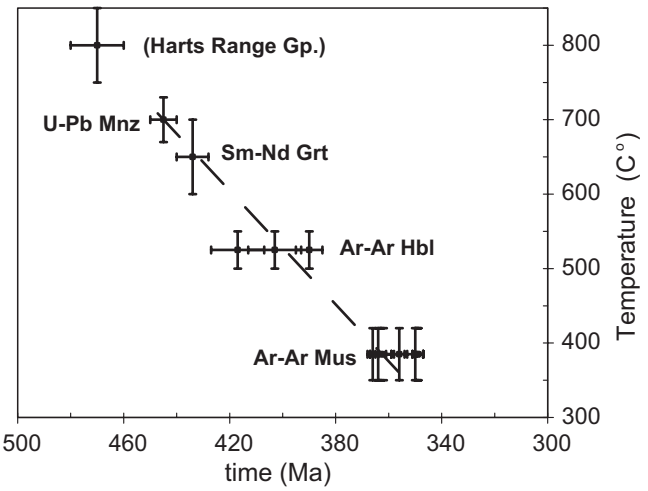

Figure 28 Inferred cooling path for the Kanandra Granulite and northern Harts Range Group in the Huckitta region, based on U-Pb, Sm-Nd and Ar-Ar geochronology

in central Australia has been discussed by Hand *et al* (1999a) and Mawby *et al* (1999). During metamorphism of the Harts Range Group in the Early Ordovician, the eastern Arunta Province was basement to the deepest part of a broad transcratonic seaway (Gorter 1991). This suggests that peak metamorphism and deformation occurred in an extensional tectonic setting (Hand *et al* 1999a). An abrupt change in basin tectonics at 450 Ma reflects the onset of compressional deformation, and this was accompanied by a shift in the locus of sedimentation to the central Amadeus Basin and increased clastic input. The compressional event included deformation on the EPSZ, and has been recognised in the Amadeus Basin as the Rodingan Movement (Shaw *et al* 1991). In the Dulcie Syncline of the Georgina Basin, immediately to the north of the Huckitta area, the youngest preserved marine sediments are Early Ordovician (Freeman and Woyzbun 1986), and a low angle unconformity separates them from Early to Late Devonian non-marine sequences of the Dulcie Sandstone.

In the northern Amadeus basin, an unconformity at the base of the Pertnjara Group is ascribed to the Pertnjara Movement (Shaw *et al* 1991), which occurred at about the end of the Early Devonian (390-380 Ma). The Pertnjara Movement is coeval with deformation in the Strangways Range and Mallee Bore (Ballèvre *et al* 2000, Buick *et al* in press) and may also be reflected in the hornblende Ar-Ar age of 390 Ma for mylonitised amphibolite in the Huckitta area. Syn-orogenic Devonian sedimentation of the Pertnjara Group culminated with the deposition of a thick alluvial fan conglomerate (Brewer Conglomerate) in the Late Devonian. Palynological dating of the top of the Brewer Conglomerate indicates that it was deposited in the late Famennian at about 360 Ma (Jones 1991). The Brewer Conglomerate accumulated during major uplift on thick-skinned structures such as the Redbank Thrust (Shaw 1991). The synchronicity of movement on the DSZ with deposition of the Pertnjara Group is consistent with the DSZ forming part of large-scale thick-skinned deformation and exhumation event during the Devonian. Existing chronological data for Palaeozoic movement on the Redbank Thrust (Shaw and Black 1991) suggests that it was also active during the Devonian and that this activity was synchronous with movement on the DSZ. The time of cessation of deformation on the DSZ (360 Ma) corresponds with final deposition in the Amadeus and Georgina Basins, and may reflect a fundamental change in the tectonics of the Alice Springs Orogeny at the Devonian-Carboniferous boundary.

Tectonic implications for Palaeozoic deformation in central Australia

The existence of steeply-dipping Palaeozoic structures in the Huckitta basement area has implications for the tectonics of the eastern Arunta Province during intraplate deformation. The EPSZ is a steep, sinistral strike-slip transpressional structure. It was active at the rear of a shallowly south-vergent thrust wedge during the onset of compressional deformation in the eastern Arunta Province at 450-440 Ma. The deformation style of the EPSZ differs markedly from shear zones of similar age in the Harts Range in terms of orientation and kinematics. Whereas the Bruna Detachment Zone and Florence-Muller

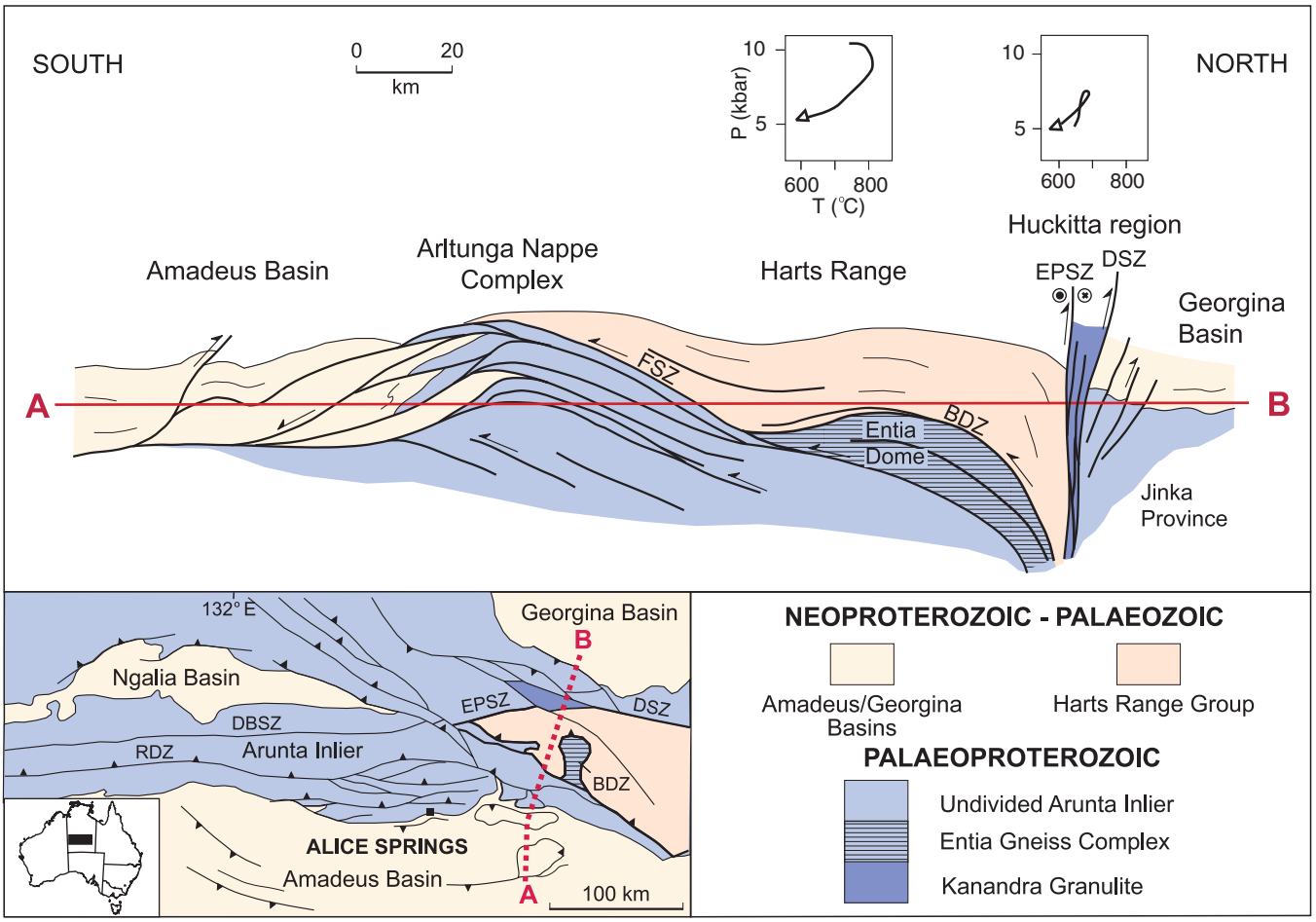

Figure 29 Schematic north-south cross-section across the eastern Arunta Province (adapted and modified from Dunlap and Teyssier 1995). Abbreviations as in Figure 1

Shear Zone in the Harts Range are shallowly dipping, south-directed thrusts, the EPSZ is steeply south dipping, has shallowly plunging lineations and a sinistral strike-slip sense of movement (Figure 29). This implies that compressional deformation associated with the 450-440 Ma event was more complex than simple south-directed compression, and involved significant partitioning of strain, with dominantly dip-slip movement in the south and strike-slip movement in the north. The existence of a steeply-dipping strike-slip zone (typically within a reverse hinterland-directed component) located behind a thrust-dominated wedge is a feature of numerous orogenic belts worldwide, particularly along the Alpine-Himalayan system (Periadriatic/Insubric Line in the Alps, Schmid *et al* 1989; Altyn Tagh Fault, Tibet, Tapponier *et al* 1986; Karakoram Fault, Ladakh, Searle *et al* 1998).

The DSZ was active during the Devonian, with most ductile deformation occurring by 360 Ma. The DSZ formed part of a large scale, thick skinned tectonic orogenic belt, in which crustal scale structures such as the Redbank Thrust intersected the moho. Deformation on the DSZ involved steep north vergent deformation, which juxtaposed upper amphibolite Palaeozoic rocks in the south against sub-greenschist Neoproterozoic sediments to the north (Figure 29). Thus, although most of the exposed late Ordovician to Carboniferous structures in the Arunta Province are south-vergent (Dunlap *et al* 1995), the orogen can be considered, as a whole, to be doubly-vergent (Collins and Teyssier 1989), with significant exhumation along steep structures at the back of the south-vergent thrust stack (Figure 29). Therefore, in spite of the current intraplate setting of Palaeozoic compression in central Australia, the large-scale geometry of the orogen has affinities with the collisional stage of Alpine-type orogens (eg Dewey *et al* 1986, Beaumont *et al* 1996). The lack of significant Carboniferous deformation and exhumation in the northeastern Arunta Province suggests that large scale thick-skinned tectonics may have ceased by the Late Devonian, with ensuing tectonics in the Carboniferous dominated by more localised thick skinned deformation and the development of south-vergent nappes (Arltunga Nappes, Dunlap *et al* 1995).

GEOLOGICAL HISTORY

The earliest geological event recognised in the Huckitta area was the deposition of the sedimentary-volcanic protoliths of the Deep Bore and Cackleberry Metamorphics, and the Kanandra Granulite. The Deep Bore Metamorphics have a maximum deposition age of 1805 ± 7 Ma, which may represent the timing of volcaniclastic sedimentation, while the Kanandra Granulite has a less well defined maximum deposition age of 1817 ± 15 Ma. Sedimentary precursors were intruded by granite, including the Dneiper Granite at 1770 Ma, as part of the Early Strangways Event. The Kanandra Granulite may also have been intruded by granite at this time. Metamorphism associated with the early Strangways Event is poorly constrained due to overprinting by higher grade events, but it is possible that cordierite-andalusite assemblages in the Cackleberry Metamorphics may be related to this early event. Alteration and K-metasomatism in precursors to sapphirine-phlogopite schist is likely to have occurred during fluid flow between 1805 Ma and 1730 Ma.

The eastern Arunta Province underwent high grade metamorphism and deformation at 1730 ± 7 Ma during the Late Strangways Event. This event involved compression with limited crustal thickening, extensive lower crustal melting, and advection of heat to the upper crust. The Late Strangways Event resulted in granulite metamorphism in the Deep Bore Metamorphics and Kanandra Granulite, and upper amphibolite metamorphism in the Cackleberry Metamorphics. Peak metamorphism of 5-7 kbar and 800°C in the Kanandra Granulite was followed by granite intrusion and near-isobaric cooling.

The Palaeoproterozoic rocks on JINKA and DNEIPER cooled through 500°C in the period 1600-1550 Ma, reflecting exhumation or a thermal event coincident with the Chewings Orogeny in the southern Arunta Province and Reynolds Range. By the mid Neoproterozoic, Deep Bore and Cackleberry Metamorphics were exposed at the surface, and were unconformably overlain by the basal units of the Georgina Basin.

Although no chronological data exist for the Harts Range Group on HUCKITTA, evidence from the Harts Range and Mallee Bore regions suggests that it was deposited in a rift setting in the late Neoproterozoic or Cambrian. The tectonic mechanism for burial of the Harts Range Group to at least 30 km depth by the early Ordovician remains unclear, but granulite metamorphism of the Harts Range Group during the Larapinta Event at 480-460 Ma is inferred to have occurred in an extensional intraplate setting. Peak metamorphism was followed by exhumation to 7 kbar by 445 ± 5 Ma. Sinistral transpression on the Entire Point Shear Zone occurred at 445 Ma, coincident with south-vergent compression in the Harts Range, and resulted in the juxtaposition of the Harts Range Group and Kanandra Granulite. Late Ordovician reworking of the Kanandra Granulite and northern Harts Range Group at upper amphibolite conditions (7 kbar, 700°C) was followed by slow cooling at a rate of about 4°CMa^{-1}.

North-vergent exhumation on steeply dipping mylonites of the Delny Shear Zone commenced with mid-amphibolite facies deformation, prior to cooling of the Kanandra Granulite through 500°C at 403 ± 10 Ma. Ductile deformation on the DSZ continued, episodically, until the Late Devonian (365-360 Ma) resulting in large scale exhumation and cooling of the Harts Range Group and Kanandra Granulite to the south. By the end of the Devonian, the terrane had cooled through 350-420°C and there is no evidence for Carboniferous metamorphism in the northeastern Arunta Province. Brittle deformation and quartz veining along the northern margin of the DSZ may be Carboniferous. Palaeozoic deformation in the Deep Bore and Cackleberry Metamorphics was restricted to brittle faulting and gentle folding at sub-greenschist facies conditions.

ACKNOWLEDGEMENTS

This study formed part of a collaborative project between the Northern Territory Geological Survey and the University of Leoben, and colleagues in both institutions are thanked for their support and input. This work benefited from numerous conversations on the geology of the eastern Arunta Province with Martin Hand, Jo Mawby and Ian Buick. Dot Close, Christine Edgoose, Chris Field and Peter Crispe are thanked for assistance and input in the field. Peter Haines and David Kelsey introduced the authors to the study area and provided details on the location of the sapphirine occurrence. Wolfgang

Frank, Richard Armstrong, Julie Smith and Jo Mawby are thanked for geochronological analyses and associated scientific input. Jodie Miller provided sample MBO-4 from Mallee Bore. Helmut Muhlhans and Hans Seiser provided high quality technical support in Leoben. The manuscript was edited by Tim Munson and formatted by Rivella Creative. Phil Carter provided cartographic support. Tim Johnson, Daniela Rubatto, Simon Harley and Bas Hensen provided constructive criticism of early versions of parts of the manuscript.

REFERENCES

Ballèvre M, Hensen BJ and Reynard B, 1997. Orthopyroxene-andalusite symplectites replacing cordierite in granulites from the Strangways Range (Arunta Block, central Australia): A new twist to the pressure-temperature history. *Geology* 25, 215-218.

Ballèvre M, Möller A and Hensen BJ, 2000. Exhumation during crustal shortening: an Alice Springs (380 Ma) age for a prograde amphibolite facies shear zone in the Strangways Metamorphic Complex (central Australia). *Journal of Metamorphic Geology* 18, 737-747.

Beaumont C, Ellis S, Hamilton J, and Fullsack P, 1996. Mechanical model for subduction-collision tectonics of Alpine-type compressional orogens. *Geology* 24, 675-678.

Becker H, 1997. Sm-Nd garnet ages and cooling history of high-temperature garnet peridotite massifs and high-pressure granulites from Lower Austria. *Contributions to Mineralogy and Petrology* 127, 224-236.

Black LP, Shaw RD and Stewart AJ, 1983. Rb-Sr geochronology of Proterozoic events in the Arunta Inlier, central Australia. *BMR Journal of Australian Geology and Geophysics* 8, 129-138.

Black LP and Shaw RD, 1992. U-Pb zircon chronology of prograde Proterozoic events in the central and southern provinces of the Arunta Block, central Australia. *Australian Journal of Earth Sciences* 39, 153-171.

Bohlen SR, Boettcher AL and Wall VJ, 1982. The system albite-H2O-CO2: a model for melting and activities of water at high pressures. *American Mineralogist* 68, 1049-1058.

Buick IS, Cartwright I and Harley SL, 1998. The retrograde P-T-t path for low-pressure granulites from the Reynolds Range, central Australia: petrological constraints and implications for low-P/high-T metamorphism. *Journal of Metamorphic Geology* 16, 511-529.

Buick IS, Miller JA, Williams IS and Cartwright I, in press. Ordovician high-grade metamorphism of a newly-recognised late Neoproterozoic terrane in the northern Harts Range, central Australia. *Journal of Metamorphic Geology.*

Burton KW, Kohn MJ, Cohen AS and O'Nions RK, 1995. The relative diffusivities of Pb, Nd, Sr and O in garnet. *Earth and Planetary Science Letters* 133, 199-211.

Cartwright I, Buick IS, Foster DA and Lambert DD, 1999. Alice Springs age shear zones from the southeastern Reynolds Range, central Australia. *Australian Journal of Earth Sciences* 46, 355-363.

Cartwright I, Buick IS and Maas R, 1997. Fluid flow in marbles at Jervois, central Australia: oxygen isotope disequilibrium and zoning produced by decoupling of mineralogical and isotopic resetting. *Contributions to Mineralogy and Petrology* 128, 335-351.

Clarke GL, Collins WJ and Vernon RH, 1990. Successive overprinting granulite facies metamorphic events in the Anmatjira Range, central Australia. *Journal of Metamorphic Geology* 8, 65-88.

Collins WJ and Shaw RD, 1995. Geochronological constraints on orogenic events in the Arunta Inlier: a review. *Precambrian Research* 71, 69-89.

Collins WJ and Teyssier C, 1989. Crustal scale ductile fault systems in the Arunta Inlier, central Australia. *Tectonophysics* 158, 49-66.

Collins WJ and Vernon RH, 1991. Orogeny associated with anti-clockwise P-T-t paths: Evidence from low-P, high-T terranes in central Australia. *Geology* 19, 835-838.

Collins WJ, Vernon RH and Clarke GL, 1991. Discrete Proterozoic structural terranes associated with low-P, high-T metamorphism, Anmatjira Range, Arunta Inlier, central Australia: tectonic implications. *Journal of Structural Geology* 13, 1157-1171.

Cooper JA, Mortimer GE and James PR, 1988. Rate of Arunta Inlier evolution at the eastern margin of the Entia Dome, central Australia. *Precambrian Research* 40/41, 217-231.

Dempster TJ, Harrison TN, Brown PE and Hutton DHW, 1991. Low-pressure granulites from the Ketilidian Mobile Belt of southern Greenland. *Journal of Petrology* 32, 979-1004.

Dewey JF, Hempton MR, Kidd WSF, Saroglu F and Sengör AMC, 1986. Shortening of continental lithosphere: the neotectonics of Eastern Anatolia - a young collision zone. In Coward MP and Ries AC (editors) Collisional Tectonics. *Geological Society of London, Special Publications* 19, 3-36.

De Yoreo JJ, Lux DR and Guidotti CV, 1991. Thermal modeling in low-pressure/high-temperature metamorphic belts. *Tectonophysics* 188, 209-238.

Ding P and James PR, 1985. Structural evolution of the Harts Range area and its implication for the development of the Arunta Block, central Australia. *Precambrian Research* 27, 251-276.

Dobos S, 1978. Phase relations, element distributions and geochemistry of metamorphic rocks from the eastern Arunta Block, NT. *PhD thesis, Macquarie University, Sydney.*

Dunlap WJ and Teyssier C, 1995. Palaeozoic deformation and isotopic disturbance in the southeastern Arunta Block, central Australia. *Precambrian Research* 71, 229-250.

Dunlap WJ, Teyssier C, McDougall I and Baldwin S, 1995. Thermal and structural evolution of the intracratonic Arltunga nappe complex, central Australia. *Tectonics* 14, 1182-1204.

Fitzsimons ICW, 1996. Metapelitic migmatites from Brattsrand Bluffs, east Antarctica - metamorphism, melting and exhumation of the mid-crust. *Journal of Petrology* 37, 395-414.

Fitzsimons ICW and Harley SL, 1994. Garnet coronas in scapolite-wollastonite calc-silicates from East Antarctica: the application and limitation of activity corrected grids. *Journal of Metamorphic Geology* 12, 761-777.

Freeman MJ, 1986. Huckitta, Northern Territory. 1:250 000 geological Map Series. *Northern Territory Geological Survey, Explanatory Notes* SF53-11.

Goscombe B, 1992. High-grade reworking of central Australian granulites: Metamorphic evolution of the Arunta Complex. *Journal of Petrology* 33, 917-962.

Graham CM and Powell R, 1984. A garnet-hornblende geothermometer: calibration, testing, and application to the Pelona Schist, Southern California. *Journal of Metamorphic Geology* 2, 13-21.

Grant JA, 1985. Phase equilibria in low-pressure partial melting of pelitic rocks. *American Journal of Science* 285, 409-435.

Grant JA and Frost BR, 1990. Contact metamorphism and partial melting of pelitic rocks in the aureole of the Laramie Anorthosite Complex, Morton Pass, Wyoming. *American Journal of Science* 290, 425-472.

Green TH and Hellman PL, 1982. Fe-Mg partitioning between coexisting garnet and phengite at high pressure, and comments on a garnet-phengite geothermometer. *Lithos* 15, 253-266.

Greenfield JE, Clarke GL and White RW, 1998. A sequence of partial melting reactions at Mt Stafford, central Australia. *Journal of Metamorphic Geology* 16, 363-378.

Hand M, Fanning M and Sandiford M, 1995. Low-P, high-T metamorphism and the role of high-heat producing granites in the northern Arunta Inlier. *Geological Society of Australia, Abstracts* 40, 60-61.

Hand M, Mawby J, Kinny P and Foden, J. 1999a. U-Pb ages from the Harts Range, central Australia: evidence for early-Ordovician extension and constraints on Carboniferous metamorphism. *Journal of the Geological Society of London* 156, 715-730.

Hand M, Mawby J, Miller JA, Ballèvre M, Hensen BJ, Möller A and Buick IS, 1999b. Tectonothermal evolution of the Harts and Strangways Range region, eastern Arunta Inlier, central Australia, field guide 4. *Geological Society of Australia, Specialist Group in Geochemistry, Mineralogy and Petrology*.

Harley SL and Green DH, 1982. Garnet-orthopyroxene barometry for granulites and peridotites. *Nature* 300, 697-701.

Hodges KV and Crowley PD, 1985. Error estimation and empirical geothermobarometry for pelitic systems. *American Mineralogist* 70, 702-709.

Hodges KV and Spear FS, 1982. Geothermometry, geobarometry and the Al_2SiO_5 triple point at Mt. Moosilauke, New Hampshire. *American Mineralogist* 67, 1118-1134.

Hoisch TD, 1990. Empirical calibration of six geobarometers for the mineral assemblage quartz + muscovite + biotite + plagioclase + garnet. *Contributions to Mineralogy and Petrology* 104, 225-234.

Holdaway MJ, 1971. Stability of andalusite and the aluminium silicate phase diagram. *American Journal of Science* 271, 97-131.

Holdaway MJ and Lee SM, 1977. Fe-Mg cordierite stability in high-grade pelitic rocks based on experimental, theoretical and natural observations. *Contributions to Mineralogy and Petrology* 63, 175-198.

Holland TJB and Powell R, 1998. An internally consistent thermodynamic dataset for phases of petrological interest. *Journal of Metamorphic Geology* 16, 309-343.

Hussey KJ, Smith J and Donnellan N, 1999. Some regional implications of new geochronological constraints from the Tennant Creek and Arunta Inliers, central Australia. *Geological Society of Australia, Abstracts* 54, 50-51.

James PR, Macdonald P and Parker M, 1989. Strain and displacement in the Harts Range detachment zone: a structural study of the Bruna Gneiss from the western margin of the Entia Dome, central Australia. *Tectonophysics* 158, 23-48.

Johannes W and Holtz F, 1990. Formation and composition of H_2O-undersaturated granitic melts. In Ashworth JR and Brown M (editors) *High-temperature metamorphism and crustal anatexis*. Unwin-Hyman, London, 87-104.

Jones BG, 1991. Fluvial and lacustrine facies in the Middle to Late Devonian Pertnjara Group, Amadeus Basin, Northern Territory, and their relationship to tectonic events and climate. *Bureau of Mineral Resources, Australia, Bulletin* 236, 429-462.

Kelsey D, 1998. Controls on the localisation of Palaeozoic deformation in the northeastern Arunta Inlier. *BSc (Hons) thesis, University of Adelaide, Adelaide*.

Kerrick DM, 1990. The Al_2SiO_5 polymorphs. *Mineralogical Society of America, Reviews in Mineralogy* 22.

Kerrick DM and Speer JA, 1988. The role of minor element solid solution on the andalusite-sillimanite equilibrium in metapelites and peraluminous granitoids. *American Journal of Science* 288, 152-192.

Kerrick DM and Woodsworth GJ, 1989. Aluminium silicates in the Mount Raleigh pendant, British Columbia. *Journal of Metamorphic Geology* 7, 547-563.

Kohn MJ and Spear FS, 1990. Two new barometers for garnet amphibolites with applications to eastern Vermont. *American Mineralogist* 75, 89-96.

Kretz R, 1983. Symbols for rock forming minerals. *American Mineralogist* 68, 277-279.

Lafrance B, Clarke GL, Collins WJ and Williams IS, 1995. The emplacement of the Wuluma Granite: melt generation and migration along steeply dipping extensional fractures at the close of the late Strangways orogenic event, Arunta Block, central Australia. *Precambrian Research* 72, 43-67.

Lanzarotti A and Hanson GN, 1996. Geochronology and geochemistry of multiple generations of monazite from the Wepawaug Schist, Connecticut, USA: implications for monazite stability in metamorphic rocks. *Contributions to Mineralogy and Petrology* 125, 332-340.

Le Breton N and Thompson AB, 1988. Fluid-absent (dehydration) melting of biotite in metapelites in the early stages of crustal anatexis. *Contributions to Mineralogy and Petrology* 99, 226-237.

Loosveld RJH and Etheridge MA, 1990. A model for low-pressure facies metamorphism during crustal thickening. *Journal of Metamorphic Geology* 8, 257-267.

Ludwig KR, 1998. On the treatment of concordant uranium-lead ages. *Geochimica et Cosmochimica Acta* 62, 665-676.

Ludwig KR, 1999. Isoplot/Ex version 2.00: A Geochronological Toolkit for Microsoft Excel. *Berkeley Geochronology Center, Special Publication* 1a.

Manning DAC and Pichavant M, 1983. The role of fluorine and boron in the generation of granitic melts. In Atherton MP and Gribble CD (editors) *Migmatites, Melting and Metamorphism*. Shiva Publishing Ltd, Nantwich, England, 94-109.

Mawby J, Hand M and Foden J, 1999. Sm-Nd evidence for Ordovician granulite facies metamorphism in an intraplate setting in the Arunta Inlier, central Australia. *Journal of Metamorphic Geology* 17, 653-668.

McLellan EL, 1983. Contrasting textures in metamorphic and anatectic migmatites: an example from the Scottish Caledonides. *Journal of Metamorphic Geology* 1, 241-262.

Miller JA, Buick IS, Williams IS and Cartwright I, 1998. Re-evaluating the metamorphic and tectonic history of the eastern Arunta Block, central Australia. *Geological Society of Australia, Abstracts* 49, 316.

Miller JA, Cartwright I and Buick IS, 1997. Granulite facies metamorphism in the Mallee Bore area, northern Harts Range: implications for the thermal evolution of the eastern Arunta Inlier, central Australia. *Journal of Metamorphic Geology* 15, 613-629.

Moine B, Sauvan P and Jarosse J, 1981. Geochemistry of evaporite-bearing series: A tentative guide to the identification of evaporites. *Contributions to Mineralogy and Petrology* 76, 401-411.

Möller A, Armstrong R, Hensen BJ and Williams IS, 1999. Dating metamorphic events and deformation: SHRIMP U-Pb zircon examples from the Strangways Metamorphic Complex, Arunta Inlier, Australia. *Journal of Conference Abstracts* 4, 711.

Newton RC, and Perkins D III, 1982. Thermodynamic calibration of geobarometers based on the assemblages garnet - plagioclase - orthopyroxene (clinopyroxene) - quartz. *American Mineralogist* 67, 203-222.

Nichols GT, Berry RF, and Green DH, 1992. Internally consistent gahnitic spinel-cordierite-garnet equilibria in the FMASHZn system: geothermobarometry and applications. *Contributions to Mineralogy and Petrology* 111, 362-377.

Pattison DRM, 1989. P-T conditions and the influence of graphite on pelitic phase relations in the Ballachulish Aureole, Scotland. *Journal of Petrology* 30, 1219-1244.

Pattison DRM, 1992. Stability of andalusite and sillimanite and the Al_2SiO_5 triple point: Constraints from the Ballachulish Aureole, Scotland. *Journal of Geology* 100, 423-446.

Pattison DRM and Harte B, 1991. Petrography and mineral chemistry of pelites. In Voll G, Pattison DRM and Seifert F (editors) *Equilibrium and Kinetics in Contact Metamorphism: The Ballachulish Igneous Complex and its Aureole.* Springer-Verlag, Heidelberg, 135-179.

Pattison DRM and Tracy RJ, 1991. Phase equilibria and thermobarometry of pelites. In Kerrick DM (editor) Contact Metamorphism. *Mineralogical Society of America, Reviews in Mineralogy* 25, 105-206.

Powell R and Holland TJB, 1988. An internally consistent thermodynamic dataset with uncertainties and correlations: 3. Applications to geobarometry, worked examples and a computer program. *Journal of Metamorphic Geology* 6, 173-204.

Richardson SW, Gilbert MC and Bell PM, 1969. Experimental determination of kyanite-andalusite and andalusite-sillimanite equilibrium: the aluminosilicate triple point. *American Journal of Science* 267, 259-272.

Rubatto D and Gebauer D, 2000. Use of Cathodoluminescence for U-Pb zircon dating by ion microprobe: some examples from the Western Alps, In Pagel M, Barbin V, Blanc P and Ohnenstetter D (editors) *Cathodoluminescence in Geosciences*. Springer-Verlag, Berlin.

Rubenach MJ, 1992. Proterozoic low-pressure/high-temperature metamorphism and an anti-clockwise P-T-t path for the Hazaldene area, Mount Isa Inlier, Queensland, Australia. *Journal of Metamorphic Geology* 10, 333-346.

Sandiford M and Hand M, 1998. Australian Proterozoic high-temperature, low-pressure metamorphism in the conductive limit. In Treloar PJ and O'Brien PJ (editors) What drives Metamorphism and Metamorphic Reactions? *Geological Society of London, Special Publication* 138, 23-46.

Sandiford M and Powell R, 1991. Some remarks on high temperature-low pressure metamorphism in convergent orogens. *Journal of Metamorphic Geology* 9, 333-340.

Schmid SM, Aebli HR, Heller F and Zingg A, 1989. The role of the Periadriatic Line in the tectonic evolution of the Alps. In Coward MP, Dietrich D and Park RG (editors) Alpine Tectonics. *Geological Society of London, Special Publication* 45, 153-171.

Scrimgeour I and Raith JG, in press. High-grade reworking of Proterozoic granulites during Ordovician intraplate transpression, eastern Arunta Inlier, central Australia. In Miller JA, Buick IS, Hand M and Holdsworth RE (editors) Continental Reworking and Reactivation. *Geological Society of London, Special Publication*.

Scrimgeour I, Smith, JB and Raith JG, in press. Palaeoproterozoic high-T, low-P metamorphism and dehydration melting of metapelites from the Mopunga Range, Arunta Inlier, central Australia. *Journal of Metamorphic Geology*.

Searle MP, Weinberg RF and Dunlap WJ, 1998. Transpressional tectonics along the Karakoram Fault Zone, northern Ladakh: constraints on Tibetan extrusion. In Holdsworth RE, Strachan RA and Dewey JD (editors) Continental Transpressional and Transtensional Tectonics, *Geological Society, London, Special Publication* 135, 307-326.

Shaw RD, 1991. The tectonic development of the Amadeus Basin, central Australia. *Bureau of Mineral Resources, Australia, Bulletin* 236, 429-462.

Shaw RD, Etheridge MA and Lambeck K, 1991. Development of the late Proterozoic to mid-Palaeozoic intracratonic Amadeus Basin in central Australia: A key to understanding tectonic forces in plate interiors. *Tectonics* 10, 688-721.

Shaw RD and Warren RG, 1975. Alcoota, Northern Territory, 1:250 000 geological sheet and explanatory notes. *Bureau of Mineral Resources, Australia*.

Shaw RD, Warren RG, Offe LA, Freeman MJ and Horsfall CL, 1984. Geology of Arunta Block in the southern part of the Huckitta 1:250 000 sheet area-Preliminary data 1980 survey. *Bureau of Mineral Resources, Australia, Record* 1984/3.

Shaw RD, Warren RG, Senior BR and Yeates AN, 1975. Geology of the Alcoota 1:250 000 sheet area, NT, *Bureau of Mineral Resources, Australia, Record* 1975/100.

Sheraton JW, England RN and Ellis DJ, 1982. Metasomatic zoning in sapphirine-bearing granulites from Antarctica. *BMR Journal of Australian Geology and Geophysics* 3, 76-79.

Smith JB, 2000a. NTGS-AGSO geochronology project. Report 1. *AGSO professional opinion* 2000/17.

Smith JB, 2000b. NTGS-AGSO geochronology project. Report 3. *AGSO professional opinion*, 2000/

Spear FS, Kohn MJ and Cheney JT, 1999. P-T paths from anatectic pelites. *Contributions to Mineralogy and Petrology* 134, 17-32.

Stevens G, Clemens JD and Droop GTR, 1997. Melt production during granulite-facies anatexis: experimental data from 'primitive' metasedimentary protoliths. *Contributions to Mineralogy and Petrology* 128, 352-370.

Tapponnier P, Peltzer G, and Armijo R, 1986. On the mechanics of the collision between India and Asia. In Coward MP and Ries AC (editors) Collisional Tectonics. *Geological Society of London, Special Publication* 19, 115-157.

Tucker RD, Ashwal LD, Handke MJ, Hamilton MA, LeGrange M and Rambeloson RA, 1999. U-Pb geochronology and isotope geochemistry of the Archaean and Proterozoic rocks of north-central Madagascar. *Journal of Geology* 107, 135-153.

Vernon RH, 1987. Oriented growth of sillimanite in andalusite, Placitas-Juan Tabo area, New Mexico, USA. *Canadian Journal of Earth Sciences* 24, 580-590.

Vernon RH, Clarke GL and Collins WJ, 1990. Local, mid-crustal granulite facies metamorphism and melting: an example in the Mount Stafford area, central Australia. In Ashworth JR and Brown M (editors) *High-temperature metamorphism and crustal anatexis*. Unwin-Hyman, London. 272-319.

Vielzeuf D and Holloway JR, 1988. Experimental determination of the fluid-absent melting reactions in the pelitic system: consequences for crustal differentiation. *Contributions to Mineralogy and Petrology* 98, 257-276.

Vry JK and Cartwright I, 1994. Sapphirine-kornerupine rocks from the Reynolds Range, central Australia: constraints on the uplift history of a Proterozoic low pressure terrain. *Contributions to Mineralogy and Petrology* 116, 78-91.

Vry JK, Compston W and Cartwright I, 1996. SHRIMP II dating of zircons and monazites: reassessing the timing of high-grade metamorphism and fluid flow in the Reynolds Range, northern Arunta Block, Australia. *Journal of Metamorphic Geology* 14, 335-350.

Walther JV and Wood BJ, 1984. Rate and mechanism in prograde metamorphism. *Contributions to Mineralogy and Petrology* 88, 246-259.

Warren RG, 1978. Delny-Mount Sainthill Fault System, eastern Arunta Block, central Australia. *BMR Journal of Australian Geology and Geophysics* 3, 76-79.

Warren RG, 1979. Sapphirine-bearing rocks with sedimentary and volcanogenic protoliths from the Arunta Block. *Nature* 278, 159-161.

Warren RG, 1983. Metamorphic and tectonic evolution of granulites from the Arunta Block, central Australia. *Nature* 305, 300-303.

Warren RG, Hensen BJ and Ryburn RJ, 1987. Wollastonite and scapolite in Precambrian calc-silicate granulites from Australia and Antarctica. *Journal of Metamorphic Geology* 5, 213-223.

Warren RG and Hensen BJ, 1987. Peraluminous sapphirine from the Aileron district, Arunta Block, central Australia. *Mineralogical Magazine* 51, 409-415.

Warren RG and Hensen BJ, 1989. The P-T evolution of the Proterozoic Arunta Block, central Australia, and implications for tectonic evolution. In Daly JS, Cliff RA and Yardley, BWD (editors) Evolution of Metamorphic Belts. *Geological Society of London, Special Publication 43*, 349-355.

Warren RG and Shaw RD, 1985. Volcanogenic Cu-Pb-Zn bodies in granulites of the central Arunta Block, central Australia. *Journal of Metamorphic Geology* 3, 481-499.

Whittington A, Harris N and Baker J, 1998. Low-pressure crustal anatexis: the significance of spinel and cordierite from metapelitic assemblages from Nanga Parbat, northern Pakistan. In Treloar PJ and O'Brien PJ (editors) What drives Metamorphism and Metamorphic Reactions? *Geological Society of London, Special Publication* 138, 183-198.

Willett S, Beaumont C and Fullsack P, 1993. A mechanical model for the tectonics of doubly-vergent compressional orogens. *Geology* 21, 371-374.

Wolf MB and Wyllie PJ, 1994. Dehydration-melting of amphibolite at 10 kbar; the effects of temperature and time. *Contributions to Mineralogy and Petrology* 115, 369-383.

Wyllie PJ and Wolf MB, 1993. Amphibolite dehydration-melting: sorting out the solidus. In Pritchard HM, Alabaster T, Harris NBW and Neary CR (editors) Magmatic Processes and Plate Tectonics. *Geological Society of London, Special Publication* 76, 405-416.

Xu G, Will TM and Powell R, 1994. A calculated petrogenetic grid for the system K_2O-FeO-MgO-Al_2O_3-SiO_2-H_2O, with particular reference to contact metamorphosed pelites. *Journal of Metamorphic Geology* 12, 99-119.

Young DN, Fanning CM, Shaw RD, Edgoose CJ, Blake DH, Page RW and Camacho A, 1995. U-Pb zircon dating of tectonothermal events in the northern Arunta Inlier, central Australia. *Precambrian Research* 71, 45-68.

Zhao Jianxin and Bennett VC, 1995. SHRIMP U-Pb zircon geochronology of granites in the Arunta Inlier, central Australia: implications for Proterozoic crustal evolution. *Precambrian Research* 71, 17-43.

Zhao Jianxin and McCulloch MT, 1995. Geochemical and Nd isotopic systematics of granites from the Arunta Inlier, central Australia: implications for Proterozoic crustal evolution. *Precambrian Research 71, 265-299.*

APPENDIX 1

List of all samples used for petrology and geochronology (samples and thin sections stored at NTGS, Alice Springs). Abbreviations: TS - thin section; P - polished; Nl - normal; EPSZ - Entire Point Shear Zone; DSZ - Delny Shear Zone; Met – Metamorphics; mineral abbreviations after Kretz (1983).

Fieldwork: July-August 1998 (All samples prefixed by ISHU98).

Sample	Region	Easting	Northing	Lithology	Description	TS	Geochron
3	W of Yam Creek Bore	53 554 590	7 484 065	Kanandra (EPSZ)	oriented sample of Grt-bearing mylonite	Nl,P	
8	W of Yam Creek Bore	53 555 125	7 484 350	Kanandra Granulite	mafic rock recrystallised to Grt-Hbl	P	
16	NE of Marshall Bore	53 565 680	7 481 235	Harts Range Group	Grt-Bt-Sil fabric - overprints earlier fabric	Nl	
20	NE of Marshall Bore	53 567 440	7 482 820	Kanandra (EPSZ)	mylonitic Bt-Grt-Sil fabric	P	
22	NE of Marshall Bore	53 567 145	7 483 100	Kanandra (EPSZ)	mafic rock recrystallised to Grt-Hbl	Nl	
23	NE of Marshall Bore	53 568 500	7 481 535	Harts Range Group	Bt-Sil-Grt rock with large Grt porphyroclasts	Nl,P	
30	Deep Bore	53 557 342	7 490 500	Deep Bore Met	Crd-Bt-Opx gneiss, Crd in melt patches	Nl,P	U-Pb zircon
32	Deep Bore	53 556 540	7 490 260	Deep Bore Met	Crd-Bt gneiss	Nl	
32A	Deep Bore	53 556 540	7 490 260	Deep Bore Met	Grt-Crd-Bt gneiss	P	
32B	Deep Bore	53 556 540	7 490 260	Deep Bore Met	Bt-Crd gneiss	P	
32C	Deep Bore	53 556 540	7 490 260	Deep Bore Met	Spl-Sil-Crd-Bt intergrowths in melt patches	Nl,P	
36A	Deep Bore	53 555 920	7 489 395	Deep Bore Met	Grt-bearing high strain granulite	P	
40	N of Halfway Dam	53 547 250	7 490 970	Cackleberry Met	massive aluminous Sil-Crd-Ms-Bt rock	Nl,P	
40C	N of Halfway Dam	53 547 250	7 490 970	Cackleberry Met	massive aluminous Sil-Crd-Ms-Bt rock	P	
42A	Near No 4 Dam	53 537 925	7 498 830	Cackleberry Met	Grt-bearing psammitic layer	P	
42C	Near No 4 Dam	53 537 925	7 498 830	Cackleberry Met	Grt-bearing psammitic layer	P	
42D	Near No 4 Dam	53 537 925	7 498 830	Cackleberry Met	typical gneiss from region - And-Crd-Bt-Ksp	Nl	
42E	Near No 4 Dam	53 537 925	7 498 830	Cackleberry Met	And-Sil-Bt gneiss with Crd porphyroblasts	P	
42F	Near No 4 Dam	53 537 925	7 498 830	Cackleberry Met	Bt-Sil rich schistose pelite	P	
42G	Near No 4 Dam	53 537 925	7 498 830	Cackleberry Met	And-Crd-Bt-Ksp-Qtz-Sil pelite	P	
42I	Near No 4 Dam	53 537 925	7 498 830	Cackleberry Met	And-Crd-Bt-Sil gneiss with Crd-bearing melt	Nl,P	
42J	Near No 4 Dam	53 537 925	7 498 830	Cackleberry Met	Bt-Sil rich gneiss	P	
44	Black Point	53 514 437	7 484 390	Kanandra Granulite	Grt-Crd pelite	P	
44B	Black Point	53 514 437	7 484 390	Kanandra Granulite	pelitic granulite - Sil + Spl inclusions in Grt	Nl	
44C	Black Point	53 514 437	7 484 390	Kanandra Granulite	pelite with Bt-Sil wrapping Grt	Nl	
44D	Black Point	53 514 437	7 484 390	Kanandra Granulite	pelite with Bt-Sil wrapping Grt	Nl	
44E	Black Point	53 514 437	7 484 390	Kanandra Granulite	Grt-bearing psammite	Nl	
45	Black Point	53 514 300	7 484 230	Kanandra Granulite	pelite with strong fabric deforming Grt + Spl	Nl	
46	Black Point	53 513 600	7 484 015	Kanandra Granulite	pelite with Grt breaking down to Spl-Bt-Crn	Nl,P	
52	Near Dingo Dam	53 506 560	7 484 650	Kanandra Granulite	Grt-Crd-Bt gneiss	P	
53A	Near Dingo Dam	53 506 337	7 486 852	Kanandra Granulite	Sil-bearing Grt-Crd pelite	P	
54D	S of highway	53 569 979	7 457 810	Harts Range Group	Wo calc-silicate with Scp, Grt	Nl	
57A	S of Mt. Sainthill	53 571 343	7 481 975	Kanandra Granulite	Bt-Sil-Grt pelite	P	
64	W of Yam Creek Bore	53 559 650	7 483 880	Kanandra Granulite	folded pelite with Bt-Sil axial planar fabric?	Nl	
70	W of Yam Creek Bore	53 557 495	7 483 541	Kanandra Granulite	migmatitic pelitic gneiss, no later fabric	Nl	
72	E of Halfway Dam	53 552 164	7 484 185	Kanandra (EPSZ)	Bt-Grt-Ms mylonite	P	
72A	E of Halfway Dam	53 552 164	7 484 230	Kanandra Granulite	Grt-Bt-Sil granulite with strong S_2 fabric	Nl	
75	E of Halfway Dam	53 552 590	7 485 625	Kanandra (DSZ)	Grt-Bt mylonite	Nl,P	
78	E of Halfway Dam	53 552 012	7 485 160	Kanandra (EPSZ)	Bt-Sil-Grt mylonitic fabric	Nl	
78B	E of Halfway Dam	53 552 000	7 485 060	Kanandra (EPSZ)	fine grained Bt-Sil-Grt mylonite	P	
81C	S of Marshall River	53 555 750	7 479 640	Harts Range Group	strained pelite retrogressed to Chl-Ms	Nl	
82	S of Marshall River	53 554 440	7 479 510	Harts Range Group	Grt-Hbl migmatite	P	
89	Huckitta-Dneiper fence	53 540 575	7 483 688	Harts Range Group	Grt-Hbl gneiss	P	
91	Huckitta-Dneiper fence	53 540 413	7 484 700	Kanandra (EPSZ)	Grt-Hbl-Cpx-Ttn-Ep-Qtz-Pl rock	P	
92	Huckitta-Dneiper fence	53 540 555	7 484 850	Kanandra Granulite	Grt-Bt-Sil gneiss, uncertain structural setting	Nl	
93A	Huckitta-Dneiper fence	53 540 739	7 485 120	Kanandra (EPSZ)	Grt-Sil-Bt mylonite	P	
93C	Huckitta-Dneiper fence	53 540 739	7 485 120	Kanandra (EPSZ)	Grt-Hbl mylonite	Nl	
93D	Huckitta-Dneiper fence	53 540 739	7 485 120	Kanandra (EPSZ)	oriented sample (felsic)	Nl	
99	Huckitta-Dneiper fence	53 540 100	7 485 085	Kanandra (DSZ)	Bt-Ms schist	Nl	
101A	Deep Bore	53 558 495	7 488 120	Deep Bore Met	Sil-Crd-Spl migmatite	Nl	
101C	Deep Bore	53 558 495	7 488 120	Deep Bore Met	Sil-Crd-Spl migmatite	Nl	
102	Deep Bore	53 558 600	7 488 290	Deep Bore Met	Grt-Crd-Bt gneiss	Nl	
102A	Deep Bore	53 558 600	7 488 290	Deep Bore Met	Grt-Crd-Bt gneiss	P	
102C	Deep Bore	53 558 600	7 488 290	Deep Bore Met	Sil-Crd-Spl migmatite	Nl,P	
102X	Deep Bore	53 558 600	7 488 290	Deep Bore Met	Crd-Spl migmatite	Nl	
107	N of Yam Creek Bore	53 562 020	7 484 950	Kanandra Granulite	Bt-Grt-Sil pelite, S_2 fabric	P	
124	E of Halfway Dam	53 553 540	7 483 675	Kanandra (EPSZ)	Grt-Bt-Sil-Ms mylonite	P	
125	E of Halfway Dam	53 553 360	7 483 800	Kanandra (EPSZ)	calc-silicate in S_3 - Scp-Cal-Di-Qtz-Ttn	Nl	

APPENDIX 1 (Continued)

Sample	Region	Easting	Northing	Lithology	Description	TS	Geochron
129	E of Halfway Dam	53 553 610	7 484 730	Kanandra Granulite	Bt-Sil-Grt, may be S_2 or S_3 mylonite	P	
131	E of Halfway Dam	53 553 820	7 484 770	Kanandra Granulite	granulite facies pelite, strong S_2	P	
131A	E of Halfway Dam	53 553 820	7 484 770	Kanandra Granulite	Grt-Crd-Sil-Bt metapelite	Nl,P	
131B	E of Halfway Dam	53 553 820	7 484 770	Kanandra Granulite	Grt-Crd-Sil-Bt metapelite	P	
132	E of Halfway Dam	53 553 850	7 484 890	Kanandra (EPSZ)	Grt-Sil-Bt mylonite	Nl	
135	E of Halfway Dam	53 553 960	7 483 780	Kanandra (EPSZ)	Grt-Sil-Bt mylonite	P	
139B	S of Marshall River	53 553 070	7 482 740	Harts Range Group	Grt-Hbl mafic with Grt bearing melts	P	
139E	S of Marshall River	53 553 070	7 482 740	Harts Range Group	amphibolite with coarse early Cpx in melt	Nl	
140	S of Marshall River	53 552 650	7 482 450	Harts Range Group	pelite with leucosomes & early Grt preserved	P	
146	W of Halfway Dam	53 548 045	7 486 840	Kanandra (DSZ)	low-grade Ms-Bt ± Chl mylonite	Nl	
147	W of Halfway Dam	53 547 250	7 487 690	Kanandra (DSZ)	pelitic granulite, retrogressed to Bt-Ms-Chl	Nl	
149	W of Yam Creek Bore	53 554 820	7 483 680	Kanandra (EPSZ)	Bt-Grt-Sil mylonite (oriented)	P	
155	W of Yam Creek Bore	53 555 670	7 484 310	Kanandra (EPSZ)	Grt-Hbl rock in S_3a mylonite cutting mafic	P	
156	W of Yam Creek Bore	53 555 640	7 484 400	Kanandra (EPSZ)	Grt-Hbl rock in S_3a mylonite cutting mafic	P	Sm-Nd Ar-Ar
158	W of Yam Creek Bore	53 555 486	7 485 000	Kanandra (EPSZ)	Grt-Hbl rock in S_3a mylonite cutting mafic	P	
168	W of Yam Creek Bore	53 558 070	7 484 010	Kanandra (DSZ)	Bt-Grt mylonite	Nl	
169	W of Yam Creek Bore	53 558 145	7 484 335	Kanandra Granulite	sample of pelite with Sil in S_2	P	
170B	W of Yam Creek Bore	53 558 010	7 484 540	Kanandra (DSZ)	Grt-Ms (± Chl & Bt) mylonite	P	
172A	S of Marshall Bore	53 561 790	7 477 090	Harts Range Group	massive Grt-rich rock with more mafics	P	
172B	S of Marshall Bore	53 561 725	7 477 210	Harts Range Group	massive Grt-Hbl felsic gneiss	P	
173	S of Marshall Bore	53 561 940	7 477 280	Harts Range Group	metapelite retrogressed to Chl-Ms	Nl	
174	Entire Point Fault	53 543 790	7 485 925	Kanandra (EPSZ)	Bt-Sil mylonite, no Grt	Nl	
176	Entire Point Fault	53 545 380	7 486 450	Kanandra (DSZ)	St-Bt-Ms mylonite	Nl	
179	Huckitta-Dneiper fence	53 542 380	7 487 060	Kanandra Granulite	pelite with strong S_2 defined by Sil	P	
184	Huckitta-Dneiper fence	53 544 240	7 488 140	Kanandra (DSZ)	Qtz-Ms mylonite with S-C fabrics (oriented)	Nl	
195	Huckitta-Dneiper fence	53 542 710	7 486 340	Kanandra Granulite	mafic granulite with S_2 high strain fabric	Nl	
195B	Huckitta-Dneiper fence	53 542 650	7 486 330	Kanandra Granulite	pelite from S_2 high strain zone	Nl	
203	Entire Point Fault	53 540 530	7 484 900	Kanandra (DSZ)	retrogressed Bt-Ms rock	Nl	
204	Entire Point Fault	53 540 420	7 484 880	Kanandra (EPSZ)	Grt-Hbl rock	P	
205A	Entire Point Fault	53 540 150	7 484 930	Kanandra Granulite	mafic rock recrystallised in S_2	Nl	
211A	Huckitta-Dneiper fence	53 541 090	7 485 150	Kanandra (EPSZ)	mafics recrystallised to Grt-Hbl	P	
215	Huckitta-Dneiper fence	53 540 790	7 485 900	Kanandra (DSZ)	mylonite with stable Grt	P	
218A	Huckitta-Dneiper fence	53 541 510	7 486 250	Kanandra Granulite	mafic granulite? with S_2 fabric	Nl	
219	Huckitta-Dneiper fence	53 541 510	7 485 470	Kanandra Granulite	mafic granulite recrystallised to Grt-Hbl	P	
221	Entire Point Fault	53 542 900	7 485 010	Harts Range Group	mafic rock recrystallised to Grt-Hbl	P	
221A-D	Entire Point Fault	53 542 900	7 485 010	Harts Range Group	mafic rock recrystallised to Grt-Hbl	Nl	
222	Entire Point Fault	53 543 870	7 485 090	Harts Range Group	Bt-Sil-Grt pelite with strong lineation	P	
223	E of Halfway Dam	53 552 850	7 484 075	Kanandra (EPSZ)	Bt-Grt-Sil mylonite zone (section 223A)	Nl,P	
224	E of Halfway Dam	53 553 080	7 484 280	Kanandra Granulite	meta-ultramafic - tremolite-rich	Nl	
225	E of Halfway Dam	53 553 190	7 484 500	Kanandra (EPSZ)	Bt-Sil-Grt mylonite	Nl,P	
225B	E of Halfway Dam	53 553 190	7 484 500	Kanandra (EPSZ)	Oriented sample of pelitic mylonite	Nl	
227	E of Halfway Dam	53 553 000	7 485 400	Kanandra (EPSZ)	Grt-Bt-Sil mylonite	Nl,P	
232	E of Halfway Dam	53 554 390	7 484 390	Kanandra (EPSZ)	mylonite with Grt-Hbl assemblage	P	
236	E of Halfway Dam	53 551 150	7 485 020	Kanandra Granulite	granulite facies metapelite	P	
237	E of Halfway Dam	53 552 475	7 484 190	Kanandra (EPSZ)	Bt-Grt-Sil mylonite	Nl,P	U-Pb monazite

Fieldwork: June 1999 (All samples prefixed by ISHU99.)

Sample	Region	Easting	Northing	Lithology	Description	TS	Geochron
241A	E of Halfway Dam	53 555 841	7 485 486	Kanandra (DSZ)	pegmatite, recrystallised in S_4, Ms in fabric	Nl	Ar-Ar Ms
241C	E of Halfway Dam	53 555 841	7 485 430	Kanandra (DSZ)	cummingtonite-tremolite? schist	Nl	
243	E of Halfway Dam	53 555 260	7 484 611	Kanandra (DSZ)	coarse Bt-Ms in recrystallised felsic mylonite		Ar-Ar Ms, Bt
250	Dneiper-Huckitta fence	53 540 907	7 486 616	Kanandra (DSZ)	D_4 shear zone, Ms-bearing felsic mylonite		Ar-Ar Ms
250A	Dneiper-Huckitta fence	53 540 907	7 486 616	Kanandra (DSZ)	D_4 shear zone, Hbl-amphibolite		Ar-Ar Hbl
251	Dneiper-Huckitta fence	53 541 088	7 489 774	Kanandra (DSZ)	Qtz-Ms phyllite, northern DSZ	Nl	Ar-Ar Ms
252	Dneiper-Huckitta fence	53 541 421	7 490 490	Cackleberry Met	para-amphibolite	Nl	Ar-Ar Hbl
253	Dneiper-Huckitta fence	53 541 083	7 490 275	Kanandra (DSZ)	Qtz-Ms-Chl phyllite northern edge of DSZ	Nl	Ar-Ar Ms
254	Dneiper-Huckitta fence	53 541 335	7 488 676	Kanandra (DSZ)	Hbl-amphibolite in DSZ	P	Ar-Ar Hbl
255	Dneiper-Huckitta fence	53 541 512	7 488 350	Kanandra (DSZ)	Hbl-amphibolite, only suitable for cooling age		Ar-Ar Hbl
255A,B	Dneiper-Huckitta fence	53 541 512	7 488 350	Kanandra (DSZ)	Ms-bearing felsic rock, recrystallised in S_4		Ar-Ar Ms

APPENDIX 1 (Continued)

Sample	Region	Easting	Northing	Lithology	Description	TS	Geochron
263	E of Yam Creek Bore	53 553 070	7 482 740	Harts Range Group	Hbl amphibolite		Ar-Ar Hbl
266	3 km S of Deep Bore	53 559 850	7 488 040	Deep Bore Met	Grt-Crd-Opx-Bt gneiss (*Thin section 266A)	P	
266B	3 km S of Deep Bore	53 559 850	7 488 040	Deep Bore Met	Grt-Crd-Opx-Bt gneiss	P	
266C	3 km S of Deep Bore	53 559 850	7 488 040	Deep Bore Met	Grt-Crd-Bt gneiss	P	
267	E of Yam Creek Bore	53 554 100	7 481 030	Harts Range Group	amphibolite with Grt-bearing melts	P	
270A	E of Yam Creek Bore	53 553 700	7 480 430	Harts Range Group	Grt-Hbl rock from planar S_2 fabric	P	
270B	E of Yam Creek Bore	53 553 700	7 480 430	Harts Range Group	Grt-Bt-Sil metapelite, relatively low S_2 strain	P	
271	E of Yam Creek Bore	53 553 180	7 480 850	Harts Range Group	Bt gneiss with Cpx-Scp bearing layers	Nl	
279A	E of Yam Creek Bore	53 552 300	7 477 280	Harts Range Group	Hbl amphibolite recrystallised in S_2h		Ar-Ar Hbl
279B	E of Yam Creek Bore	53 552 300	7 477 280	Harts Range Group	pelite retrogressed to Chl-Ms	Nl	Ar-Ar Ms
281	E of Yam Creek Bore	53 554 710	7 478 980	Harts Range Group	Grt-Bt-Sil pelite with S_2h fabric	P	
283	NE of Yam Creek Bore	53 555 305	7 483 840	Kanandra Granulite	mafic granulite with S_2 - no Palaeozoic	Nl	Ar-Ar Hbl
284	Northern DSZ	53 557 130	7 486 080	Kanandra (DSZ)	northern edge of DSZ - amphibolite boudin	Nl	Ar-Ar Hbl
285A	Northern DSZ	53 558 747	7 486 140	Kanandra (DSZ)	Bt-epidote schist	Nl	
286	3 km S of Deep Bore	53 559 850	7 488 080	Deep Bore Met	Crd-Bt-Spl-Crn gneiss	Nl	
286A	3 km S of Deep Bore	53 559 850	7 488 080	Deep Bore Met	Crd gneiss	Nl	
287	3 km S of Deep Bore	53 559 740	7 488 060	Deep Bore Met	Grt-Crd-Opx gneiss (Bt poor)	P	
288A	3 km S of Deep Bore	53 559 460	7 488 050	Deep Bore Met	Di-Qtz-Scp calc-silicate	Nl	
289A	3 km S of Deep Bore	53 559 500	7 488 035	Deep Bore Met	Grt-Crd-Bt gneiss	Nl	
289B	3 km S of Deep Bore	53 559 500	7 488 035	Deep Bore Met	Sil-Crd-Spl migmatite	P	
289C	3 km S of Deep Bore	53 559 500	7 488 035	Deep Bore Met	Grt-Crd-Bt gneiss	P	
289D	3 km S of Deep Bore	53 559 500	7 488 035	Deep Bore Met	Grt-Crd-Bt gneiss	P	
291B	3 km S of Deep Bore	53 559 850	7 488 040	Deep Bore Met	Sil-Crd migmatite	P	

Fieldwork: January 2000 (All samples prefixed by ISHU99).

Sample	Region	Easting	Northing	Lithology	Description	TS	Geochron
296	Western Mopunga R	53 537 950	7 498 680	Cackleberry Met	Crd-Sil-Bt gneiss with Crd-bearing melt	P	
298B	Western Mopunga R	53 540 925	7 496 640	Cackleberry Met	Spr-Phl schist	P	
298D	Western Mopunga R	53 540 925	7 496 640	Cackleberry Met	unusual Crd-Oam? rock	P	
298E	Western Mopunga R	53 540 925	7 496 640	Cackleberry Met	unusual Crd-Oam? rock - higher strain	P	
298G	Western Mopunga R	53 540 925	7 496 640	Cackleberry Met	Spr-Spl-Crn-Crd-Phl schist	P	
298H	Western Mopunga R	53 540 925	7 496 640	Cackleberry Met	Phl-Crn-Crd schist	Nl	
299A	Western Mopunga R	53 538 833	7 498 030	Cackleberry Met	Crd-Bt-Sil/And gneiss	Nl	
299B	Western Mopunga R	53 538 833	7 498 030	Cackleberry Met	Sil-Bt rich rock, after andalusite?	Nl	
300	Western Mopunga R	53 538 800	7 498 480	Cackleberry Met	Crd-rich rock in low strain zone	Nl	
301A	Western Mopunga R	53 536 938	7 500 590	Cackleberry Met	Crd gneiss with strong Bt-Sil fabric	P	

APPENDIX 2

Whole rock geochemical data of a sapphirine-phlogopite schist (298G) and corundum-phlogopite schist (298H) and selected microprobe analyses from sample 298G. Abbreviations: incl – mineral occurring as inclusion; retr – mineral occurring as a retrograde phase consuming sapphirine; mineral abbreviations after Kretz (1983).

Sample	298G Spr-Phl	298H Crn-Phl
SiO_2	34.30	38.30
TiO_2	1.90	1.52
Al_2O_3	26.10	25.30
Fe_2O_3	1.56	1.98
FeO	2.10	1.30
MnO	0.03	0.04
MgO	19.60	16.30
CaO	0.57	0.48
Na_2O	0.59	0.40
K_2O	5.87	7.75
ZnO	0.01	0.01
P_2O_5	0.28	0.23
F	0.21	0.19
LOI	6.36	4.56
Total	**99.48**	**98.36**
	(ppm)	
Ba	650	850
Ce	190	135
Cs	40	53
Cr	5	2
Ga	26	24
La	98	71
Nb	28	20
Ni	19	18
Rb	360	750
Sr	24	25
Th	45	50
U	2	3
V	97	100
Y	27	25
Zr	550	460

Mineral	Spr	Spl incl	Spl retr	Pinite repl Crd	Phl coarse	Phl retr	Chl retr 1	Chl retr 2
SiO_2	11.10	0.06	0.11	47.16	39.94	40.32	28.33	27.57
TiO_2	0.00	0.00	0.00	0.00	0.70	0.61	0.00	0.00
Al_2O_3	66.53	66.67	66.59	31.67	20.13	21.77	24.37	24.99
Cr_2O_3	0.06	0.00	0.00	0.00	0.00	0.06	0.00	0.00
FeO	3.21	9.39	7.85	1.87	2.78	2.99	3.65	3.77
MnO	0.06	0.11	0.03	0.02	0.03	0.00	0.06	0.06
MgO	18.32	23.15	22.52	7.50	23.23	21.65	31.55	30.33
CaO	0.00	0.00	0.00	0.00	0.00	0.00	0.00	0.00
Na_2O	0.00	0.00	0.00	0.00	0.88	0.81	0.00	0.09
K_2O	0.00	0.00	0.00	3.76	8.86	8.77	0.00	0.13
ZnO	0.04	0.94	3.62	0.00	0.00	0.00	0.00	0.00
Total	**99.32**	**100.32**	**100.72**	**91.98**	**96.55**	**96.98**	**87.96**	**86.94**
Oxygens	**20**	**4**	**4**	**11**	**11**	**11**	**14**	**14**
Si	1.299	0.001	0.003	3.124	2.743	2.747	2.642	2.606
Ti	0	0	0	0	0.036	0.031	0	0
Al	9.178	1.936	1.939	2.474	1.630	1.749	2.680	2.785
Cr	0.006	0	0	0	0	0.003	0	0
Fe^{3+}	0.216	0.061	0.055	0.073	0.024	0.021	0.033	0.034
Fe^{2+}	0.098	0.132	0.107	0.031	0.136	0.150	0.251	0.264
Mn	0.006	0.002	0.001	0.001	0.002	0	0.005	0.005
Mg	3.198	0.850	0.829	0.741	2.377	2.199	4.390	4.273
Ca	0	0	0	0	0	0	0	0
Na	0	0	0	0	0.117	0.107	0	0.016
K	0	0	0	0.318	0.777	0.763	0	0.016
Zn	0	0.017	0.066	0	0	0	0	0
Total	**14.001**	**2.999**	**3.000**	**6.762**	**7.842**	**7.770**	**10.001**	**9.999**
X_{Mg}	0.91	0.81	0.84	0.88	0.94	0.93	0.94	0.93
OR	0.69	0.32	0.34	0.70	0.15	0.12	0.12	0.11

APPENDIX 3 (A)

Summary of conventional P-T estimates and Thermocalc results for selected samples from the Kanandra Granulite.

Errors on averaged conventional estimates are standard deviation from the mean; value after the semi-colon is the number of estimates from which the mean is derived. 2σ error is calculated by dividing the average 1σ error by the square root of the number of analyses and dividing this number by two. Errors for individual samples are 1σ. *- denotes sample from Harts Range Group; # composition of M3a garnets are outside of the range for which the Kohn and Spear (1990) barometer is calibrated. Abbreviations: HS82 - Hodges and Spear (1982); HC85 - Hodges and Crowley (1985); H90 - Hoisch (1990); GP - Graham and Powell (1982); KS90 - Kohn and Spear (1990); PH88 - Powell and Holland (1988); HP98 - Holland and Powell (1998); GH82 - Green and Hellman (1982); mineral abbreviations after Kretz (1983).

	Grt-Bt	GASP	Grt-Bi-Pl-Qtz		Thermocalc			Grt-Hbl	Grt-Hbl-Pl-Qtz		Thermocalc	
	HS82	HC85	H90		PH88, HP98			GP82	KS90		PH88, HP98	
			Mg	Fe	avP	avT			Fe	Mg	avP	avT
M1	T (@6 kb)	P (@800C)			aH2O = 0.35		# M3a	T(@6 kbar)	P (@650C)		aH2O=0.35	
57A	696-865	6.0-6.6	5.5-6.3	6.2-7.1	6.0±2.0	789±52	*8*	625-659	5.6-6.0	4.5-5.1	4.6±1.3	661±105
	782±65; 7	6.3±0.2; 7	5.9±0.3; 7	6.6±0.4; 7				632±12; 5	5.7±0.2; 4	4.7±0.3; 4		
131A	749-824	5.5-6.1	5.7-6.0	5.5-6.0	6.1±0.8	800±62	*156*	619-649	5.3-6.0	4.1-4.6	5.4±2.6	632±121
	801±35; 4	5.8±0.2; 4	5.9±0.2; 4	5.8±0.2; 4				64 ±15; 4	5.5±0.3; 4	4.3±0.2; 4		
169	750-839	5.6-6.2	5.7-5.9	5.8-6.2	5.7±1.6	767±49	*211A*	610-645	5.6-7.0	4.4-5.3	4.3±1.0	735±102
	804± 3; 7	5.8±0.2; 7	5.8±0.1; 7	5.9±0.2; 7				630±19; 3	6.2±0.7; 3	4.9±0.5; 3		
236	810-866	5.6-6.1	5.0-5.4	4.8-5.4	5.9±1.6	817±49	*221*				5.3±2.3	672±107
	829±32; 3	5.8±0.2; 4	5.2±0.2; 3	5.1±0.4; 3								
average (2σ error)					**5.9±1.5**	**793±53**					**4.9±1.8**	**673±109**
M2	T (@6 kb)	P (@750C)					M3b	T(@6 kbar)	P (@700C)			
131A	740-792	5.7-6.5	6.0-6.5	5.9-6.5	5.4±0.7	753±40	*211A*	580-701	7.2-8.2	5.2-7.6	-	-
	762±18; 6	6.2±0.4; 6	6.2±0.2; 4	6.2±0.2; 4				647±54; 4	7.6±0.4; 4	6.5±0.9; 4		
179	692-778	4.9-5.3	4.7-5.1	5.0-5.3	4.9±0.5	760±51	*219*	622-666	6.1-8.6	5.2-7.9	-	-
	736±35; 4	5.1±0.2; 4	4.9±0.2; 4	5.2±0.1; 4				641±19; 4	7.8±1.2; 4	7.0±1.3; 4		

	Grt-Bt	Grt-Phe	GASP	Grt-Bt-Pl-Qtz		Grt-Pl-Ms-Bt	Grt-Pl-Ms-Qtz		Grt-Pl-Ms-Sil	Grt-Ms-Bt-Sil	Thermocalc	
	HS82	GH82	HC85	H90		HC95	HC95	H90	HC95	HC95	PH88, HP98	
				Mg	Fe		Fe	Mg			avP	avT
M3b	T (@7 kb)		P (@700C)								aH2O = 0.35	
72	640-728	672-703	6.6-7.1	6.6-6.9	6.6-7.0	6.6-7.0	7.0-7.1	6.2-6.4	6.6-6.8	6.5-7.0	6.8±1.3	686±43
	695±37; 5	685±15; 5	6.9±0.2; 6	6.7±0.1; 4	6.8±0.2; 4	6.8±0.1; 5	7.1±0.1; 3	6.4±0.2; 3	6.7±0.1: 4	6.8±0.2; 5		
93A	619-725		6.1-6.6	5.8-6.4	6.2-6.8						6.3±1.3	666±45
	653±40; 6		6.4±0.2; 6	6.2±0.2; 6	6.5±0.2; 6							
227	674-695		6.4-7.2	6.3-6.8	6.5-7.2						7.2±1.1	709±45
	681±10; 4		6.7±0.3; 5	6.6±0.2; 5	6.8±0.3; 5							
237	640-763	702-786	6.6-7.6	6.5-7.5	6.8-7.3	6.7-7.4	6.7-7.8	6.0-7.2	6.7-8.2	6.6-7.4	7.2±1.3	699±30
	689±42; 7	728±32; 5	7.2±0.4; 5	6.9±0.5; 4	7.1±0.4; 4	7.1±0.3; 4	7.4±0.5; 5	6.4±0.5; 5	7.7±0.6; 5	7.1±0.4; 5		
*23**	722-780		5.9-6.9	6.4-6.6	6.2-6.3						6.3±1.4	698±43
	743±25; 2		6.6±0.5; 4	6.5±0.1; 3	6.3±0.1; 3							
average (2σ error)											**6.8±1.1**	**692±37**
M4	T(@5kb)			P (@ 650C)							aH2O = 1.0	
170B	607-660	608-656		3.7-4.4	3.7-4.9	4.2-6.0	4.4-6.0	3.3-5.3			5.1±1.3	653±34
	634±19; 6	636±14; 6		4.1±0.3; 6	4.4±0.5; 6	5.0±0.6; 6	5.2±0.6; 6	4.1±0.7; 6				

APPENDIX 3 (B)

Representative P-T analyses from the Deep Bore and Cackleberry Metamorphics. Abbreviations: HS82 - Hodges and Spear (1982); FS w/B Ferry and Spear (1978) with Berman (1990) garnet activity model; PD93 - Patino Douce *et al* (1993); N92 - Nichols *et al* (1992); SB82 - Sen and Bhattacharya (1988); HG82 - Harley and Green (1982); H84 - Harley (1984); H90 - Hoisch (1990); mineral abbreviations after Kretz (1983). * calculated at P=3 kbar; † - calculated at T=800°C for Deep Bore Metamorphics, and at 650°C for Cackleberry Metamorphics. Errors are single standard deviations on averaged estimates from 5-7 mineral pairs from each sample.

Representative P-T analyses from the Mopunga Range using THERMOCALC (Powell & Holland, 1988)

Average T calculations for sample ISHU98.42, Cackleberry Metamorphics (Bt-Crd-And-Ksp-Qtz)

	phl	ann	east	crd	fcrd	and	san	q
activities (a)	0.03300	0.05200	0.04800	0.39000	0.18000	1.00	1.00	1.00
σ[ln(a)]	0.40181	0.35353	0.36589	0.11163	0.19888	0	0	0

Independent set of reactions at P = 3.0 kbar	**T(P)**	**σ(T)**	**a**	**σ(a)**	**b**	**c**	**ln_K**	**sd(ln_K)**
1) 2east + crd + q = 2phl + 4and	613	331	-18.25	6.97	0.03294	-4.257	0.192	1.093
2) 10phl + 21and = 9east + 6crd + san + H_2O	640	185	163.59	31.43	-0.27585	26.794	1.134	5.238
3) 2phl + 3fcrd = 2ann + 3crd	753	4247	-29.34	2.50	0.00237	-0.213	3.229	1.270

Average temperatures [for $a(H_2O) = 0.9$]

P	1.0	1.5	2.0	2.5	3.0	3.5	4.0	4.5	5.0
av T	599	635	650	666	684	704	723	743	763
σ(T)	20	21	20	20	21	21	21	21	21
σ(fit)	0.6	0.5	0.4	0.3	0.2	0.1	0.1	0.2	0.2

All average T estimates, Cackleberry Metamorphics, at P=3.0 kbar (for $a(H_2O) = 0.9$)

Sample	42A	42E	42F	42I	301A	**Average (± 2 σ)**
aveT ± σ(T)	684 ± 21	669 ± 19	671 ± 19	667 ± 20	675 ± 20	**673 ± 17**

Average P-T calculations for sample ISHU98.266C, Deep Bore Metamorphics (Grt-Bt-Crd-Qtz-Ksp)

	crd	fcrd	py	alm	phl	ann	east	q	san
activities (a)	0.4900	0.115	0.01070	0.430	0.0470	0.0570	0.0124	1.0	1.0
σ[ln(a)]	0.0780	0.262	0.54706	0.150	0.3680	0.3477	0.5315	0	0

Independent set of reactions [for $a(H_2O) = 0.3$]	**P(T)**	**σ(P)**	**a**	**σ(a)**	**b**	**c**	**ln_K**	**σ(ln_K)**
1) py + east + 3q = crd + phl	2.2	1.48	-26.18	3.50	-0.0298	5.206	5.157	0.851
2) 3fcrd + 4ann + 3q = 6alm + 4H_2O + 4san	4.1	0.94	66.86	5.04	-0.1053	-16.587	12.883	1.834
3) 3crd + 2alm = 3fcrd + 2py	7.9	14.27	136.64	1.54	-0.0493	0.801	-11.736	1.400
4) 3fcrd + 2py + 2east + 6q = 5crd + 2ann	0.88	1.67	-81.75	7.53	-0.0573	10.200	15.047	1.892

aCO_2	**aH_2O**	**T**	**σ(T)**	**P**	**σ(P)**	**σ(fit)**
0.25	0.2	736	60	2.7	0.9	0.94
0	0.3	784	80	3.4	1.1	1.23
0.50	0.3	785	80	3.6	1.1	1.23
0.25	0.4	838	101	4.2	1.3	1.45

All average P-T estimates, Deep Bore Metamorphics (for $a(H_2O) = 0.3$)

Sample	**36A**	**102A**	**266A**	**266B**	**266C**	**189C**	**Average (± 2σ)**
aveP ± σ(P)	2.8 ± 0.8	2.9 ± 0.9	4.3 ± 1.1	4.9 ± 1.0	3.4 ± 1.1	2.2 ± 1.3	**3.4 ± 0.8**
aveT ± σ(T)	763 ± 65	784 ± 59	771 ± 80	770 ± 57	784± 80	770 ± 91	**773 ± 59**

Summary of conventional P-T estimates

		Deep Bore Metamorphics						**Cackleberry**
Thermometers		***102A***	***266A***	***266B***	***266C***	***287***	***289C***	***42C***
Grt-Bt	HS82	871 ± 20	826 ± 43	842 ± 27	748 ± 21		774 ± 16	
Grt-Bt	FS w/B	862 ± 34	801 ± 42	818 ± 38	734 ± 21		760 ± 18	
Grt-Bt	PD93	794 ± 36	754 ± 41	764 ± 25	704 ± 20		714 ± 13	
Grt-Crd	N92	742 ± 38	615 ± 30	708 ± 11	542 ± 20	711 ± 25	656 ± 30	
Grt-Opx	SB82		732 ± 28	802 ± 18		795 ± 58		
Grt-Opx	H84		670 ± 27	732 ± 10		743 ± 23		
Barometers†								
Grt-Opx	HG82		2.9 ± 0.3	3.0 ± 0.5		2.3 ± 0.2		
GBPQ	H90 (Mg)							2.5 ± 0.3
GBPQ	H90 (Fe)							3.7 ± 0.2

APPENDIX 4 (A)

SHRIMP U-Th-Pb data for zircon, Deep Bore Metamorphics (Sample ISHU98.130). f206 % represents % of ^{206}Pb that is common Pb; nd - not detectable; % Conc is percentage concordance; Pb* is the concentration of radiogenic lead; data is corrected for ^{204}Pb using the Cumming and Richards (1975) model; [a] rim age; [b] core age; [d] discordant data; [i] inheritance or component of inheritance.

Grain spot	U ppm	Th ppm	Th/U	Pb* (ppm)	^{204}Pb (ppb)	f206 %	$\frac{^{206}Pb}{^{238}U}$	± (1σ)	$\frac{^{207}Pb}{^{235}U}$	± (1σ)	$\frac{^{207}Pb}{^{206}Pb}$	± (1σ)	Age 6/38	Age 7/6	% Conc
403.1[a]	861	7	0.009	250	7	0.05	0.3045	0.0047	4.469	0.079	0.1064	0.0007	1714±23	1739±13	99
405.1[a]	613	11	0.019	179	6	0.06	0.3051	0.0061	4.477	0.094	0.1064	0.0005	1716±30	1739±9	99
412.1[a]	554	5	0.010	164	4	0.04	0.3114	0.0066	4.527	0.100	0.1054	0.0004	1748±33	1722±7	102
416.1[a]	857	9	0.011	251	12	0.08	0.3068	0.0055	4.475	0.084	0.1058	0.0005	1725±27	1728±8	100
418.1[a]	678	6	0.009	188	32	0.30	0.2909	0.0048	4.188	0.080	0.1044	0.0008	1646±24	1704±14	97
419.1[a]	902	28	0.031	248	17	0.12	0.2876	0.0044	4.167	0.078	0.1051	0.0010	1629±22	1716±17	95
421.2[a]	957	6	0.006	287	2	0.01	0.3147	0.0050	4.612	0.082	0.1063	0.0007	1764±24	1737±12	102
422.1[a]	623	7	0.010	188	0	0.00	0.3159	0.0048	4.631	0.080	0.1063	0.0007	1770±24	1737±12	102
424.1[a]	716	8	0.012	213	1	0.01	0.3113	0.0050	4.551	0.079	0.1060	0.0005	1747±25	1732±8	101
426.1[a]	891	74	0.083	260	4	0.03	0.3005	0.0045	4.432	0.080	0.1070	0.0009	1694±22	1748±15	97
427.1[a]	583	7	0.012	172	2	0.02	0.3089	0.0067	4.519	0.109	0.1061	0.0008	1735±33	1734±15	100
431.1[a]	816	20	0.025	242	11	0.08	0.3103	0.0052	4.498	0.105	0.1051	0.0015	1742±26	1716±27	102
402.1[b]	198	91	0.462	68	3	0.09	0.3232	0.0067	4.855	0.116	0.1089	0.0010	1806±33	1782±17	101
404.1[b]	157	78	0.496	54	nd	nd	0.3195	0.0062	4.842	0.116	0.1099	0.0013	1787±30	1798±22	99
405.2[b]	231	133	0.573	83	5	0.11	0.3268	0.0061	4.918	0.107	0.1091	0.0010	1823±30	1785±17	102
406.1[b]	228	102	0.447	77	nd	nd	0.3138	0.0072	4.796	0.123	0.1109	0.0010	1759±35	1814±17	97
407.1[b]	254	155	0.611	90	3	0.08	0.3204	0.0068	4.836	0.113	0.1095	0.0008	1792±33	1791±14	100
409.1[b]	201	86	0.427	69	0	0.01	0.3218	0.0055	4.888	0.094	0.1102	0.0008	1798±27	1802±13	100
410.1[b]	386	170	0.441	134	2	0.03	0.3253	0.0052	5.017	0.089	0.1119	0.0006	1816±25	1830±10	99
411.1[b]	285	173	0.605	103	1	0.03	0.3256	0.0052	4.903	0.093	0.1092	0.0009	1817±25	1787±15	102
413.1[b]	315	102	0.323	102	2	0.03	0.3106	0.0068	4.649	0.128	0.1086	0.0015	1743±34	1776±26	98
414.1[b]	220	82	0.372	76	1	0.02	0.3295	0.0066	5.124	0.123	0.1128	0.0012	1836±32	1845±20	100
415.1[b]	300	181	0.603	109	nd	nd	0.3270	0.0059	5.010	0.143	0.1111	0.0022	1824±28	1818±37	100
416.2[b]	321	197	0.614	116	nd	nd	0.3257	0.0061	4.954	0.100	0.1103	0.0006	1817±30	1805±10	101
417.1[b]	255	126	0.495	93	1	0.03	0.3378	0.0066	5.282	0.118	0.1134	0.0010	1876±32	1855±16	101
420.2[b]	138	61	0.440	48	1	0.05	0.3221	0.0060	4.872	0.103	0.1097	0.0009	1800±29	1795±15	100
421.1[b]	418	221	0.528	148	nd	nd	0.3249	0.0062	4.952	0.105	0.1105	0.0008	1814±30	1808±12	100
426.2[b]	270	149	0.552	95	1	0.02	0.3220	0.0065	4.869	0.129	0.1097	0.0016	1800±32	1794±27	100
428.1[b]	256	121	0.471	91	1	0.03	0.3327	0.0059	5.044	0.100	0.1100	0.0007	1852±29	1799±12	103
429.1[b]	208	115	0.553	74	3	0.08	0.3271	0.0070	4.920	0.121	0.1091	0.0011	1824±34	1784±18	102
430.1[b]	281	126	0.447	96	4	0.08	0.3194	0.0078	4.810	0.132	0.1092	0.0011	1787±38	1786±19	100
431.2[b]	224	121	0.539	79	nd	nd	0.3232	0.0059	4.926	0.103	0.1105	0.0010	1805±29	1808±16	100
419.2[d]	888	349	0.393	281	131	0.87	0.3020	0.0053	4.803	0.104	0.1153	0.0012	1701±26	1885±19	90
420.1[d]	1255	17	0.014	268	229	1.48	0.2253	0.0047	3.061	0.071	0.0985	0.0008	1310±25	1596±15	82
423.1[d]	1008	11	0.011	263	2	0.01	0.2737	0.0051	3.997	0.101	0.1059	0.0016	1560±26	1730±28	90
401.1[i]	459	379	0.825	179	1	0.02	0.3348	0.0051	5.271	0.090	0.1142	0.0007	1862±25	1867±11	100
408.1[i]	595	139	0.234	293	2	0.01	0.4654	0.0079	10.563	0.264	0.1646	0.0027	2463±35	2504±28	98
425.1[i]	594	808	1.360	288	2	0.02	0.3717	0.0057	6.369	0.102	0.1243	0.0004	2037±27	2019±6	101

APPENDIX 4 (B)

SHRIMP U-Th-Pb data for monazite, Entire Point Shear Zone (Sample ISHU98.237). Summary of Sm-Nd analytical data for sample ISHU98.156.

Grain spot	U (ppm)	Th (ppm)	Th/U	Pb* (ppm)	$^{204}Pb/^{206}Pb$	f206 %	$^{208}Pb/^{232}Th$	± 1σ	$^{206}Pb/^{238}U$	± 1σ	$^{207}Pb/^{235}U$	± 1σ	$^{207}Pb/^{206}Pb$	± 1σ	$^{208}Pb/^{232}Th$	± 1σ	$^{206}Pb/^{238}U$	± 1σ	$^{207}Pb/^{235}U$	± 1σ	$^{207}Pb/^{206}Pb$	± 1σ	Conc %
							Radiogenic Ratios								Ages (in Ma)								
1.1	745	5107	6.86	149	0.000099	0.18	0.0224	0.0005	0.0738	0.0015	0.570	0.015	0.0561	0.0007	448	10	459	9	458	9	454	28	101
1.2	999	6285	6.29	186	0.000088	0.16	0.0222	0.0006	0.0717	0.0016	0.545	0.016	0.0552	0.0009	443	11	446	10	442	10	420	35	106
2.1	935	3772	4.04	130	0.000043	0.08	0.0212	0.0005	0.0709	0.0017	0.552	0.015	0.0564	0.0006	424	11	441	10	446	10	470	23	94
2.2	765	6396	8.36	167	0.000175	0.32	0.0214	0.0005	0.0699	0.0015	0.529	0.016	0.0549	0.0010	429	10	435	9	431	10	410	39	106
2.3	1231	7299	5.93	216	0.000131	0.24	0.0217	0.0005	0.0708	0.0015	0.539	0.016	0.0552	0.0009	433	10	441	9	438	10	420	38	105
3.1	537	6139	11.44	150	0.000068	0.12	0.0218	0.0006	0.0702	0.0017	0.543	0.016	0.0561	0.0009	435	11	437	10	440	11	456	36	96
4.1	872	6575	7.54	180	0.000095	0.17	0.0218	0.0005	0.0707	0.0015	0.546	0.017	0.0560	0.0011	436	10	440	9	442	11	452	42	97
5.1	1159	6873	5.93	205	0.000071	0.13	0.0218	0.0005	0.0714	0.0016	0.545	0.017	0.0554	0.0011	435	10	444	9	442	11	430	43	104
6.1	1213	7222	5.96	213	0.000259	0.47	0.0216	0.0005	0.0700	0.0016	0.530	0.021	0.0550	0.0016	433	10	436	9	432	14	411	67	106
7.1	1088	4868	4.47	165	0.000053	0.10	0.0220	0.0005	0.0728	0.0016	0.566	0.015	0.0564	0.0007	439	10	453	9	455	10	467	29	97
8.1	968	9004	9.30	238	0.000068	0.12	0.0224	0.0005	0.0723	0.0016	0.559	0.015	0.0561	0.0008	447	10	450	9	451	10	457	31	99
8.2	671	6833	10.19	170	0.000202	0.37	0.0215	0.0006	0.0696	0.0016	0.520	0.018	0.0542	0.0012	430	11	433	10	425	12	379	51	114
9.1	871	7058	8.10	187	0.000193	0.35	0.0215	0.0005	0.0708	0.0016	0.535	0.023	0.0548	0.0019	429	10	441	9	435	15	405	79	109
9.2	2053	11680	5.69	362	0.000010	0.02	0.0223	0.0005	0.0727	0.0015	0.562	0.013	0.0561	0.0004	447	10	452	9	453	8	455	16	99
10.1	729	6636	9.10	176	0.000084	0.15	0.0222	0.0005	0.0726	0.0016	0.558	0.016	0.0558	0.0009	444	11	452	10	450	11	443	35	102
11.1	1323	6043	4.57	207	0.000159	0.29	0.0226	0.0005	0.0739	0.0015	0.567	0.016	0.0556	0.0009	451	10	460	9	456	10	436	37	105

Summary of SHRIMP results for monazite from ISHU98.237

Method	Analyses	MSWD	Probability	Age (Ma)*
$^{238}U/^{206}Pb$	All data	0.75	0.73	445 ± 5
$^{208}Pb/^{232}Th$	All data	0.63	0.86	438 ± 5
$^{207}Pb/^{206}Pb$	All data	0.44	0.97	447 ± 16
Concordia Age	All data	0.59†	0.97†	446 ± 5

* 95% confidence limits, except for the Concordia Age which is 2σ

† Calculated for concordance and equivalence

Summary of Sm-Nd analytical data for sample ISHU98.156

Sample	Sm (ppm)	Nd (ppm)	$^{147}Sm/^{144}Nd$	$^{143}Nd/^{144}Nd$	± 2σ
Garnet	0.77	1.05	0.444	0.513056	0.0007
Hornblende	4.74	13.92	0.206	0.512403	0.0050
Whole Rock	3.07	11.64	0.160	0.512241	0.0008

0.3% error is used for $^{147}Sm/^{144}Nd$ $^{143}Nd/^{144}Nd$ ratios are normalised to $^{146}Nd/^{144}Nd = 0.7129$